EPRI
Electric Power
Research Institute

Topics:
Transmission towers
Transmission lines
Foundations
Soils
Design
Testing

EPRI EL-5918
Project 1493-4
Final Report
August 1988

Analysis and Design of Drilled Shaft Foundations Socketed Into Rock

Prepared by
Cornell University
Ithaca, New York

REPORT SUMMARY

SUBJECTS: Overhead electrical transmission / Overhead transmission structures and foundations

TOPICS:
- Transmission towers
- Transmission lines
- Foundations
- Soils
- Design
- Testing

AUDIENCE: Transmission managers and engineers

Analysis and Design of Drilled Shaft Foundations Socketed Into Rock

This comprehensive evaluation of the behavior of rock-socketed foundations provides a consistent and broad-based approach to rock foundation design. It presents new procedures for realistic modeling of the rock-socket mass system.

BACKGROUND: Because natural rock masses are among the most variable of all engineering materials, designers of rock sockets have relied largely on simple empirical models. Although complex numerical methods can account for geomechanical properties of rock sockets, they are not readily accessible, and when available, they are difficult to use. The numerical approach may show promise when fully evolved, but at present neither method provides cost-effective design. EPRI and the Empire State Electric Energy Research Corporation have cofunded a large foundation-research effort. EPRI report EL-2870 provides information on transmission line structure foundations for uplift-compression loading; report EL-3771 is a critical review of design methods for foundations under axial uplift and compression loading; and report EL-3777 discusses load transfer mechanisms in rock sockets and anchors.

OBJECTIVES: To develop, implement, and demonstrate improved procedures for analyzing and designing drilled shaft foundations socketed into rock.

APPROACH: Geologic characterization of the rock mass provided the basis for a geomechanical model of the foundation–rock mass system. The project team reviewed and summarized analytic techniques for predicting the ultimate capacity of axial, lateral, and torsional loading, as well as techniques for predicting load-displacement for the three loading modes. They compared analytic model results with full-scale test data and developed a design example.

RESULTS: The report provides methods for geologic characterization of the rock mass and a mechanical model that uses simple closed-form equations to evaluate the strength and deformation properties of the rock mass. Analytic techniques consider rock-mass behavior under axial, lateral, and torsional loading (assuming no coupling between modes) and can predict deformations of shaft foundations under each loading. The report presents

guidelines for identifying and resolving special problems, considers the application of analytic techniques to reported full-scale load tests, and gives an example of the use of these techniques in design.

EPRI PERSPECTIVE

Until a comprehensive, three-dimensional finite-element model is developed and verified, the results of this research provide a design method, based on a rational, analytic approach, for drilled shaft foundations in rock. This design method departs from the commonly used empirical models for rock-socket design. The model presented here will significantly assist engineers in analyzing and designing more cost-effective and reliable rock foundation systems.

Related EPRI reports evaluate procedures for predicting foundation uplift movements (EL-4107), describe the undrained uplift behavior of drilled shaft foundations (EL-5323), analyze drilled shaft foundations under repeated axial loads and drained conditions (EL-5325), and report on drilled shaft foundation load tests (EL-5915). Volume 16 of the TLWorkstation Code™ (report EL-4540-CCM) provides a user's manual for compression uplift foundation analysis and design.

PROJECT

RP1493-4
EPRI Project Manager: Vito J. Longo
Electrical Systems Division
Contractor: Cornell University

For further information on EPRI research programs, call EPRI Technical Information Specialists (415) 855-2411.

Analysis and Design of Drilled Shaft Foundations Socketed Into Rock

EL-5918
Research Project 1493-4

Final Report, August 1988

Prepared by

CORNELL UNIVERSITY
Geotechnical Engineering Group
Hollister Hall
Ithaca, New York 14853

Authors
J. P. Carter
F. H. Kulhawy

Principal Investigator
F. H. Kulhawy

Prepared for

Empire State Electric Energy Research Corporation
1155 Avenue of the Americas
New York, New York 10036

and

Electric Power Research Institute
3412 Hillview Avenue
Palo Alto, California 94304

EPRI Project Manager
V. J. Longo

Overhead Transmission Lines Program
Electrical Systems Division

ORDERING INFORMATION

Requests for copies of this report should be directed to Research Reports Center (RRC), Box 50490, Palo Alto, CA 94303, (415) 965-4081. There is no charge for reports requested by EPRI member utilities and affiliates, U.S. utility associations, U.S. government agencies (federal, state, and local), media, and foreign organizations with which EPRI has an information exchange agreement. On request, RRC will send a catalog of EPRI reports.

NOTICE

Prepared by
Cornell University
Ithaca, New York

ABSTRACT

A comprehensive investigation has been made of the behavior of drilled shaft foundations socketed into rock. Methods of analysis have been presented to predict the ultimate capacity and the load-displacement behavior under axial load (compression or uplift), lateral load or moment, and torsion. Simple approximate models have been developed which allow closed form predictions for all of these loading modes. The models for axial loading have been used in the interpretation of 25 load tests from the literature to deduce the likely range of design parameters. Only two load tests were available for lateral load analysis, and no torsional load tests were available. More data are needed from these loading modes for model verification. A detailed design example also is included to illustrate the use of the design equations presented.

ACKNOWLEDGMENTS

This study was conducted at Cornell University while the first author was on sabbatical leave from the University of Sydney, Sydney, N.S.W., Australia. Appreciation is expressed to the University of Sydney for the leave opportunity and partial financial support.

During the course of this study, C. H. Trautmann of Cornell University was a constructive critic and reviewer who provided much assistance. L. Crouse did an excellent job on typing the draft text, A. Avcisoy drafted the figures with style and character, and K. Stewart typed the final text.

Several colleagues graciously responded to a request for review and evaluation of the first draft of this report. These included: R. A. Bragg, GAI Consultants; J. C. Burton, San Diego Gas and Electric; M. W. O'Neill, University of Houston; T. E. Rodgers, Virginia Power; J. W. Rustvold, Bonneville Power Administration; and J. P. Stewart, Syracuse University.

CONTENTS

ILLUSTRATIONS

TABLES

SYMBOLS

ENGLISH LETTERS - UPPER CASE

A - area: of sidewall socket (A_s)

B - foundation width or diameter

D - foundation depth: in soil (D_s), in rock (D_r)

E - Young's modulus: of rock (E_r), of concrete shaft (E_c), of rock below tip (E_b), equivalent for lateral loading (E_e)

G - shear modulus: of rock (G_r), of rock below tip (G_b), equivalent for torsional loading (G_e)

G* - equivalent shear modulus of rock mass, equal to $G_r(1 + 3\nu_r/4)$

H - horizontal or shear load: ultimate (H_{ult}), at soil-rock contact (H_o)

J - bearing capacity correction factor; polar moment of inertia

K - coefficient of horizontal soil stress: maximum passive limit (K_p)
- normal (K_n) or shear (K_s) stiffness of discontinuity

L_t - travel distance along socket wall profile

M - moment: at soil-rock contact (M_o)

N - bearing capacity factor: on cohesion (N_c), on friction (N_γ), on overburden (N_q), for jointed rock (N_{cr}), for oriented discontinuities (N_{cs})

P - jack load at tip

P_{sf} - peak side resistance

Q - axial load: in compression at butt (Q_c), in compression at tip (Q_{tip}), in uplift at butt (Q_u), in uplift at tip (Q_{ut}), at soil-rock contact (Q_o), at initiation of full slip (Q_{fs}), at intercept of slip behavior (Q_i), at maximum value (Q_{max}), ultimate (Q_{ult})

R - plastic radius at limit condition; radius at which vertical displacements vanish

RQD - rock quality designation

S - mean discontinuity spacing
- stiffness of load-displacement curve: initial elastic (S_1), during slip (S_2), for tip (S_3), at maximum value ($S_f = 0$)

T - torque or torsional moment: ultimate (T_{ult}), at tip (T_{tip}), at soil-rock contact (T_o)

ENGLISH LETTERS - LOWER CASE

a - cavity radius

$\bar{a}$ - average height of asperities along socket

b - empirical coefficient

c - cohesion: of rock (c_r), of joint or discontinuity (c_j)

e - eccentricity

f'_c - concrete uniaxial compressive strength

m - empirical strength parameter

p_a - atmospheric pressure

p_L - limit stress

p_u - distribution of soil resistance

q - surcharge or overburden stress ($= \gamma D$)

q_a - allowable contact stress

q_u - rock uniaxial compressive strength

q_{ult} - ultimate bearing stress

r - radial distance

r_o - radius of cylinder or shaft

s - empirical strength parameter

s_u - undrained shearing resistance of soil

u - radial or horizontal displacement: of concrete (u_c), of rock (u_r), between ground surface and soil-rock contact (u_{AB})

v - circumferential displacement

w - vertical displacement: of concrete shaft or butt in compression (w_c), of rock (w_r), of tip in compression (w_{ct}), of butt in uplift (w_u), of tip in uplift (w_{ut}), at soil-rock contact (w_o), between ground surface and soil-rock contact (w_{AB})

z - depth: to center of rotation (z_c)

GREEK LETTERS - UPPER CASE

Δ - change

Φ - rotation under torsional load: at shaft tip (Φ_{tip}), between ground surface and soil-rock contact (Φ_{AB})

GREEK LETTERS - LOWER CASE

α - strength reduction factor

α_E - modulus reduction factor

γ - unit weight; shear strain

δ - angle of friction for soil-shaft interface

ϵ - strain: vertical (ϵ_z), radial (ϵ_r)

$\dot{\epsilon}^p$ - plastic strain increment: major principal ($\dot{\epsilon}_1^p$), minor principal ($\dot{\epsilon}_3^p$)

ζ - $ln[5(1 - \nu_r)D/B]$

ζ_{xs} - bearing capacity shape factors: on $N_c(\zeta_{cs})$, on $N_\gamma(\zeta_{\gamma s})$, on $N_q(\zeta_{qs})$

θ - rotation under lateral load or moment: between ground surface and soil-rock contact (θ_{AB})

λ - E_c/G_r for axial and lateral, G_e/G_r for torsion

μ - $(2/B)(2/\zeta\lambda)^{1/2}$ for axial and lateral, $(1/B)(32/\lambda)^{1/2}$ for torsion

ν - Poisson's ratio: of rock (ν_r), of concrete shaft (ν_c), of rock below tip (ν_b), equivalent for lateral loading (ν_e)

ξ - G_r/G_b

σ - normal stress: major principal (σ_1), minor principal (σ_3), in-situ horizontal (σ_{hi}), at butt (σ_b), radial (σ_r), vertical (σ_z), at tip (σ_{tip})

$\bar{\sigma}_v$ - vertical effective stress

τ - shear stress: at radius $r_o(\tau_o)$, along soil-shaft interface (τ_f), circumferential on horizontal planes (τ_{zo}), circumferential on cylindrical surface ($\tau_{r\theta}$)

$\bar{\tau}_{max}$ - maximum unit side resistance

ϕ - angle of friction: of rock (ϕ_r), of joint or discontinuity (ϕ_j)

$\bar{\phi}$ - effective stress angle of friction

ψ - dilation angle: of rock (ψ_r)

ω - discontinuity orientation

SUMMARY

This report has been prepared for the Electric Power Research Institute (EPRI) as an account of work on Research Project 1493, "Uplift/Compression Transmission Line Structure Foundation Research". The general objectives of this research are the development and implementation of rational analysis and design procedures for the foundations of transmission line structures.

Overall, this report provides a comprehensive evaluation of the behavior of drilled shaft foundations socketed into rock. Methods of analysis are presented to predict the ultimate capacity and the load-displacement behavior under axial load (compression or uplift), lateral load or moment, and torsion. All of the methods have been presented in simple, approximate, closed form equations for ease in use. Comparisons with limited available load test data illustrate the usefulness of the methods presented.

CURRENT DESIGN METHODS

Current design practice for foundations socketed into rock is less than satisfactory. A variety of empirical design rules lie at one extreme. Gross simplification of rock mass behavior is needed to employ these rules and, fundamentally, they do not incorporate the load-displacement behavior of the socket-rock mass system. At the other extreme, sophisticated numerical methods can be used. These methods have the potential to analyze the socket-rock mass behavior realistically, but the computer codes and systems are not commonly available to every designer. Neither extreme is convenient or appropriate for cost-effective design. The procedures presented in this report allow for realistic modeling of the socket-rock mass system through approximate closed form solutions which are convenient for design.

GEOLOGICAL AND GEOMECHANICAL MODELING

The initial stage in the design process is to characterize the rock mass. First, it is necessary to evaluate the general geological setting and the rock types present. Some guidelines are presented for the identification and resolution of special problems which may be encountered. Second, a mechanical model of the rock

mass is necessary to allow evaluation of the strength and deformation properties of the rock mass. Using a simple geomechanical model, it is shown how approximate correlations can be established between the RQD (rock quality designation) and both strength and modulus reduction factors to evaluate the necessary rock mass properties.

AXIAL, LATERAL, AND TORSIONAL LOAD CAPACITY

Axial capacity includes both tip and side resistance. The tip resistance is a bearing capacity problem, and pertinent solutions to this problem are presented. The side resistance is a problem of bond, gradual bond breakage, and subsequent shear or slip along the socket as a function of displacement. Methods are presented to evaluate the side resistance for the range of displacement conditions likely to occur in practice. Lateral capacity is evaluated as a limit stress problem similar to the expansion of a cylindrical cavity. This approach allows a direct solution for the capacity. The torsional capacity is approximated as a straightforward cylindrical equilibrium problem.

AXIAL LOAD-DISPLACEMENT RESPONSE

The axial uplift and compression behavior is modeled using an elastic shaft in an elastic rock mass, where the socket-rock mass interface can be elasto-plastic. An overlying soil layer also can be included. Equations are presented for the bounding cases of no slip (full bond) and full slip along the interface, and numerous examples illustrate the behavior for a variety of material parameters and loading cases. Comparisons of the closed form equations with finite element solutions and load tests gave good agreement.

LATERAL AND MOMENT LOAD-DISPLACEMENT RESPONSE

The lateral and moment behavior for both flexible and rigid shafts was modeled parametrically using finite element methods. Based on these solutions, simple, approximate, closed form equations were developed for the full range of loading conditions, material parameters, and socket-rock mass stiffness encountered in practice. These results are in good agreement with available solutions for the limiting flexible and rigid cases. The solutions give both horizontal groundline displacements and rotations and can incorporate an overlying soil layer.

TORSION LOAD-DISPLACEMENT RESPONSE

The torsion behavior is modeled as an elastic inclusion in an elastic rock mass. Assuming that the circumferential shear stress on horizontal planes is negligible, simple closed form equations result for the torsion-rotation problem. These results are in good agreement with more general numerical solutions. The solutions also can incorporate an overlying soil layer.

ANALYSIS OF FIELD LOAD TESTS

A comparison of the solutions developed herein was made with available field load test data. For the 25 axial load tests, good agreement was found for both the no slip and full slip conditions. In addition, the solutions can be used to back-calculate the model parameters needed. From this procedure, positive correlations resulted between the uniaxial compressive strength of the intact rock and the socket-rock mass interface strength parameters. For the two lateral load tests, essentially a linear behavior was observed at working load levels. No torsional load test data were found for comparison.

CONCLUSIONS

This study demonstrates that drilled shaft foundations socketed into rock can be modeled effectively using simple closed form equations. Both the capacity and load-displacement behavior can be analyzed for axial load (compression or uplift), lateral load or moment, and torsion. A design example illustrates that the solution procedure is very straightforward. However, the available load test data are quite limited, and more test results are necessary to provide complete verification.

This study represents a major advance to current design practice and will assist engineers significantly in the analysis and design of more cost-effective foundation systems.

Section 1

INTRODUCTION

Significant economy normally can be realized in design if a foundation can be constructed on or in the surface or near-surface rock. However, designers can not blindly follow the old adage, "when in doubt, put it on rock", because natural rock masses are among the most variable of all engineering materials. It is mostly for this reason that the design of foundations on or in rock has been largely empirical until recent years. Fortunately, there have been many recent studies which have improved vastly our understanding of the mechanical behavior of rock masses, making possible more rational analytical treatments of rock-foundation systems. In this report, the more pertinent of these recent analytical studies are coupled with new analytical procedures to provide a consistent and broad-based approach to the design of foundations in rock.

PROBLEM STATEMENT

The foundation type considered in this study is the concrete drilled shaft which is embedded, either partially or completely, within a rock mass, as shown in Figure 1-1. In the case of partial embedment in rock, a soil layer overlies the rock mass. These foundations are constructed by auger or drill and blast excavation and then casting concrete (often reinforced) into the cylindrical hole excavated in the rock mass. The axis of the cylinder usually coincides with the vertical direction, but may be battered. Large batters are uncommon because of the associated construction difficulties.

In general, the socketed shaft can be used to resist three modes of loading: (1) axial, either compression or uplift; (2) lateral, either moment and/or shear applied at ground level; and (3) torsional.

For single-pole transmission line structures, subjected typically to wind and ice loading and unbalanced line tensions, all three modes of loading can be transmitted to the foundation element. For lattice tower structures, the significant foundation loadings are axial uplift and perhaps lateral.

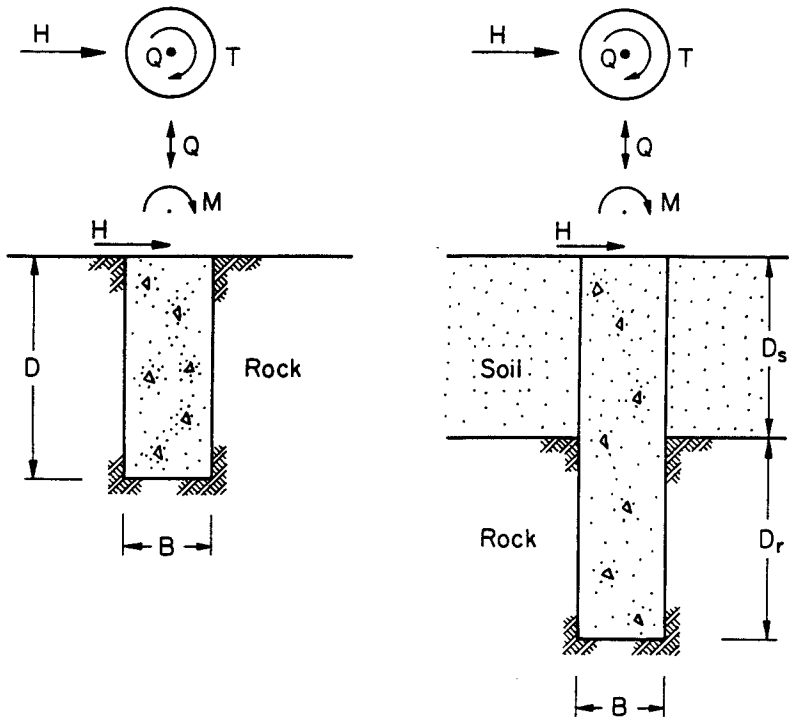

a) Rock at Ground Surface b) Overlying Soil

Figure 1-1. Cylindrical Shaft in Rock

The major design problem is to select the foundation dimensions to meet the design criteria discussed below. In this report, single shaft foundations are considered and group effects are not included. Each mode of loading is treated separately, and possible interaction effects are not considered. At present, there are very few data, if any, to determine the significance of coupling between the three loading modes.

DESIGN CONSIDERATIONS

Foundations in rock must satisfy the same design criteria as any other type of foundation: adequate stability, tolerable deformations, and cost-effectiveness. Adequate load capacity and tolerable deformations under the applied loading must be ensured with respect to all three possible modes of loading discussed above. The final design also must be feasible to construct at a reasonable cost.

The primary difference between foundations in soil and those in rock is that rock masses can be extremely variable and can surprise the designer who has not

developed a thorough understanding of the site geology. This variability often makes the characterization of a rock mass difficult because the behavior of the mass will be influenced not only by the nature of the rock material, but also by the discontinuities which are pervasive throughout almost all natural rock masses.

From a practical standpoint, some limiting structural factors may ultimately control the foundation design process, particularly in "good" rock. Most "good" rock masses have relatively high strength, low compressibility, and no unfavorable discontinuities. When these "good" rock masses are encountered, the structural design factors may control the foundation size. One example is when the "allowable" concrete stress is less than that for the rock mass, in which case the concrete design criteria will dictate the foundation size. When this situation occurs, the use of higher strength concrete should be considered in an effort to optimize the foundation sizing.

In other than "good" quality rock masses, the geotechnical considerations will normally control the design, barring any construction limitations. The question then is how to approach the geotechnical design. Four different general approaches can be adopted: full-scale load tests, building code criteria, empirical rules, and analytical methods. Load tests provide the most direct approach because a full-scale foundation is constructed in accordance with the proposed production techniques and then is tested, preferably to failure. Proper interpretation of these data should lead to a sound design. However, load tests are costly and are not warranted on most projects and at remote sites. Therefore, alternative approaches must be adopted for the majority of design cases.

A second approach is to use the allowable stresses for compression loading given in building codes. Little, if any, geotechnical information is required to design on this basis in most codes, other than a knowledge of the rock type. Type and function of the structure, loading conditions, tolerable deformations, etc. also are not included. Therefore, building code criteria tend to be very conservative. A further problem is that foundation movements will be unknown. Critical evaluation of these code values suggests that actual design values can be significantly larger. Depending on particulars, increases by factors of two to more than ten may be appropriate. However, for simple and lightly loaded structures on relatively good rock masses, it may be reasonable to use code values, primarily because they are sufficiently high that little economy may be realized by increasing the design values, given the structural limitations noted previously.

Another approach to the design of foundations is to use empirical rules. One of the more useful of these is shown in Figure 1-2, which addresses compression loading through an empirical correlation between the allowable bearing stress and the RQD (1), which is a modified core recovery index. The RQD (rock quality designation) is an approximate measure of the intensity of jointing, which in turn is a general indicator of the rock mass compressibility. This figure was developed for a reasonably sound rock mass with discontinuities that "are tight or are not open wider than a fraction of an inch". The authors contend that, with these design values, the foundation settlement should not exceed 13 mm (0.5 in). However, settlements can not be computed directly from this chart. An interesting observation can be made from this figure. If 20 MN/m^2 (2900 psi) concrete was used, with a working stress of say 0.45 f'_c (9 MN/m^2 or 1300 psi), all allowable stresses in the rock corresponding to RQD values above 65 percent could not be used. This illustrates one of the structural limitations noted previously and points out that higher strength concrete would be useful to utilize the available rock capacity more effectively.

Building codes and empirical rules provide some insight into the design process, but they do not address the problem directly or provide guidelines applicable for transmission line structures. In addition, they do not provide procedures for computing both the load capacity and deformations of the foundation. In the remainder of this report, a general procedure is presented to focus directly on these factors.

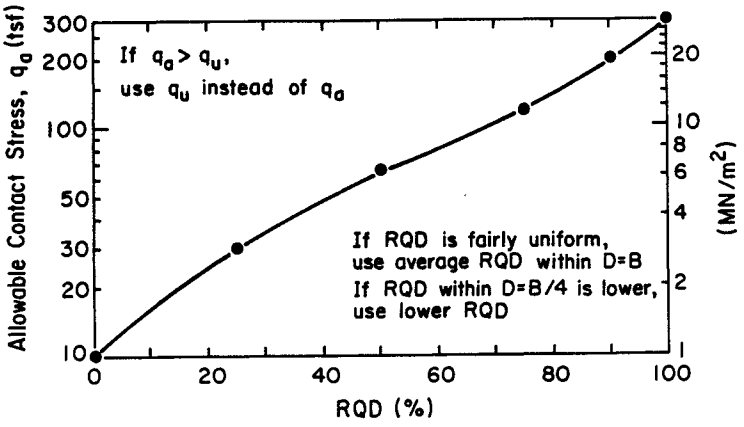

Figure 1-2. Allowable Bearing Stress on Jointed Rock

Source: Based on Peck, Hanson, and Thornburn (1).

ORGANIZATION OF REPORT

Section 2 focuses on geological characterization of the rock mass, the first step in the design process. Once this characterization is accomplished, a geomechanical model is required to allow analytical treatment of the foundation-rock mass system. Both of these issues are considered in Section 2.

The ultimate capacity of drilled shaft foundations under the three modes of loading (axial, lateral, and torsional) is addressed in Section 3. Each mode is considered separately.

In Sections 4, 5, and 6, analytical techniques are presented for the prediction of the deformations of shaft foundations under axial, lateral, and torsional loading. The behavior under each mode of loading is considered separately, and no coupling between modes is assumed. These sections contain only the details of the analyses.

The application of the analytical techniques to reported full-scale load tests is considered in Section 7, while an example of the use of these techniques in design is presented in Section 8. Concluding remarks are contained in Section 9.

REFERENCES

1. Peck, R. B., Hanson, W. E., and Thornburn, T. H., Foundation Engineering, 2nd Ed., John Wiley and Sons, New York, 1974, 514 p.

Section 2

GEOLOGICAL AND GEOMECHANICAL MODELING

Rational design procedures for rock-socketed shafts employ analytical techniques that are based on a conceptual model of the foundation-rock mass system. The development of this model normally involves data gathering, from which idealizations can be made about the nature, extent, and mechanical behavior of the rock mass. The end result of this modeling process is a mathematical formulation which is used to analyze the response of the foundation to applied load. In achieving this end, a number of basic problems must be addressed. First, a geological model of the rock mass must be developed to characterize the nature and extent of the rock mass. Second, the mechanical behavior of the natural material must be idealized in the form of a geomechanical model. Both stages in the modeling process involve simplifications to keep the mathematical analysis tractable. Common techniques for data gathering and some of the more usual simplifications are discussed below.

GEOLOGICAL CHARACTERIZATION

The first step in the design process is geological characterization of the rock mass. Rock masses are inhomogeneous, discontinuous media composed of the rock material and naturally occurring discontinuities such as joints, seams, faults, and bedding planes. The rock materials may have engineering properties that are anisotropic, nonlinear, and stress-dependent. The discontinuities may range from soft and weathered, to hard and unweathered, and their spacings and attitudes (strike and dip) may vary considerably. The resulting rock mass exhibits the characteristics of both the material and the discontinuities which, together, tend to make the rock mass highly directional in its deformability and strength properties.

Site Exploration

The goal of site exploration is to characterize the rock mass, with particular emphasis on establishing the type of rock material present, the size, frequency, and spatial distribution of the discontinuities, the water table, and perhaps in-situ measurements of engineering properties. For large or special structures,

such as tall buildings, major bridges, high dams, power plants, etc., extensive and specialized exploration programs are normally carried out. Commonly these consist of vertical and inclined borings, detailed geologic mapping, down-hole and cross-hole measurements, etc. Extensive laboratory testing is done on the rock, and in-situ testing may be done to measure the strength and deformation properties of the rock mass. Furthermore, load tests are warranted for these kinds of structures. With the data obtained, the rock mass and its properties can be characterized well.

For more conventional structures, and particularly for transmission line structures, the exploration and testing will be more limited, typically consisting of vertical borings, limited mapping, some simple laboratory core testing, and perhaps a few down-hole measurements. With these more limited data, the characterization is less complete, and increased reliance is placed on prior information and correlations in the literature. Judgment and experience enter more prominently into the design process in this case.

Regardless of the level of detail, the exploration program should provide sufficient information to: (1) allow the development of a geological model of the site being investigated, and (2) establish the engineering properties necessary. These are the necessary input data for the analysis and design.

Special Geological Problems

During the characterization process, special geological features should be identified because they have the potential to influence the design strongly. Many of these have been discussed in detail (1, 2). The following is a brief discussion of the key concerns related to weathering, chemical effects, solution phenomena, creep, subsidence, and collapse structures.

Weathering is a process of rock alteration which increases in significance as the climate becomes warmer and more humid. There can be a deep profile of complexly weathered rock between the overlying residual soil and the underlying unweathered rock. In extreme cases, this weathered zone may be deeper than 50 meters (150 ft). In this weathered zone, a gradual grading occurs from soil with rock pieces, to rock blocks in a soil matrix, to rock with weathered discontinuity zones. This variability with depth has to be identified carefully during exploration because it may control the design process (i.e., is it soil-like or rock-like?) and influence the field construction operations.

In some rock types, chemical effects can result in serious heaving problems. Among the potentially troublesome rocks are those which contain reactive minerals such as pyrite, pyrrhotite, marcasite, and anhydrite. For example, in the "alum shales", which are pyrite-bearing, black, carbonaceous shales of Paleozoic age, significant swelling problems have occurred because of the growth of crystals of gypsum or jarosite resulting from the oxidization of pyrite and the reaction of the breakdown products with calcium carbonate. Sulfuric acid, also produced in the reaction, has been known to attack foundation concrete vigorously. Placement of a moisture barrier between the rock and foundation can minimize this problem substantially.

Solution problems often present themselves in more soluble rock types, such as limestone, gypsum, and salt. Exploration, design, and construction problems can arise because of irregular bedrock surfaces, open vertical joints, clay seams, cavities, and sinkholes.

Creep is a common problem when dealing with some of the softer rock types, such as salt, gypsum, and, to a lesser degree, compaction shales. Creep is analogous to secondary compression in soil and can be analyzed in a similar manner, using laboratory creep test data. If the overburden stress on these rocks is reduced significantly, time-dependent heave may result. This phenomenon also may be addressed using laboratory heave test data.

Subsidence is a problem in many mining regions of the world. For modern room and pillar or longwall mines, the designs are based on assessment of the surface subsidence from the mining operation. The surface subsidence trough can be determined and a foundation-structure system can be developed to accommodate the subsidence pattern. However, over older abandoned mines, caution must be exercised because of the potential for mine degradation, pillar collapse, etc. which may result in residual subsidence or surface collapse. Extraordinary foundation schemes may be necessary to minimize these potential problems.

A final geological problem to consider is the possibility of pore collapse under structural loads. This is possible in the young, soft, carbonate rocks, and in volcanic cinders and friable tuff. With their weakly cemented porous structure, an imposed stress exceeding the threshold stress can break down the cement or crush the interpore webs, causing a sudden collapse. These types of rocks must be pre-collapsed, or the foundation stresses must be maintained well below the threshold stress.

GEOMECHANICAL MODELS

Analytical predictions in geotechnical engineering require the adoption of a model of the behavior of the real material. For example, to predict the short term bearing capacity of a foundation on a layer of clay soil, it is customary to assume that the clay behaves in an undrained manner and that the real material can be idealized as being purely cohesive. Predictions of the bearing capacity then are based on the theory for a rigid punch indenting an ideal rigid-perfectly plastic half-space. In the application of this theory, the designer must choose an appropriate value for the undrained shear strength of the clay, and the accuracy of the prediction will depend on the accuracy of the strength value and the model for the clay behavior.

The same general principles apply to the prediction of the mechanical behavior of a rock mass, because the success of the analytical prediction depends on the appropriate choice of an ideal material to model the rock behavior, as well as the selection of the basic input parameters for that model. Invariably, the choice of the ideal material will depend on the type of prediction to be made and on how much information is available. It would be pointless to adopt a highly sophisticated model for the rock mass if the necessary geological information and test data were not available to support its use.

For predicting the ultimate load capacity of a foundation in rock, a strength model of the rock mass is required. Alternatively, if predictions of the foundation movements caused by the applied loading are required, then a constitutive (or deformation) model must be selected. Usually, the ultimate load capacity and the deformations are considered as separate problems, requiring the adoption of a different material model for each. Constitutive models which combine the strength and deformation issues have been developed, allowing the prediction of the complete load-deformation behavior of the foundation from initial loading to failure. At present, these find major use in the research environment and rarely find application in design practice, although this is likely to change with forthcoming increases in computing power and usage.

In this report, the two issues of ultimate load capacity and deformations under working loads will be treated separately. This approach is consistent with current design practice and results in greatly simplified design methods.

Rock Strength

The general problem of evaluating the strength of rock materials and rock masses is beyond the scope of this report, but useful treatments of this problem are given elsewhere (e.g., 3, 4, 5). The problem considered herein is the ultimate load capacity of drilled shafts subjected to either axial, lateral, or torsional loading, and different types of strength parameters will be applicable in each case. It is assumed that the concrete shaft is able to resist the applied loading adequately, so that the ultimate strength of the foundation will depend on the strength of the rock mass or the concrete-rock interface and not upon the structural strength of the concrete section.

For axial loading, the resistance will be provided by a combination of shear stresses developed along the cylindrical interface between the concrete and rock and the normal stress developed at the tip of the shaft. For lateral loading, the ultimate capacity of the shaft will be a function largely of the maximum compressive stress that can develop normal to the shaft along its leading face (with respect to the loading) and, to a lesser extent, the tensile and shear capacities of the back and sides of the shaft-rock mass interface. Under torsional loading, the capacity will be primarily a function of the circumferential shear stress that may be developed either at or near the interface between the rock and concrete. Some resistance also may be provided by torsional shear stresses developed at the tip of the shaft.

The limiting values of each of the stresses described above may themselves be dependent on more fundamental strength parameters of the rock mass. Further details are given in Section 3 where predictions of the ultimate shaft capacity are given in detail.

Rock Mass Displacements

As with foundations in soil, the displacements of foundations in rock normally control the design. With rock masses, however, a model must be established to address their discontinuous nature, taking into account the properties of the rock material and the discontinuities. When dealing with the displacements of foundations in rock, it is usual to idealize the discontinuous rock mass as an elastic continuum.

A geomechanical model has been suggested to establish equivalent rock mass properties from the individual elastic properties of the rock material and the

discontinuities (6). In general, the model considers the case of three orthogonal discontinuity sets, as shown in Figure 2-1. The rock material is defined by the Young's modulus and Poisson's ratio, E_r and ν_r, and subsequently the shear modulus, G_r, while the discontinuities are described by a normal stiffness, K_n, shear stiffness, K_s, and mean discontinuity spacing, S. Anisotropic rock material properties also could be used, as long as the attitude of the property principal planes was coincident with the attitude of the discontinuity planes. For this model, the properties of the equivalent orthotropic elastic mass are given as (7):

$$E_i = \left(\frac{1}{E_r} + \frac{1}{S_i\ K_{ni}}\right)^{-1} \tag{2-1}$$

$$G_{ij} = \left(\frac{1}{G_r} + \frac{1}{S_i\ K_{si}} + \frac{1}{S_j\ K_{sj}}\right)^{-1} \tag{2-2}$$

$$\nu_{ij} = \nu_{ik} = \nu_r\ \frac{E_i}{E_r} \tag{2-3}$$

for i = x, y, z with j = y, z, x and k = z, x, y. These equations describe the rock mass elastic properties completely.

For engineering convenience, it is useful to define a modulus reduction factor, α_E, which represents the ratio of the rock mass to rock material modulus. This factor can be obtained by re-writing Equation 2-1 as:

$$\alpha_E = \frac{E_i}{E_r} = \left(1 + \frac{E_r}{S_i\ K_{ni}}\right)^{-1} \tag{2-4}$$

This relationship is plotted in Figure 2-2. This figure shows smaller values of α_E in rock masses with softer discontinuities (larger E_r/K_n values).

Unfortunately, the mean discontinuity spacing is not easy to obtain directly and, in normal practice, RQD values are determined instead. Using a physical model, the RQD can be correlated (6) with the number of discontinuities per 1.5 meter (5 ft) core run, a common measure in practice. This relationship is shown in Figure 2-3. Other models presented in the literature, using statistical or random number premises, generally have confirmed this approach. Combining Figures 2-2 and 2-3 yields Figure 2-4, which relates α_E to RQD as a function of E_r/K_n.

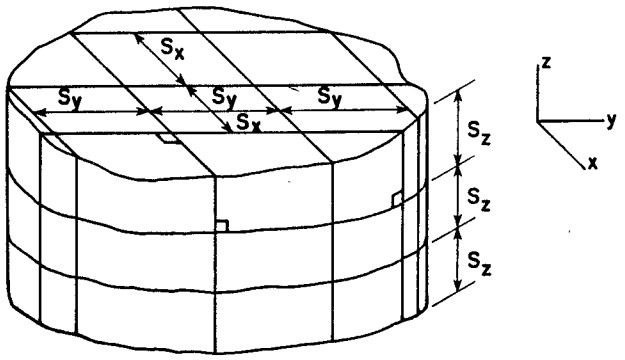

Figure 2-1. Rock Mass Model

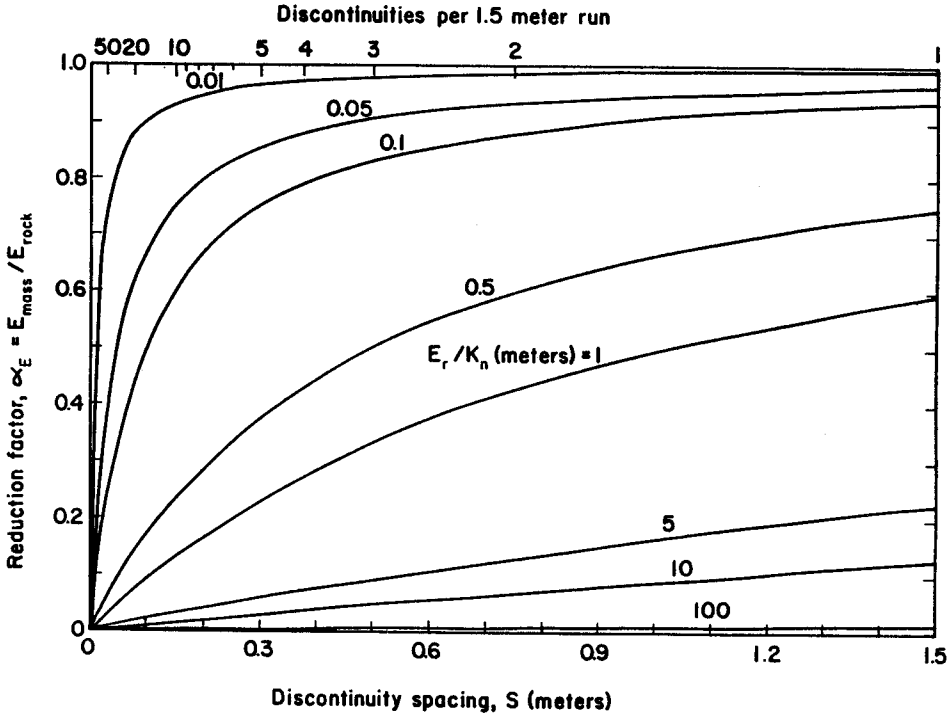

Figure 2-2. Modulus Reduction Factor vs. Discontinuity Spacing

Source: Kulhawy (6), p. 216.

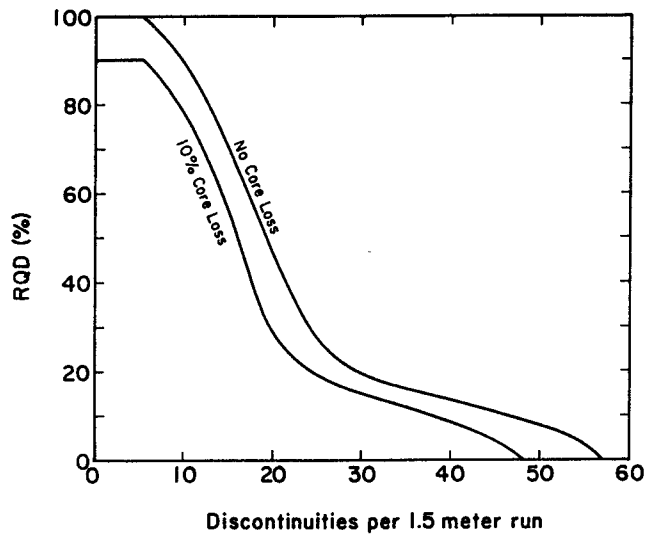

Figure 2-3. RQD vs. Number of Discontinuities

Source: Kulhawy (6), p. 217.

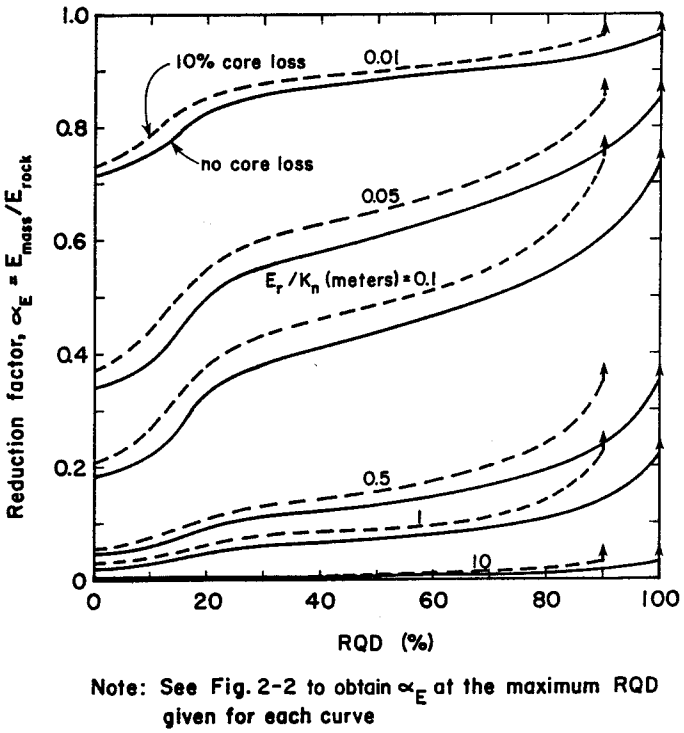

Figure 2-4. Modulus Reduction Factor vs. RQD

Source: Kulhawy (6), p. 218.

This model is most effective when good quality geological data are available to define the discontinuity sets adequately. When the data are not sufficient to define the x and y discontinuities adequately, the model must be simplified to deal with the z values only. In the majority of rock masses, S_z is normally less than S_x and S_y and tends to control settlement under compression loading. The assumption of an isotropic mass based on S_z and K_{nz} normally gives a conservative upper bound on the settlement.

Good physical property data also are needed. These should be obtained for the anticipated effective stress range to be applied in the field, in tests which impose strains compatible with those expected. If full-scale load tests or field deformation tests are conducted, α_E can be determined easily by dividing the field test E by the value of E from laboratory tests on intact core. When the field and laboratory testing is more limited, the values given in Table 2-1 can provide some general guidelines. The complete details of these data are given in (8). As a first approximation, the designer can select a mean value of $E_r/K_n = 1$ m, which yields $\alpha_E \approx 0.1$ for an RQD less than about 70 percent, and progressively higher α_E values varying linearly up to 0.6 at an RQD of 100 percent.

Table 2-1

TYPICAL RANGES IN ROCK PROPERTIES

Property	Units	Number of Values	Maximum	Minimum	Mean
Elastic Modulus, E_r	GN/m^2 kip/in^2	261	111.6 16,180	0.006 0.87	34.60 5,020
Poisson's Ratio, ν_r	-	138	0.46	0.02	0.20
Normal Stiffness, K_n	GN/m^3 kip/in^3	12	67.59 249	0.24 0.88	13.00 47.9
Shear Stiffness, K_s	GN/m^3 kip/in^3	167	31.60 116	0.01 0.037	2.82 10.4
K_n/K_s for same rock	-	12	83.0	0.84	17.8
E_r/K_n for same rock	m ft	9	4.23 13.9	0.21 0.69	1.22 4.00

Source: Kulhawy (6), pp. 218-223.

SUMMARY

To apply analytical techniques to the design of foundations in rock, a geological model of the site and a geomechanical model of the rock mass must be developed. The general principles involved have been outlined in this section. Some special geological problems that may be encountered at the site also have been discussed. A geomechanical model was described that may be used in the prediction of the displacement of foundations in rock. Idealizations of the rock mass behavior have been discussed briefly, but a more detailed treatment of this issue will be given in Section 3.

REFERENCES

1. Peck, R. B., "Rock Foundations for Structures", Proceedings, Rock Engineering for Foundations and Slopes, Vol. 2, ASCE, New York, 1976, pp. 1-21.

2. Kulhawy, F. H. and Goodman, R. E., "Foundations in Rock", Chapter in Ground Engineers Reference Book, Ed. F. G. Bell, Butterworths, London, in press.

3. Goodman, R. E., Introduction to Rock Mechanics, John Wiley and Sons, New York, 1980, 478 p.

4. Hoek, E. and Brown, E. T., Underground Excavations in Rock, Institution of Mining and Metallurgy, London, 1980, 527 p.

5. Brady, B. H. G. and Brown, E. T., Rock Mechanics for Underground Mining, George Allen and Unwin, London, 1985, 527 p.

6. Kulhawy, F. H., "Geomechanical Model for Rock Foundation Settlement", Journal of the Geotechnical Engineering Division, ASCE, Vol. 104, No. GT2, Feb. 1978, pp. 211-227.

7. Duncan, J. M. and Goodman, R. E., "Finite Element Analyses of Slopes in Jointed Rock", Contract Report S-68-3, U.S. Army Engineer Waterways Experiment Station, Vicksburg, 1968, 271 p.

8. Kulhawy, F. H., "Stress-Deformation Properties of Rock and Rock Discontinuities", Engineering Geology, Vol. 9, No. 4, Dec. 1975, pp. 327-350.

Section 3

ULTIMATE LOAD CAPACITY OF DRILLED SHAFTS IN ROCK

Normally the design of foundations socketed into rock will be governed by displacement considerations. Nevertheless, the ultimate capacity of the foundation must always be evaluated to determine the degree of safety of the proposed design. This evaluation requires consideration of two important issues. First, the foundation element itself must be able to resist the applied loading adequately. Second, the rock mass surrounding the shaft must be capable of providing resistance to the loading. In both cases, a reasonable margin of safety must be provided. The first case is a structural design problem which is not addressed herein, while the second is the subject of this section.

CAPACITY AS A FUNCTION OF ROCK PROPERTIES

Assuming that the concrete shaft has been designed correctly for structural considerations, its capacity will depend on the strength of the rock mass. Three separate modes of loading are considered herein: axial, lateral, and torsional. These three modes are treated separately, and no coupling of the modes is considered. The prediction of failure under simultaneously applied axial, lateral, and torsional loading is exceedingly difficult, and no satisfactory solutions of general applicability have been developed. Because of the uncertainty which exists about the significance of interaction between modes, it is recommended that conservative factors of safety be used in the design of shafts subjected to more than one mode of loading.

AXIAL COMPRESSION CAPACITY

Theoretically, compressive loads applied to the shaft butt are transmitted to the surrounding rock mass through both tip resistance and side resistance. The relative importance of these resistances in determining the capacity depends on the geometry of the shaft and the relative stiffness of the shaft concrete and the rock mass. There also may be some interdependence between the tip and side resistances, especially in jointed rock where both strength and stiffness will depend on the confining stress.

Tip Resistance

It has been demonstrated from elasticity solutions (e.g., 1, 2) that, at working loads, only a small proportion of the compressive load applied at the shaft butt is actually transmitted to the tip. In Section 4, it will be shown that, even for a relatively stiff, stubby shaft, the proportion of applied load transmitted to the tip is typically within the range of 10 to 20 percent of the butt load; for more slender shafts, the percentage is much less. Furthermore, the tip resistance component of the compression capacity will be mobilized only after significant displacements have occurred, at loads large enough to cause slip (relative movement between concrete and rock) along the full length of the shaft. Even then a clean, undisturbed surface is required to mobilize the full tip resistance. In practice, this condition may be difficult to achieve (3, 4) and, by the time the full capacity of the shaft has developed, the displacements may be excessive. For this reason, it has been suggested (e.g., 5) that the tip resistance should be ignored when determining the axial compression capacity. However, the designer may have to assume that full slip of the shaft will occur under working load conditions (e.g., when large loads are applied to relatively rigid, short stubby shafts), and in these cases some reliance has to be placed on the mobilized tip resistance. Under these circumstances, the accurate prediction of tip resistance is necessary.

The typical tip resistance or bearing capacity failure modes for rock masses are shown in Figure 3-1 (6). These depend on the discontinuity spacing or rock layering, as described below.

For a thick rigid layer overlying a weaker one, failure may be by flexure. The flexural strength is approximately twice the tensile strength of the rock material, and the tensile strength is of the order of 5 to 10 percent of the compressive strength. For a thin layer overlying a weaker one, failure can be by punching which, in effect, is manifested by a tensile failure in the rock material. It is important to realize that, in both of these cases, failure in the underlying layer could occur first by one of the other failure modes.

For loading applied to a rock mass with open joints, where the joint spacing is less than the foundation width (or diameter), failure is likely to occur by uniaxial compression of rock columns. If the rock mass is idealized as a cohesive-frictional material, the ultimate capacity is given by the Mohr-Coulomb failure criterion as:

$$q_{ult} = q_u = 2c \tan(45° + \phi/2) \qquad (3\text{-}1)$$

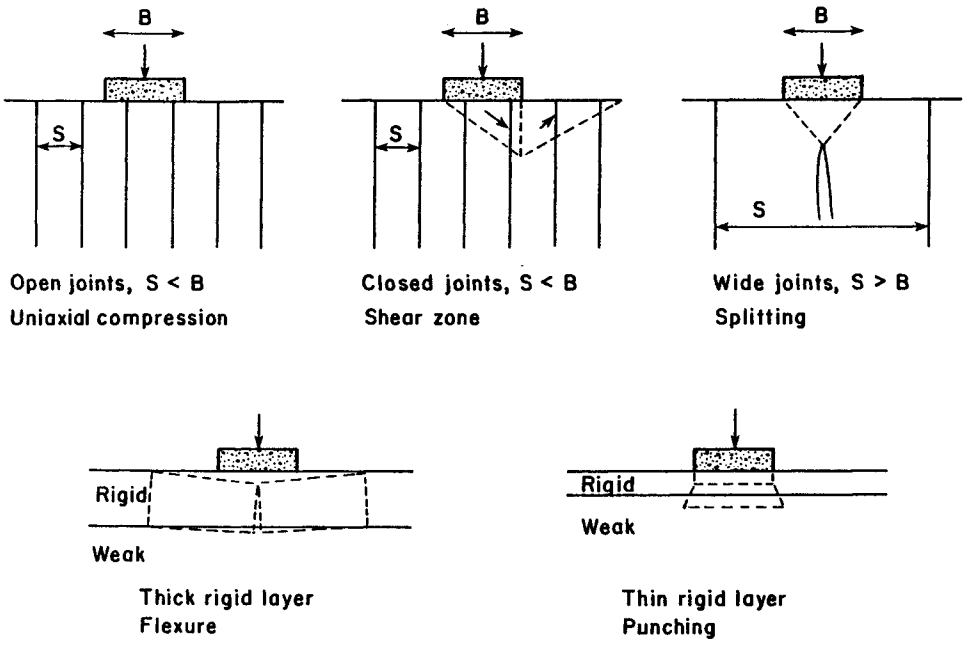

Figure 3-1. Bearing Capacity Failure Modes

Source: Sowers (6), p. 490.

in which q_{ult} = ultimate bearing capacity, q_u = uniaxial compressive strength, c = cohesion intercept, and ϕ = friction angle. The values of q_u, c, and ϕ are rock mass (rather than intact rock) properties.

If the rock mass contains closely spaced, closed joints, a general wedge type of failure mode may develop, as shown in Figure 3-1. The ultimate bearing capacity in this case is given by the Bell solution (7) for plane strain conditions:

$$q_{ult} = cN_c + \frac{B}{2} \gamma N_\gamma + \gamma D N_q \qquad (3\text{-}2)$$

in which B = foundation width, D = foundation depth, γ = effective unit weight of the rock mass, and N_c, N_γ, and N_q are bearing capacity factors given in Figure 3-2. For a cylindrical shaft of diameter B and depth D, Equation 3-2 should be modified to allow for the circular foundation shape:

$$q_{ult} = \zeta_{cs} cN_c + \zeta_{\gamma s} B\gamma N_\gamma/2 + \zeta_{qs} \gamma D N_q \qquad (3\text{-}3)$$

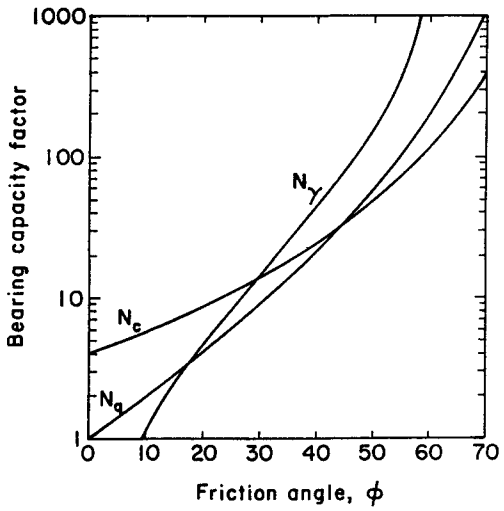

Figure 3-2. Wedge Bearing Capacity Factors

in which $\zeta_{cs} = 1 + N_q/N_c$, $\zeta_{\gamma s} = 0.6$, and $\zeta_{qs} = 1 + \tan\phi$. For foundations at the rock surface, D = 0. Also, the second term is normally small compared to the other terms and is often neglected.

For cases in which the joints are spaced more widely than the foundation width, failure occurs by splitting beneath the foundation, which eventually leads to general shear failure. This problem has been evaluated, assuming no stress is transmitted across the vertical discontinuity (8), to give:

$$q_{ult} \approx JcN_{cr} \qquad (3\text{-}4)$$

in which N_{cr} = bearing capacity factor in Figure 3-3, and J = correction factor given in Figure 3-4.

In the evaluation of the tip resistance outlined above, it is important to note that the strength parameters of the rock mass, and not of the intact rock, must be used. Values of c and ϕ obtained for the intact rock material are considerably higher than those for the rock mass, and their use will result in an overestimate of the actual bearing capacity.

If the actual rock mass properties are not evaluated, it has been suggested (8) that the values of c or q_u for the intact rock be reduced by the parameter α_E, as described previously for the rock mass modulus in Section 2. Values of ϕ

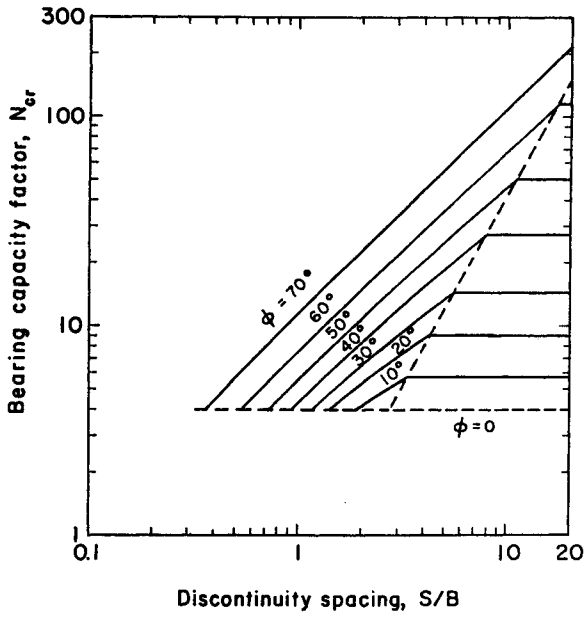

Figure 3-3. Bearing Capacity Factor for Open Joints

Source: Kulhawy and Goodman (8), p. 215.

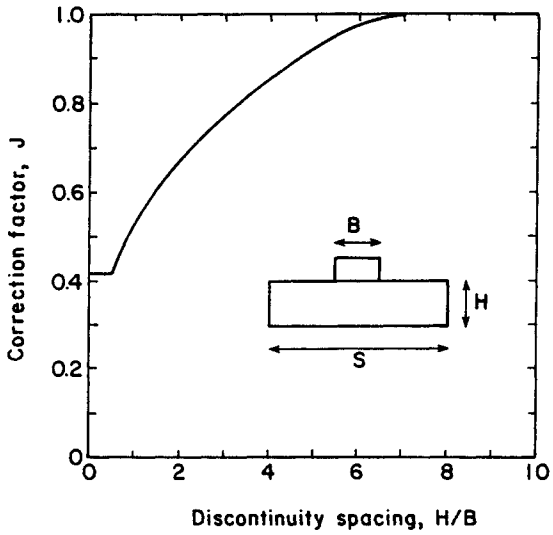

Figure 3-4. Correction Factor for Discontinuity Spacing

Source: Bishnoi (9), p. 77.

for the rock mass are typically 50 to 75 percent of the ϕ values for the intact rock material.

Alternatively, a strength criterion for jointed rock masses (10) may be used to determine the bearing capacity. This curved strength envelope can be expressed as:

$$\sigma_1 = \sigma_3 + (mq_u\sigma_3 + sq_u^2)^{1/2} \qquad (3\text{-}5)$$

in which σ_1 = major principal effective stress, σ_3 = minor principal effective stress, q_u = uniaxial compressive strength of the intact rock, and s and m = empirically determined strength parameters for the rock mass, which are somewhat analogous to c and ϕ of the Mohr-Coulomb failure criterion.

An analysis of the bearing capacity of a rock mass obeying this criterion can be made using the same approximate technique as used in the Bell solution. The details of this approach are described in Figure 3-5. A lower bound to the failure load is calculated by finding a stress field which satisfies both equilibrium and

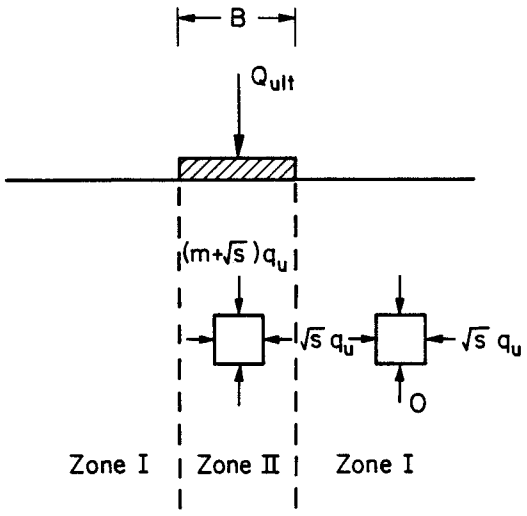

Rock Mass Failure Criterion: $\sigma_1 = \sigma_3 + \sqrt{(mq_u\,\sigma_3 + sq_u^2)}$

Figure 3-5. Lower Bound Solution for Bearing Capacity

the failure criterion. The rock mass beneath a strip footing may be divided into two zones, with homogeneous stress conditions at failure throughout each, as shown in Figure 3-5. The vertical stress in zone I is assumed to be zero, while the horizontal stress is equal to the uniaxial compressive strength of the rock mass, given by Equation 3-5 as $s^{1/2}q_u$. For equilibrium, continuity of the horizontal stress across the interface must be maintained, and therefore the bearing capacity of the strip footing may be evaluated from Equation 3-5 (with $\sigma_3 = s^{1/2}q_u$) as:

$$q_{ult} = (m + \sqrt{s})q_u \tag{3-6}$$

For a circular foundation, a similar approach may be used, with the interface between the two zones being a cylindrical surface of the same diameter as the foundation. In this axisymmetric case, the radial stress transmitted across the cylindrical surface, at the point of collapse of the foundation, may be greater than $s^{1/2}q_u$, without necessarily violating either radial equilibrium or the failure criterion. However, because of the uncertainty of this value, the radial stress at the interface also is assumed to be $s^{1/2}q_u$ for the case of a circular foundation. Therefore, the predicted (lower bound) bearing capacity is given by Equation 3-6.

Guidelines for selecting s and m for jointed rock masses are given in Table 3-1. The categories in this table are determined by the rock type and the conditions of

Table 3-1

APPROXIMATE CORRELATION BETWEEN ROCK MASS QUALITY AND STRENGTH CONSTANTS

Rock Mass Quality	Approximate Joint Spacing	CSIR Rating	NGI Rating	S Value	m Value as Function of Rock Type				
					A	B	C	D	E
Excellent	> 3 m (10 ft) intact	100	500	1	7	10	15	17	25
Very good	1-3 m interlocking	85	100	0.1	3.5	5	7.5	8.5	12.5
Good	1-3 m slightly weathered	65	10	0.004	0.7	1	1.5	1.7	2.5
Fair	0.3-1 m moderately weathered	44	1	10^{-4}	0.14	0.2	0.3	0.34	0.5
Poor	30-500 mm weathered with gouge	23	0.1	10^{-5}	0.04	0.05	0.08	0.09	0.13
Very poor	< 50 mm (2 in) heavily weathered	3	0.01	0	0.007	0.01	0.015	0.017	0.025

Rock Types:
A - Carbonate rocks with well-developed crystal cleavage (dolostone, limestone, marble)
B - Lithified argillaceous rocks (mudstone, siltstone, shale, slate)
C - Arenaceous rocks with strong crystals and poor cleavage (sandstone, quartzite)
D - Fine-grained igneous crystalline rocks (andesite, dolerite, diabase, rhyolite)
E - Coarse-grained igneous and metamorphic crystalline rocks (amphibolite, gabbro, gneiss, granite, norite, quartzdiorite)

Source: Hoek (11), p. 215.

the rock mass, and selecting an appropriate category is easier if either the CSIR (12) or NGI (13) classification data are available. The values in this table should only be used as general guidelines, and they do not replace the need for testing or other means of assessing the strength parameters more reliably.

In another study of the bearing capacity of jointed rock, a plasticity solution was obtained which incorporates the discontinuities in the rock mass (14).

Although this solution was for a strip foundation, it demonstrates the important effect of jointing. The strength of the intact material was determined by the Mohr-Coulomb criterion, with strength parameters c_r and ϕ_r. Shear failure along the joints also was determined by the Mohr-Coulomb criterion with parameters c_j and ϕ_j. The joints were assumed to be closely spaced (relative to the foundation width, B) and parallel, being inclined at an angle ω to the vertical. The results of this analysis for a range of c_j/c_r and ω, with $\phi_r = \phi_j = 35°$, are given in Figure 3-6. The horizontal line for $c_j/c_r = 1$ at the top of the figure gives the bearing capacity without any weakening from discontinuities. For comparison, the uniaxial compressive strength is also shown at the bottom of the figure. It can be seen that, for low and high values of ω, the discontinuities do not cause a very large loss of bearing capacity but, between these limits, the reduction can be large. The vertical drop for $\omega = 35°$ when $c_j/c_r = 0$ occurs because no load can be applied to a purely frictional interface if the angle of obliquity is greater than the friction angle. The other kinks in the curves arise from changes in the mode or sequence of plastic regions in the solutions.

The results of Figure 3-6 apply equally well to negative values of ω. The effect of more than one set of discontinuities has not been studied, but there are no theoretical difficulties to such an extension. In general, each additional set will cause further lowering of the bearing capacity, although not necessarily to a great extent. For example, the solution for the two sets $\omega = 0°$ and $90°$, with $c_j/c_r = 0$, is indicated in Figure 3-6, and gives a value only slightly below that for the single set $\omega = 90°$.

The results in Figure 3-6 are for zero surcharge but, by the following transformation, the effect of surcharge can be included. Consider the case with $\phi_r = \phi_j = \phi = 35°$, discontinuity cohesion = c_j, rock material cohesion = c_r, and surcharge = q. For this case, the bearing capacity will be:

$$q_{ult} = N_{cs}(c_r + q \tan\phi) + q \qquad (3\text{-}7)$$

in which N_{cs} = bearing capacity factor from Figure 3-6 using c_j/c_r modified for the surcharge as follows:

$$(c_j/c_r)_q = (c_j + q \tan\phi)/(c_r + q \tan\phi) \qquad (3\text{-}8)$$

As mentioned previously, Figure 3-6 applies only for plane strain, but the trends in behavior and the general conclusions implied should also be true for the case of

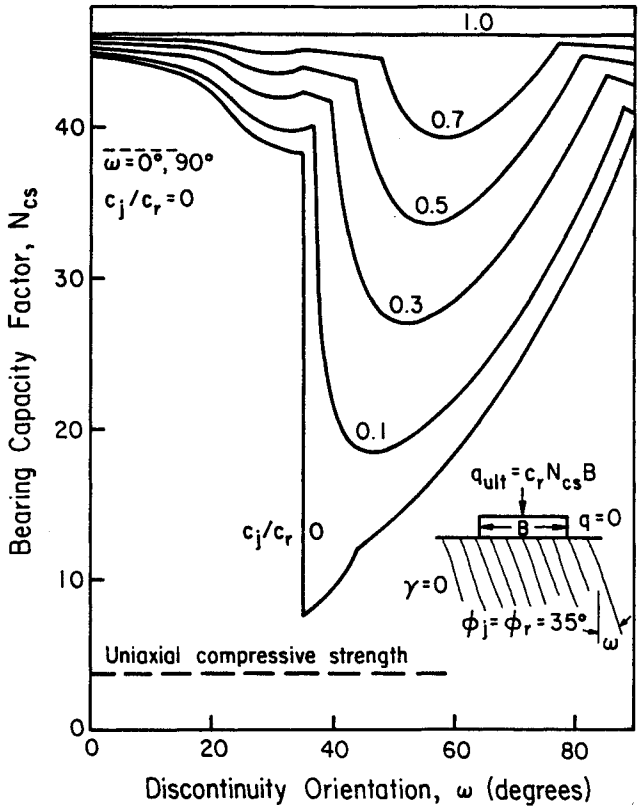

Figure 3-6. Effect of Discontinuity Orientation on Bearing Capacity of Strip Footing

Source: Davis (14), p. 89.

loading applied over a circular area.

Side Resistance

The mechanism of side resistance development in rock sockets is complex and includes both adhesion and friction effects, as well as dilatancy that may accompany shearing of a roughened interface. Very high normal stresses may develop between the shaft and surrounding rock mass, chiefly as a result of dilation at the interface (3, 15), but also may develop from the effect of Poisson's ratio and the compressive axial stresses in the shaft. In a rock mass that is capable of sustaining these high radial stresses, large shear stresses will develop along the cylindrical interface of the shaft.

To predict the side resistance of a rock socket, a constitutive model for interface

sliding is required which incorporates the coupling of the shear and normal modes of displacement (e.g., 16, 17). With such a model, the development of side resistance from initial loading until full slip of the shaft can be examined. However, these models require, as input data, accurate numerical values for parameters such as the shear and normal stiffness, cohesion intercept and friction angle, and some measure of the dilatancy and perhaps strain softening. Most of these parameters are not measured routinely either in laboratory or field tests. While the constitutive models may give good insight into the basic mechanism of shear failure, including the progressive development of slip along the shaft, they are not incorporated easily into engineering practice.

The results of most field tests on shafts and direct shear tests in the laboratory are usually summarized in the form of a unit side shear stress. For a load test on a shaft in the field, this stress is obtained by dividing the total force carried in shear along the shaft by the side area of the shaft. Values at peak and residual shear load are quoted commonly but, because of the definition used, they are average values which do not account for the distribution of shear stress along the shaft. For short, rigid shafts, this averaging process will not be important because the stress state will be relatively uniform throughout the loading. The unit side shear resistance corresponding to the peak shaft load is sometimes called, inappropriately, the bond strength of the interface.

Values of the unit side shear resistance have been measured in field and laboratory tests and have been summarized in (5, 15, 18). To date, the most comprehensive summary of the available data is given in (19), including critical evaluation of the available test data on the basis of test method, socket roughness, and reliability and type of data recorded. The suggested correlation (19) between expected unit side shear resistance, $\bar{\tau}_{max}$, and uniaxial compressive strength, q_u, for most sockets is presented as:

$$\frac{\bar{\tau}_{max}}{p_a} = 1.42 \left(\frac{q_u}{p_a}\right)^{1/2} \qquad (3\text{-}9)$$

in which p_a = atmospheric pressure. Particularly rough sockets, defined as those having grooves or undulations of depth greater than 10 mm (0.4 in) and width greater than 10 mm (0.4 in), at spacings between 50 mm (2 in) and 200 mm (8 in), were found to be stronger, and the correlation with uniaxial compressive strength was suggested as:

$$\frac{\bar{\tau}_{max}}{p_a} = 1.9 \left(\frac{q_u}{p_a}\right)^{1/2} \tag{3-10}$$

The data from which Equation 3-9 was deduced have been plotted in Figure 3-7. It can be seen that Equation 3-9 is a reasonable fit to the data; however, it does not represent a lower bound to all data points. A lower bound to most of the observed data was suggested earlier (20) and is given by:

$$\left(\frac{\bar{\tau}_{max}}{p_a}\right) = b \left(\frac{q_u}{p_a}\right)^{1/2} \tag{3-11}$$

in which b = 0.63 to 0.95. A curve with b = 0.63 also is plotted on Figure 3-7. For design purposes, a conservative estimate of the peak side resistance could be evaluated in most cases using Equation 3-11 with b = 0.63. A conservative approach also is warranted for smooth wall sockets constructed under slurry. However, values of the average stress, $\bar{\tau}_{max}$, in excess of 0.15 q_u should only be used when they are demonstrated to be reasonable by a load test, local experience, or adequate in-situ testing. After selecting a suitable value for $\bar{\tau}_{max}$, the peak side resistance then is:

$$P_{sf} = \bar{\tau}_{max} A_s \tag{3-12}$$

in which A_s = area of the socket sidewall.

Relationships as shown in Equations 3-9 to 3-11 are appealing to the designer, because of their succinct form and dependence on a single, easily measured index property (q_u). However, they can be misleading because: (1) they try to correlate a simple rock property (q_u) with the mechanical performance of a complicated shaft-rock system, and (2) they are probably only applicable to relatively uniform sound rock. In an attempt to extend the correlation to weathered and poor quality (highly jointed) rock masses (15), an additional empirical factor has been introduced which is based on the parameter α_E, the ratio between the rock mass modulus and the modulus of the intact rock material.

In some cases encountered in practice, the concrete may have a lower compressive strength (f'_c) than the intact rock (q_u). For these cases, the average bond strength is governed by the concrete, being approximately equal to 0.05 f'_c.

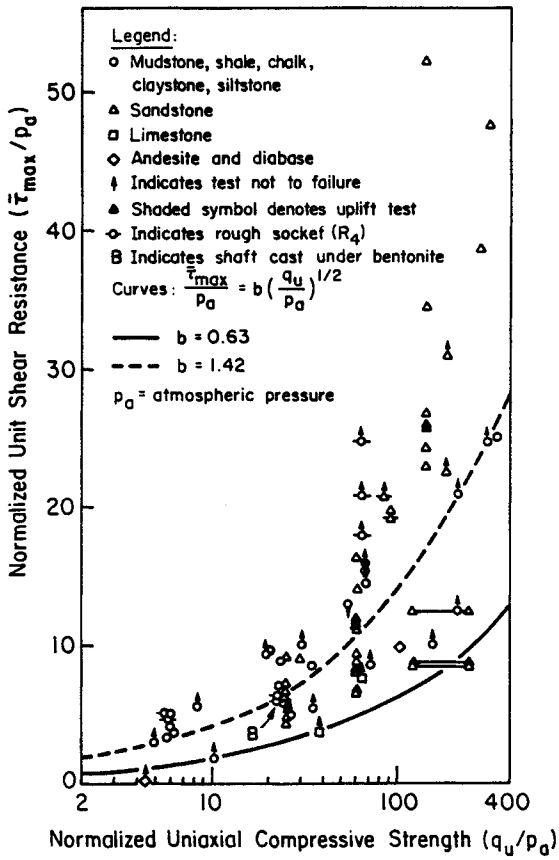

Figure 3-7. Correlations Between Bond Strength and Uniaxial Compressive Strength

Source: Rowe and Armitage (19), p. 121.

AXIAL UPLIFT CAPACITY

Socketed foundations often are used to resist uplift loads, and the uplift capacity is developed from both side and tip resistance. Tip resistance requires the development of a concrete-to-rock tensile bond at the shaft tip. For the ideal case, this tip resistance would equal the tensile strength of the weaker of the rock or concrete, multiplied by the tip area. However, considering the typical construction problems associated with cleaning out the bottom of a socket hole, it is prudent to disregard the tensile resistance developed at the tip.

The side resistance develops from socket shear stresses, as described previously. With compression sockets, there is a positive Poisson's ratio effect, resulting in lateral expansion of the shaft. In tension sockets, the Poisson's ratio effect is

negative, resulting in lateral contraction of the shaft. In the following sections, it will be shown that the effect of Poisson's ratio of the shaft material is important only in shafts which are relatively flexible, and it is unimportant if the shaft is relatively rigid. In Section 4, it will be demonstrated that a shaft is effectively rigid whenever the ratio, $(E_c/E_r)(B/D)^2$, is greater than about 4. For these cases, the behavior in uplift will be the same as that in compression. For compressible or extensible shafts, it may be prudent to reduce the unit side shear resistance in uplift below that for compression. Based upon examination of elastic solutions, a reduction of up to 30 percent has been suggested (21).

LATERAL CAPACITY

The lateral capacity of shafts socketed into rock has received very little attention in the literature. Perhaps the reason for this is that the lateral design is governed largely by displacement considerations, and therefore the capacity has been assigned lesser importance. Regardless of the reason, reliable evaluation of the lateral capacity still is important, if only to determine the likely margin of safety existing at working load levels. The problem is very difficult to solve theoretically, which also may account for the lack of published work in this area.

An approximate theoretical approach for estimating the ultimate lateral capacity is presented here. It is assumed in the following that the shaft section has sufficient moment and shear capacity to resist the applied loading, and ultimate failure of the shaft occurs when the surrounding rock mass is not able to sustain any further lateral loading, similar to the so-called "short pile" failure mode (22). This assumption must always be checked; once the limiting state of stress acting on the shaft has been determined, then the calculated maximum bending moment and shear force in the shaft should be compared to the capabilities of the reinforced concrete section. If either of these calculated values exceeds the section properties, then failure will be governed by the strength of the shaft itself.

To determine the ultimate lateral loads acting on a "short" shaft, the distribution of the limiting reaction (force per unit length acting on the shaft) is required. This may be evaluated as follows.

When a lateral load is applied at the rock mass surface, the rock mass immediately in front of the shaft will have nearly zero vertical stress, while horizontal stress is applied by the leading face of the shaft. Ultimately, the horizontal

stress may reach the uniaxial compressive strength of the rock mass and, with further increases in the lateral load, the horizontal stress may decrease as the rock mass softens during post-peak deformation. Large lateral deformations may be required for the rock mass at depth to exert a maximum reaction stress on the leading face of the shaft. Therefore, it is reasonable to assume that the reaction stress at the rock mass surface, in the limiting case of loading of the shaft, is zero or very nearly zero as a result of the post-peak softening. Along the sides of the shaft, some shearing resistance may be mobilized, and this is likely to be on the order of the unit side resistance under axial compression, $\bar{\tau}_{max}$.

At greater depth, it is reasonable to assume that the stress in front of the shaft may increase from the initial in-situ horizontal stress level, σ_{hi}, up to the limit stress, p_L, reached during the expansion of a long cylindrical cavity, i.e., the plane strain condition will apply. Behind the shaft, the horizontal stresses will decrease and, after tensile rupture of the bond between the concrete and the rock mass, the horizontal stress will reduce to zero. At the sides of the shaft, some shearing resistance also may be mobilized. Therefore, at depth, the ultimate force per unit length resisting the lateral loading is likely to be on the order of $B(p_L + \bar{\tau}_{max})$.

Closed form solutions have been presented for the limit stress developed during the expansion of a long cylindrical cavity in an elastoplastic, cohesive-frictional, dilatant material (23). This limit stress, p_L, may be determined from the following parametric equations in the nondimensional quantity ρ:

$$\frac{2G_r}{\sigma_{hi} + c_r \cot\phi_r} = \left(\frac{N - 1}{N + 1}\right) (T\rho^n - Z\rho) \tag{3-13}$$

and

$$\rho = (p_L + c_r \cot\phi_r) / (\sigma_R + c_r \cot\phi_r) \tag{3-14}$$

in which

$$T = 2\left(1 + \frac{\chi}{\alpha + \beta}\right) \tag{3-15}$$

$$Z = 2\left(\frac{\chi}{\alpha + \beta}\right) \tag{3-16}$$

$$\sigma_R = [(\frac{2N}{N + 1}) (\sigma_{hi} + c_r \cot\phi_r)] - c_r \cot\phi_r \quad (3\text{-}17)$$

$$\alpha = 1/M \quad (3\text{-}18)$$

$$\beta = 1/N \quad (3\text{-}19)$$

$$n = \frac{1 + \alpha}{1 - \beta} \quad (3\text{-}20)$$

$$M = \frac{1 + \sin\psi_r}{1 - \sin\psi_r} \quad (3\text{-}21)$$

$$N = \frac{1 + \sin\phi_r}{1 - \sin\phi_r} \quad (3\text{-}22)$$

$$\chi = \frac{(1 - \nu_r)(1 + MN) - \nu_r(M + N)}{MN} \quad (3\text{-}23)$$

and G_r = shear modulus, ν_r = Poisson's ratio, c_r = cohesion intercept, ϕ_r = friction angle, and ψ_r = dilation angle of the rock mass. The rock mass is assumed to obey the Mohr-Coulomb failure criterion and dilatancy accompanies yielding, according to the following flow rule (24):

$$\frac{\dot{\epsilon}_3^p}{\dot{\epsilon}_1^p} = -M \quad (3\text{-}24)$$

in which $\dot{\epsilon}_1^p$ and $\dot{\epsilon}_3^p$ = major and minor principal plastic strain increments, respectively.

In most practical cases, the in-situ horizontal stress, σ_{hi}, will be small compared to the cohesion, c_r, and therefore Equation 3-13 may be simplified slightly by substitution of $\sigma_{hi} = 0$. For convenience, solutions for the limit pressure p_L have been plotted in Figure 3-8 for selected values of ν_r, ϕ_r, and ψ_r. The central vertical axis on each plot indicates the ratio of the plastic radius at the limit condition, R, to the cavity radius, a. These charts may be used by entering with a value of $G/(\sigma_{hi} + c_r \cot\phi_r)$ and working clockwise around the figure, determining in turn values of R/a and $\rho = (p_L + c \cot\phi)/(\sigma_R + c \cot\phi)$, from which the limit pressure p_L can be calculated.

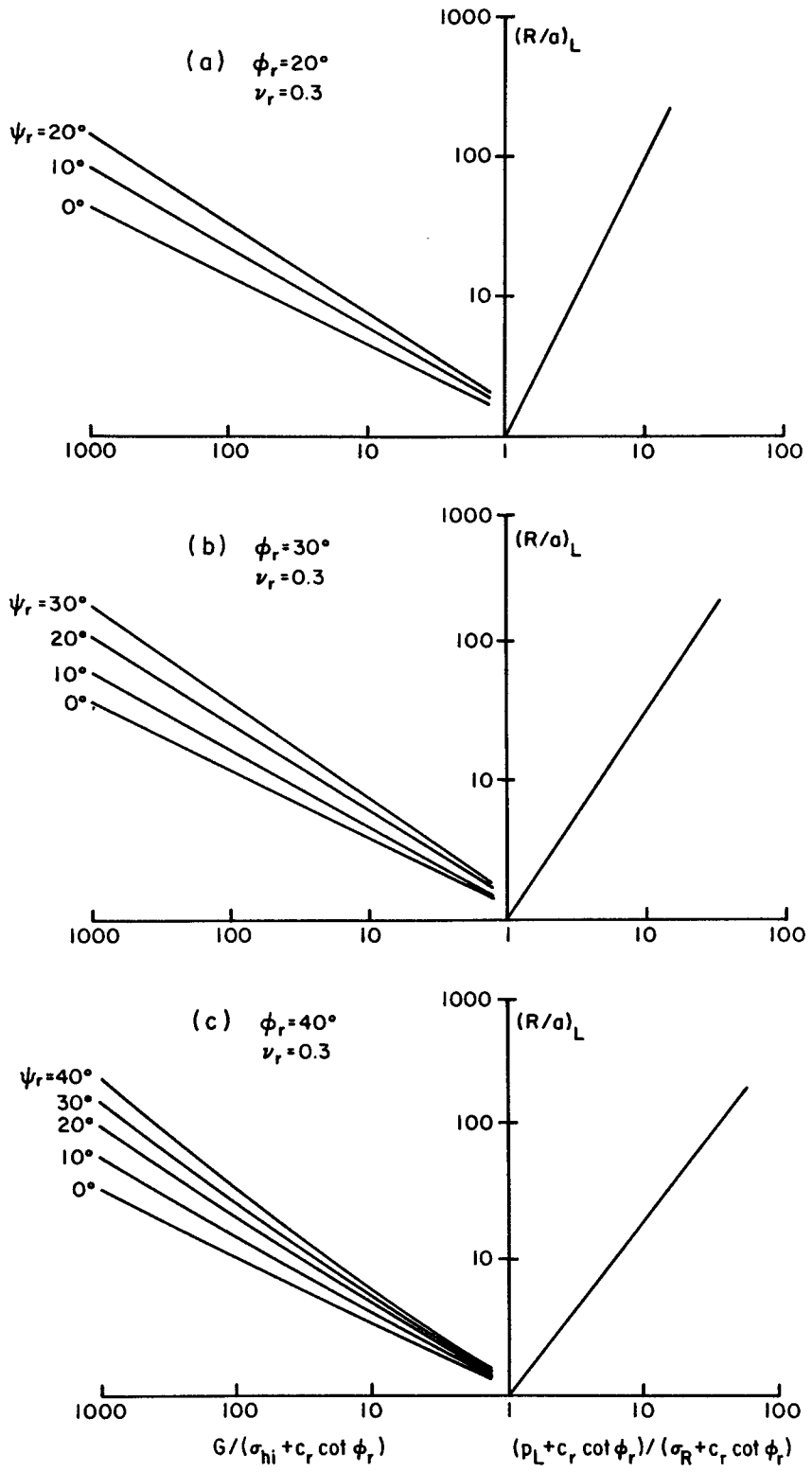

Figure 3-8. Limit Solution for Cylindrical Cavity

Source: Carter, Booker, and Yeung (23), p. 355.

One final problem remains, and that is determining the depth at which this limit stress is mobilized. In an earlier study (25), it was suggested that, in a purely cohesive material, this depth would be about three shaft diameters (3B). In the absence of any other data, this suggestion will be adopted. Therefore, the proposed distribution of ultimate force per unit length resisting the shaft is as shown in Figure 3-9.

The ultimate lateral force that may be applied for the conditions given above can be approximated by:

$$H_{ult} = (p_L D/6 + \bar{\tau}_{max}B)D \qquad \text{(for } D < 3B\text{)} \qquad (3\text{-}25a)$$

$$H_{ult} = (p_L/2 + \bar{\tau}_{max})3B^2 + (p_L + \bar{\tau}_{max})(D - 3B)B \qquad \text{(for } D > 3B\text{)} \qquad (3\text{-}25b)$$

The maximum bending moment in the shaft then is calculated from H_{ult} and the reaction distribution shown in Figure 3-9. If the lateral loading consists of a horizontal force, H, and an applied moment, M, then for purposes of calculating an appropriate bending moment distribution, these may be represented by an equivalent force of the same magnitude, but applied at a height, e = M/H, above the rock mass surface.

The theoretical approach suggested above (Equation 3-25) may be used to calculate the ultimate lateral load for a rock-socketed shaft if suitable data are available for the rock mass strength and deformation parameters c_r, ϕ_r, ψ_r, $\bar{\tau}_{max}$, G_r, and ν_r. Methods for determining appropriate values for all of these have been described previously in this section and in Section 2. This method for predicting the ultimate capacity should be used with caution because it has yet to be tested against field data. Note also that the dilation angle may be influenced by the construction method. For example, with a smooth wall socket constructed under a heavy slurry which could leave a slurry "cake" on the socket wall, the dilatancy may be minimal and the dilation angle could approach zero.

TORSIONAL CAPACITY

Almost all shaft foundations loaded laterally will also be subjected to a degree of torsional loading because of the eccentricity of the applied loading. The torsional loading mode can be particularly significant for single pole transmission line structures. However, to calculate the torsional capacity of these foundations, the lateral and torsional modes of behavior are considered to be uncoupled so that the lateral loading has no influence on the torsional capacity

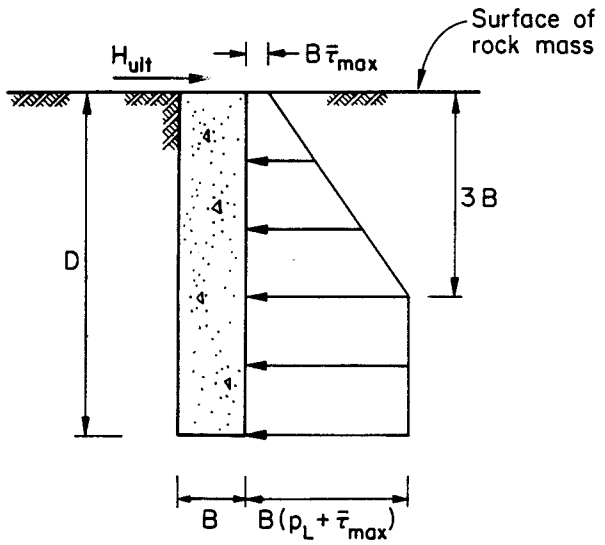

Figure 3-9. Distribution of Ultimate Lateral Force per Unit Length

and vice versa. Because of the unknown significance of any interaction between these modes, conservative factors of safety are recommended for the design of shafts subjected to combined lateral and torsional loading.

The development of the maximum torsional resistance of the foundation involves a complicated interaction between the concrete-rock bonding at the sidewalls and at the tip, the roughness of the interface, and the relative stiffness and strength of the concrete and surrounding rock mass. Assuming that the circular shaft section is able to sustain all possible applied torques, failure will be initiated by rotational slip at or close to the interface between the concrete and rock. This failure will begin near the surface of the rock mass and progress down the shaft. This progression will be rapid in the case of a torsionally rigid shaft, in which case the peak torsional shear resistance will be mobilized almost simultaneously everywhere along the shaft. For more flexible shafts, the progression of slip down the shaft will occur more slowly, and the situation may arise where the interface near the top of the shaft has reached a residual condition before the bottom of the shaft has reached a peak. In this case, the peak applied torque will be some average function of the peak and residual torsional shear behavior at the interface.

The authors have been unable to find any recorded instance in the literature where torsional load tests on rock-socketed piers have been conducted to failure. To be

able to estimate the torsional shaft capacity, data on interface shear strength obtained from axial load tests will have to be utilized. As in the case of axial uplift, it will be prudent to ignore any torsional shear resistance developed at the tip of the shaft, because of uncertainties with regard to the conditions at the bottom of the socket at the time of concrete pouring. On this basis, the maximum torque that may be applied to the foundation, T_{ult}, can be calculated from:

$$T_{ult} = \bar{\tau}_{max} A_s B/2 \qquad (3\text{-}26)$$

in which A_s = area of the socket sidewall. For design purposes, values for the unit side resistance, $\bar{\tau}_{max}$, may be obtained as previously. The maximum torque calculated by Equation 3-26 should also be compared with the torsional capacity of the circular shaft section, to check whether structural failure is likely to occur before failure at the concrete-rock interface.

SUMMARY

Methods for estimating the axial, lateral, and torsional capacity of a cylindrical shaft socketed into a homogeneous rock mass have been reviewed, and some new techniques have been presented. These techniques have been based on relatively simple models of the strength of rock masses and concrete-rock interfaces and, where possible, they have been supported by field test data. The use of these methods for layered rock masses can be approximated by simple summations over the respective layer depths.

Each loading mode has been examined separately, assuming that failure occurs in the rock mass or at the rock-concrete interface. Checks always should be made to ensure that failure is not initiated first in the concrete member. Any possible interaction between modes of loading has been ignored specifically. If these techniques are to be used in the design of shafts subjected to combined loading, conservative factors of safety for each mode should be adopted.

REFERENCES

1. Mattes, N. S. and Poulos, H. G., "Settlement of Single Compressible Pile", Journal of the Soil Mechanics and Foundations Division, ASCE, Vol. 95, No. SM1, Jan. 1969, pp. 189-207.

2. Randolph, M. F. and Wroth, C. P., "Analysis of Deformation of Vertically Loaded Piles", Journal of the Geotechnical Engineering Division, ASCE, Vol. 104, No. GT12, Dec. 1978, pp. 1465-1488.

3. Williams, A. F., "The Design and Performance of Piles Socketed Into Weak Rock", Ph.D. Dissertation, Monash University, Melbourne, 1980.

4. Williams, A. F., Johnston, I. W., and Donald, I. B., "The Design of Sockets in Weak Rock", Proceedings, International Conference on Structural Foundations on Rock, Vol. 1, Sydney, 1980, pp. 327-347.

5. Amir, J. M., Piling in Rock, A. A. Balkema, Rotterdam, 1986, 147 p.

6. Sowers, G. F., Introductory Soil Mechanics and Foundations: Geotechnical Engineering, 4th Ed., MacMillan Publishing Co., New York, 1979, 621 p.

7. Bell, A. L., "The Lateral Pressure and Resistance of Clay, and the Supporting Power of Clay Foundations", Proceedings, Institution of Civil Engineers, Vol. 199, 1915, pp. 233-272.

8. Kulhawy, F. H. and Goodman, R. E., "Design of Foundations on Discontinuous Rock", Proceedings, International Conference on Structural Foundations on Rock, Vol. 1, Sydney, 1980, pp. 209-220.

9. Bishnoi, B. L., "Bearing Capacity of a Closely Jointed Rock", Ph.D. Dissertation, Georgia Institute of Technology, Atlanta, 1968, 120 p.

10. Hoek, E. and Brown, E. T., Underground Excavations in Rock, Institution of Mining and Metallurgy, London, 1980, 527 p.

11. Hoek, E., "Strength of Jointed Rock Masses", Geotechnique, Vol. 33, No. 3, Sept. 1983, pp. 187-223.

12. Bieniawski, Z. T., "Geomechanics Classification of Rock Masses and Its Application in Tunnelling", Proceedings, 3rd International Congress of the International Society for Rock Mechanics, Vol. 2, Part A, Denver, 1974, pp. 27-32.

13. Barton, N. R., Lien, R., and Lunde, J., "Engineering Classification of Rock Masses for the Design of Tunnel Support", Rock Mechanics, Vol. 6, No. 4, Dec. 1974, pp. 189-236.

14. Davis, E. H., "A Note on Some Plasticity Solutions Relevant to the Bearing Capacity of Brittle and Fissured Materials", Proceedings, International Conference on Structural Foundations on Rock, Vol. 2, Sydney, 1980, pp. 83-90.

15. Williams, A. F. and Pells, P. J. N., "Side Resistance Rock Sockets in Sandstone, Mudstone, and Shale", Canadian Geotechnical Journal, Vol. 18, No. 4, Nov. 1981, pp. 502-513.

16. Pease, K. A. and Kulhawy, F. H., "Load Transfer Mechanisms in Rock Sockets and Anchors", Report No. EL-3777, Electric Power Research Institute, Palo Alto, Nov. 1984, 102 p.

17. Pease, K. A. and Kulhawy, F. H., "Behavior of Rock Anchors and Sockets", Proceedings, 25th U.S. Symposium on Rock Mechanics, Evanston, 1984, pp. 883-890.

18. Horvath, R. G., "Field Load Test Data on Concrete-to-Rock Bond Strength for Drilled Pier Foundations", Publication 87-07, Department of Civil Engineering, University of Toronto, Toronto, 1978, 97 p.

19. Rowe, R. K. and Armitage, H. H., "The Design of Piles Socketed Into Weak Rock", Report GEOT-11-84, University of Western Ontario, London, 1984, 366 p.

20. Horvath, R. G., "Behavior of Rock-Socketed Drilled Pier Foundations", Ph.D. Dissertation, University of Toronto, Toronto, 1982.

21. Poulos, H. G. and Davis, E. H., Pile Foundation Analysis and Design, John Wiley and Sons, New York, 1980, 397 p.

22. Broms, B. B., "Lateral Resistance of Piles in Cohesive Soils", Journal of the Soil Mechanics and Foundations Division, ASCE, Vol. 90, No. SM2, Mar. 1964, pp. 27-63.

23. Carter, J. P., Booker, J. R., and Yeung, S. K., "Cavity Expansion in Cohesive Frictional Soils", Geotechnique, Vol. 36, No. 3, Sept. 1986, pp. 349-358.

24. Davis, E. H., "Theories of Plasticity and the Failure of Soil Masses", Chapter 6 in Soil Mechanics - Selected Topics, Ed. I. K. Lee, Butterworths, London, 1968, pp. 341-380.

25. Randolph, M. F. and Houlsby, G. T., "The Limiting Pressure on a Circular Pile Loaded Laterally in Cohesive Soil", Geotechnique, Vol. 34, No. 4, Dec. 1984, pp. 613-623.

Section 4

LOAD-DISPLACEMENT RESPONSE OF AXIALLY LOADED SHAFTS

Socketed drilled shafts must satisfy the same criteria as other types of foundations, including adequate stability and tolerable deformations. To develop more rational design methods, a number of workers have devoted considerable attention to the analysis and testing of this type of foundation (e.g., 1 through 23). A detailed review of this literature has been done (16). On the basis of empirical evidence, recommendations have been made for the allowable stresses that may act on the tip and side of these shafts (e.g., 3, 23). Methods for estimating settlements at working loads also have been discussed (e.g., 3, 15, 17, 18).

In practice, the design of a socketed shaft commonly is governed by displacements, rather than by stability requirements. Most of the techniques proposed for the calculation of shaft displacements are based on the theory of elasticity. It has been usual to assume that the foundation is essentially a cylindrical elastic inclusion within a surrounding rock mass, as shown in Figures 4-1 and 4-2. In a recent study, the possibility of slip occurring at the interface between the shaft and the rock mass also was included (17, 18). From these studies, design charts have been prepared for the computation of shaft settlements under compression loading.

In this section, a simple method for computing the load-displacement behavior of a rock-socketed shaft is presented. Approximate analytical expressions are developed to describe the response of a shaft to axial compression or uplift loading. Separate expressions are developed for perfect interface bonding (no slip) and for slip along the entire cylindrical interface. These expressions are in general agreement with the results of more complicated numerical analyses of the complete problem, which include interface slip. The simplicity of these approximate closed form expressions makes them attractive for design purposes. For most practical problems, they avoid the need for a sophisticated numerical analysis or the need for a large number of chart solutions to cover the many variations in geometric and material parameters involved.

The summary of this section presents convenient flow charts for the developed

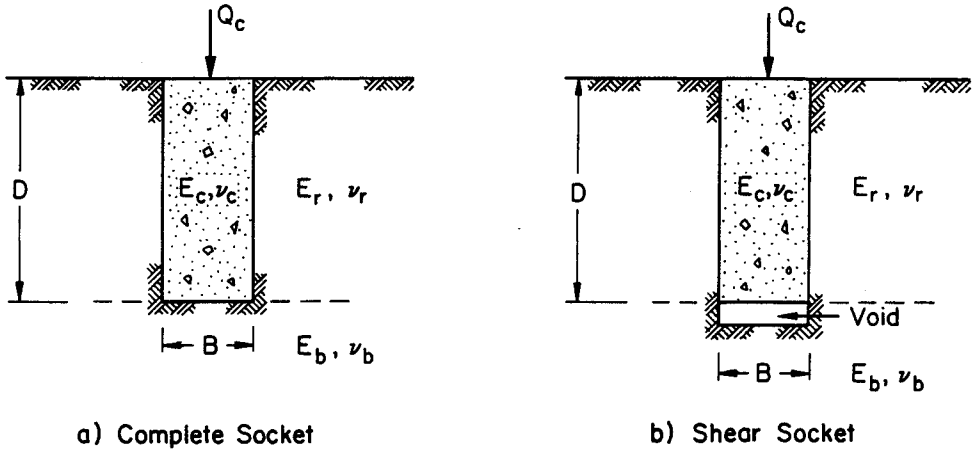

Figure 4-1. Compression Loading of Drilled Shaft

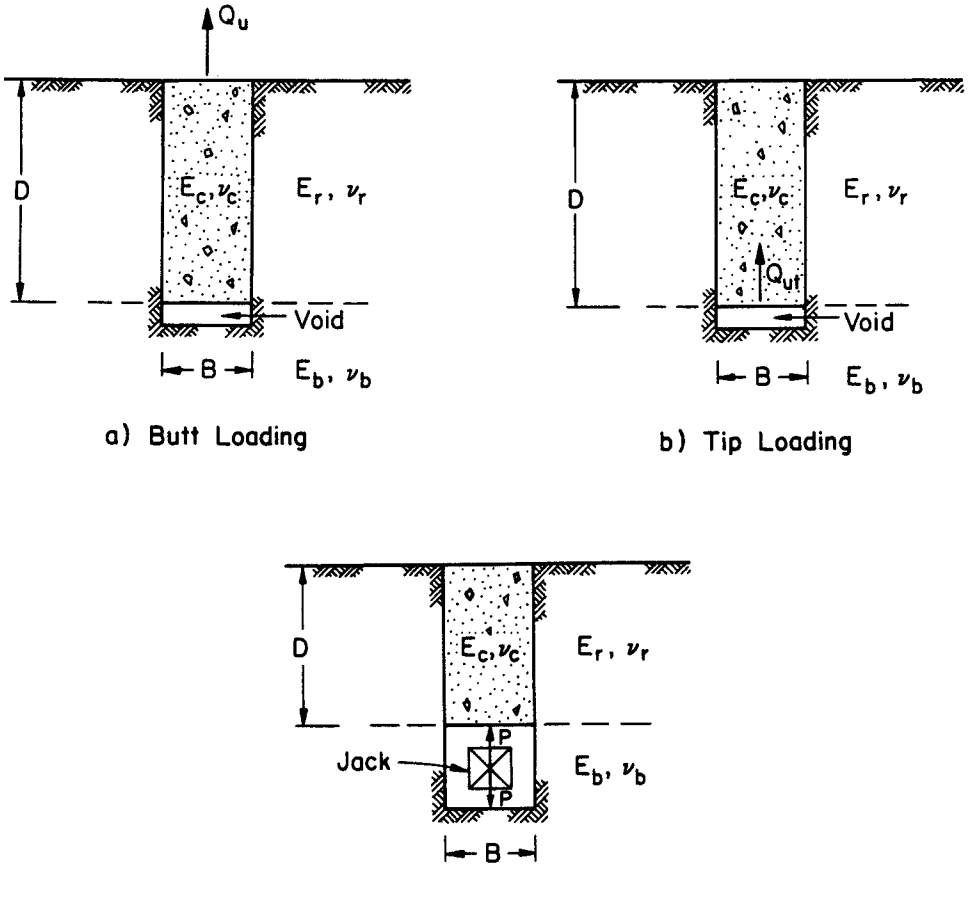

Figure 4-2. Uplift Loading of Drilled Shaft

solutions to assist in locating the appropriate expressions for a particular design case.

LOAD TRANSFER MECHANISMS

Compression Loading

When a socketed foundation is loaded in axial compression, support is provided by shear transfer along the socket wall and vertical stress transfer at the tip of the shaft. The distribution of the load between side and tip resistance is a function of the socket geometry, relative stiffness of the shaft and rock mass, socket roughness and strength, and foundation settlement. When relatively small loads are applied, the rock socket behaves essentially in a linear manner, and the load transfer can be computed using the theory of elasticity. This linear behavior is illustrated in Figure 4-3 by the line OA. As the load is increased to point A in Figure 4-3, the shear stress at some point along the interface will reach the shear strength, and the socket "bond" will begin to rupture and relative displacement (slip) will occur between the foundation and the surrounding rock. As the loading is increased further (beyond A), this process will continue along the shaft, more of the shaft will slip, and a greater proportion of the applied load will be transferred to the tip of the shaft. If loading is continued, eventually the entire shaft will slip (point B); beyond this point, a greater proportion of the total axial load will be transmitted directly to the tip.

In field studies involving compression loading, it was shown (3, 20) that slip can occur within the working load range of the shaft. As long as an adequate factor of safety on the tip resistance is maintained, it may be reasonable and economical to design these foundations for the partial or full slip conditions.

Clearly, it is desirable to be able to predict the entire load-displacement behavior of a shaft and, in the case of compression loading, to be able to estimate the proportion of the applied load transmitted to the tip. Prediction of the full load-displacement curve, including progressive slip (region AB on Figure 4-3), requires the use of numerical techniques. However, for design purposes, the initial linear elastic response (OA) and the full slip condition (the region beyond point B) provide good bounds on the overall shaft behavior. Approximate analytical solutions for the bounds are given in this section.

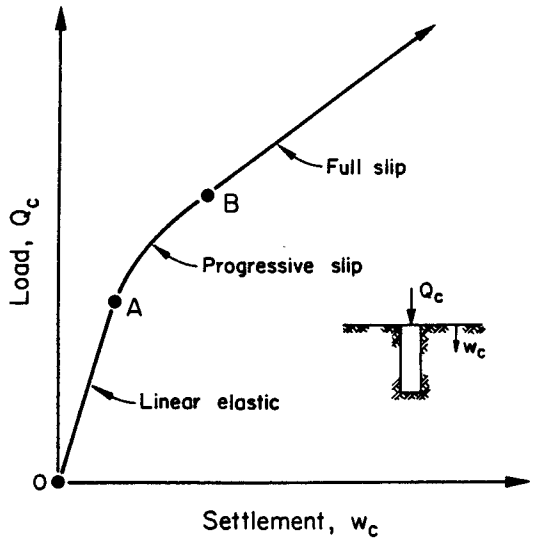

Figure 4-3. Idealized Load-Displacement Behavior

Uplift Loading

The manner in which axial uplift loads are transmitted to the rock mass depends upon the load magnitude and the way in which the load is applied to the socket. Two particular loading cases can be identified. In one case, the uplift load is applied to the butt of the shaft, as shown in Figure 4-2a. This would be the usual case in practice. The second involves a socket being pulled upwards from the tip, as shown in Figure 4-2b. In practice, this loading could develop by casting a shaft onto a plate located near the bottom of the socket, and attaching to this plate a vertical rod passing through the concrete shaft to the surface. To ensure that the uplift load is first applied to the tip, the rod connecting the base plate to the surface should not be cast directly into the concrete but should pass through a sleeve. In terms of the stiffness of the foundation system, there may be some advantage in this arrangement.

If the uplift load is applied directly to the tip (Figures 4-2b, 2c), then compressive axial stresses will develop in the shaft. Because of the Poisson's ratio effect, compressive radial stresses will be induced at the interface between the shaft and the rock mass. These compressive stresses will tend to enhance the frictional component of the side shear resistance of the shaft. If dilation also occurs at the interface as the shaft slips relative to the rock mass, further

compressive radial stresses will be generated. It is possible that, with this tip loading arrangement, the load-displacement relationship for the shaft may take the form shown in Figure 4-3. However, if no dilation occurs at the interface, or if it ceases to occur after some amount of slip, the uplift load-displacement curve eventually will be horizontal.

Where the uplift load is applied directly to the butt, the axial stresses in the shaft will be tensile and, because of the Poisson's ratio effect, the radial stress changes at the interface also will be tensile. This loading will tend to reduce the frictional component of side shear resistance and any beneficial effects that may arise from dilation at the interface.

In principle, some resistance to uplift loading also may be provided in a "complete" socket by the tensile strength of the interface between the tip of the shaft and the rock mass. However, in practice it is prudent to ignore this component of resistance because of the uncertainty about "perfect clean-out" of the socket at the time that the concrete is placed. It is usual to design these foundations to resist uplift loading on the basis of a "shear only" socket.

PROBLEM DEFINITION

The problem analyzed is that of axial loading of a socketed shaft, with either a "complete" or "shear" socket, as shown in Figures 4-1 and 4-2. The concrete shaft is modeled as an elastic cylindrical inclusion, with Young's modulus E_c and Poisson's ratio ν_c , embedded in an elastic rock mass. The shaft has depth D and diameter B. The rock mass surrounding the shaft to a depth D is homogeneous with Young's modulus E_r and Poisson's ratio ν_r. Beneath the shaft tip, the rock mass has Young's modulus E_b and Poisson's ratio ν_b. For compression, a vertical load, Q_c, is applied to the shaft butt and is considered to be distributed uniformly so that the average applied axial stress is $\sigma_b = 4Q_c/\pi B^2$. For uplift, the load may be applied either at the shaft tip or butt.

An elastic model for the shaft is consistent with current structural engineering practice. If the shaft is reinforced concrete, then E_c should be assigned the value of the equivalent section modulus. An elastic model to represent the mechanical behavior of the rock mass is a simplification of reality, and the selection of suitable properties to characterize the mass is a matter where considerable judgment and experience are required. Allowance must be made for the discontinuous nature of most natural rock masses. Modulus values determined from laboratory testing of intact core specimens are generally considered inappropriate,

because they normally overestimate the stiffness of the discontinuous mass. Suggested methods for determining representative elastic properties of the rock mass were described in Section 2.

Consider now a horizontal slice through the shaft, with the interface and rock mass at depth z, as shown in Figure 4-4. For clarity, the interface at r = B/2 has been "exploded" to show the stress components more clearly. It is assumed that the interface has zero radial thickness.

The symbols (u_c, w_c) and (u_r, w_r) will be used to denote the radial (u) and vertical (w) displacements of the concrete shaft and rock mass, respectively, at radius B/2 (i.e., the interface) and depth z. Downward vertical and outward radial displacements are positive. Symbols σ_r, σ_z, and τ (or τ_o) denote the radial, vertical, and shear stresses acting at the interface, as shown in Figure 4-4. Compressive normal stress is positive.

The analysis of two different stages in the loading history of the shaft will be considered. Initially, perfect contact (no slip) along the interface will be analyzed. Then slip between the shaft and rock mass along the full length of the interface will be examined. The former corresponds to OA in Figure 4-3, while the latter corresponds to the region beyond point B.

LINEAR ELASTIC BEHAVIOR

The approximate analysis for linear elastic behavior follows that for the deformation of vertically loaded piles in soil (24) and the behavior of resin-grouted anchor bars in a rigid rock mass (25). Perfect bonding is assumed along the shaft-rock mass interface, so that the following conditions apply:

$$u_r = u_c \tag{4-1}$$

and

$$w_r = w_c \tag{4-2}$$

Under an applied axial load, the displacements in the rock mass are predominantly vertical, and the load is transferred from the shaft to the rock mass by vertical shear stresses, with little change in vertical normal stress in the rock mass (except near the tip of a complete socket). The pattern of deformation around the

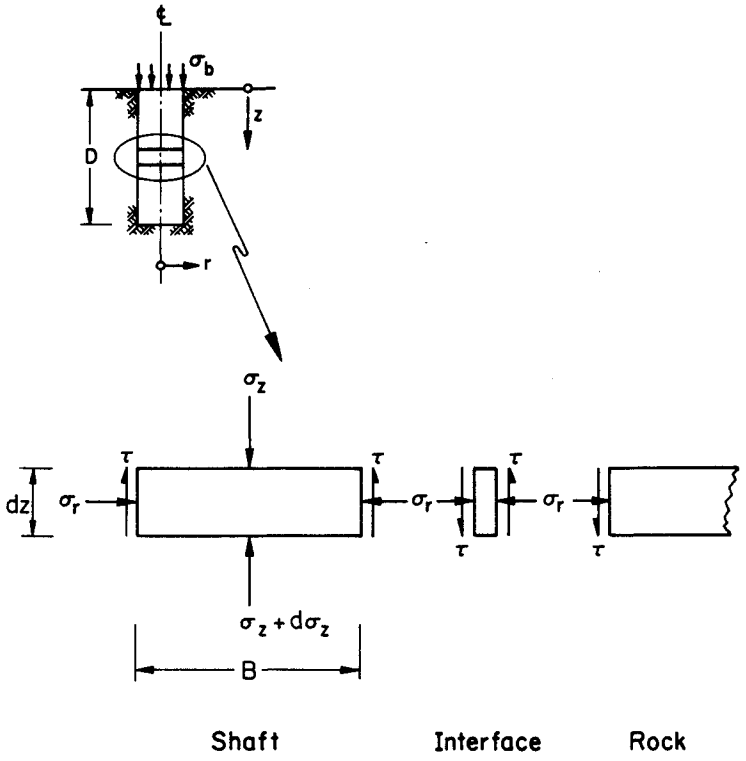

Figure 4-4. Exploded View of Horizontal "Slice" Through Socketed Shaft

shaft may be visualized as an infinite number of concentric cylinders sliding inside each other (26). For vertical equilibrium, the magnitude of the shear stress on each cylinder must decrease with the surface area of the cylinder. If the shear stress at depth z on the shaft is $\tau_o(z)$ at radius r_o (i.e., B/2), then the shear stress at radius r and depth z is given by:

$$\tau = \frac{\tau_o(z)\ r_o}{r} \tag{4-3}$$

The shear strain in the elastic rock mass is:

$$\gamma = \frac{\tau}{G_r} \tag{4-4}$$

in which $G_r = E_r/[2(1 + \nu_r)]$ is the shear modulus of the elastic rock mass. Since the major component of rock deformation will be vertical, the shear strain is approximated by:

$$\gamma \approx \frac{dw_r}{dr} \tag{4-5}$$

in which w_r is the vertical displacement of the rock mass.

If it is also assumed that at a radius R, the vertical displacements vanish, then it can be shown that the shaft displacement at depth z is given by:

$$w_r(z) = \int_{r_o}^{R} \left(\frac{\tau_o(z)\ r_o}{G_r\ r}\right) dr = \frac{\tau_o(z)\ r_o}{G_r}\ ln[R/r_o] \tag{4-6}$$

From a study of finite element predictions of pile behavior, it was deduced empirically (24) that a suitable value of R was given approximately by:

$$\left(\frac{R}{r_o}\right) \approx 2.5(1 - \nu_r)\ \left(\frac{D}{r_o}\right) \tag{4-7}$$

This expression for R provides good predictions of the axial displacements of slender piles in relatively soft soils. As will be shown later, the same expression gives reasonable predictions of the displacements for much stubbier shafts in stiffer rock masses. Therefore, Equation 4-6 can be written as:

$$w_r(z) = \frac{\tau_o(z)\ r_o\ \zeta}{G_r} = \frac{\tau_o(z)\ B\ \zeta}{2G_r} \tag{4-8}$$

in which

$$\zeta = ln[2.5\ (1-\nu_r)\ D/r_o] = ln[5\ (1-\nu_r)\ D/B] \tag{4-9}$$

Because there is no slip at the interface, Equation 4-8 also gives the vertical displacement of the shaft, w_c.

In developing the general solution for shaft displacements, compression or extension of the shaft under axial load will be taken into account. If the shaft is treated as a free standing column, subjected to known loading, then the axial strain at any level down the shaft is:

$$\epsilon_z = -\frac{dw_c}{dz} = \frac{4Q}{\pi\ B^2\ E_c} \tag{4-10}$$

with compression positive. The axial force Q will vary along the length of the shaft as load is shed into the surrounding rock mass, so that:

$$\frac{dQ}{dz} = -\pi \, B \, \tau_o(z) \tag{4-11}$$

Finally, substitution of Equations 4-2, 4-8, and 4-11 into 4-10 yields the governing equation for shaft displacements as:

$$\frac{d^2 w_c}{dz^2} = \mu^2 \, w_c \tag{4-12}$$

in which

$$(\mu D)^2 = \left(\frac{2}{\zeta\lambda}\right) \left(\frac{2D}{B}\right)^2 \tag{4-13}$$

and

$$\lambda = E_c/G_r \tag{4-14}$$

This differential equation may be solved to give w_c in terms of hyperbolic sine and cosine functions of the depth, z, as given below:

$$w_c(z) = A \sinh[\mu z] + C \cosh[\mu z] \tag{4-15}$$

Substitution of the appropriate boundary conditions into Equation 4-15 allows the constants A and C to be determined. Some particular cases are considered below.

ELASTIC SOLUTIONS

Complete Socket Under Compression Loading

When the shaft tip bears directly on the bottom of the socket hole, a contribution to the shaft settlement will arise from the displacement of the rock beneath the tip (Figure 4-1a). This case can be approximated as a rigid punch acting on the surface of an elastic half-space with Young's modulus E_b and Poisson's ratio ν_b. To retain generality, the elastic rock mass below the shaft tip may be different from that surrounding the shaft. The tip displacement is given by (e.g., 27):

$$w_{ct} = \frac{Q_{tip}\ (1 - \nu_b)}{2G_b\ B} \tag{4-16}$$

in which $G_b = E_b/[2(1 + \nu_b)]$ is the shear modulus of the elastic material beneath the shaft tip.

If this equation is used as one of the boundary conditions for the shaft, then it is found that the elastic settlement at the butt of the complete shaft, w_c, is given by:

$$\frac{G_r\ B\ w_c}{2Q_c} = \frac{1 + (\frac{4}{1 - \nu_b})\ (\frac{1}{\pi\lambda\xi})\ (\frac{2D}{B})\ (\frac{\tanh[\mu D]}{\mu D})}{(\frac{4}{1 - \nu_b})\ (\frac{1}{\xi}) + (\frac{2\pi}{\zeta})\ (\frac{2D}{B})\ (\frac{\tanh[\mu D]}{\mu D})} \tag{4-17}$$

and the proportion of the applied load transmitted to the tip is:

$$\frac{Q_{tip}}{Q_c} = \frac{(\frac{4}{1 - \nu_b})\ (\frac{1}{\xi})\ (\frac{1}{\cosh[\mu D]})}{(\frac{4}{1 - \nu_b})\ (\frac{1}{\xi}) + (\frac{2\pi}{\zeta})\ (\frac{2D}{B})\ (\frac{\tanh[\mu D]}{\mu D})} \tag{4-18}$$

in which

$$\xi = G_r/G_b \tag{4-19}$$

The solution given in Equation 4-17 has been plotted in Figure 4-5 for cases where $\nu_r = \nu_b = 0.25$ and $E_r = E_b$. A number of values of the modulus ratio, E_c/E_r, and the slenderness ratio, D/B, are shown. Also plotted are available finite element method (FEM) solutions (15). The general agreement between the two solutions is reasonable and could be considered conservative and satisfactory for most design purposes.

Shear Socket Under Compression Loading

For a shear socket under compression loading (Figure 4-1b), the boundary condition at the shaft tip is one of zero axial stress. For this case, the settlement at the shaft butt is given by:

$$\frac{E_r\ B\ w_c}{2Q_c} = (\frac{1}{\pi})\ (\frac{E_r}{E_c})\ (\frac{2}{\mu B})\ (\frac{\cosh[\mu D]}{\sinh[\mu D]}) \tag{4-20}$$

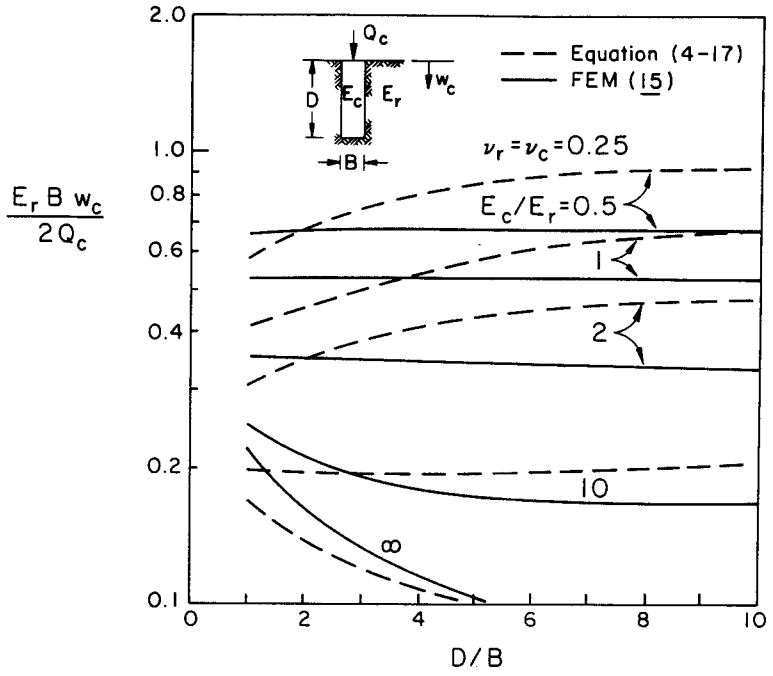

Figure 4-5. Elastic Settlement of Complete Rock Socket

This solution is plotted in Figure 4-6 and compared with finite element results (15). The accuracy of the approximate equation (4-20) is clear, particularly at larger values of the modulus ratio (E_c/E_r).

Uplift Loading Applied to Shaft Butt in Shear Socket

For this case (Figure 4-2a), the uplift displacement is simply the reverse of the settlement of the same type of socket when subjected to a compressive load equal in magnitude to the uplift load. Therefore, the magnitude of the uplift displacement is given by Equation 4-20, with $w_u = w_c$ and $Q_u = Q_c$.

Uplift Loading Applied to Shaft Tip in Shear Socket

For this case (Figure 4-2b), the appropriate boundary condition is zero axial stress at the shaft butt, which leads to the following:

$$\frac{E_r\ B\ w_u}{2Q_{ut}} = -\left(\frac{1}{\pi}\right)\left(\frac{E_r}{E_c}\right)\left(\frac{2}{\mu B}\right)\left(\frac{1}{\sinh[\mu D]}\right) \qquad (4\text{-}21)$$

in which Q_{ut} is the uplift load applied at the shaft tip, which applies a compression to the tip and therefore is given a positive sign, while the negative sign indicates an upward vertical displacement.

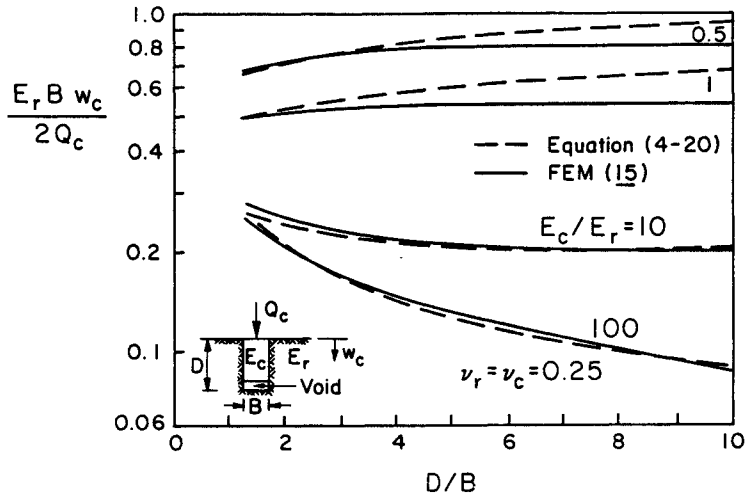

Figure 4-6. Elastic Settlement of Shear Socket

The displacement of the shaft tip, w_{ut}, may be also of interest and is given by:

$$\frac{E_r\ B\ w_{ut}}{2Q_{ut}} = -\ (\frac{1}{\pi})\ (\frac{E_r}{E_c})\ (\frac{2}{\mu B})\ (\frac{\cosh[\mu D]}{\sinh[\mu D]}) \qquad (4\text{-}22)$$

This equation has the same form as Equation 4-20, for a shear socket under compression loading, and could have been predicted by the reciprocal theorem of elasticity.

Equations 4-21 and 4-22 have been plotted in Figures 4-7 and 4-8, respectively. In general, the butt displacement for a shaft loaded in uplift at its tip is less than the displacement of the same type of shaft, subjected to the same load applied at its butt (Compare Figures 4-6 and 4-7.). It is also interesting to note that, for a shaft loaded at its tip, the displacements at the butt become smaller as the ratio E_c/E_r is reduced, but the displacements at the tip become smaller as E_c/E_r is increased. However, the difference between butt and tip displacements is only significant for very compressible or extensible shafts.

Shaft Jacked Upward

A shaft also can be loaded by a jacking force acting on the shaft tip and the

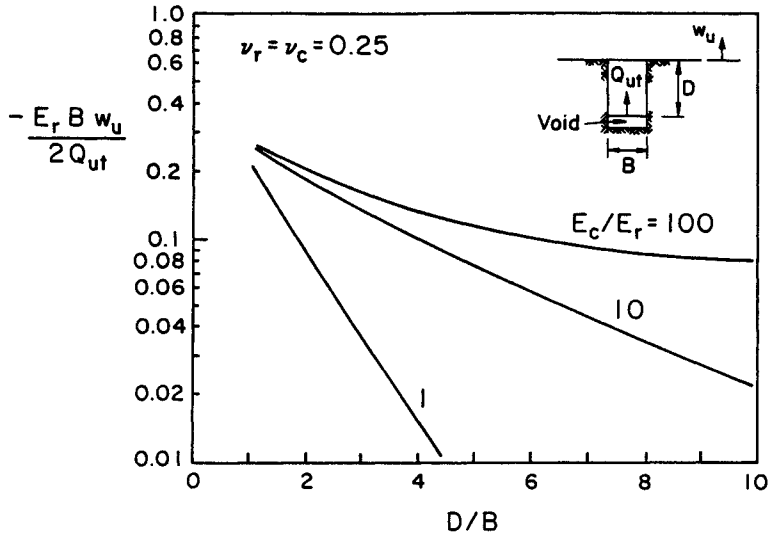

Figure 4-7. Elastic Uplift Displacement of Butt of Shaft Pulled Upward from Tip

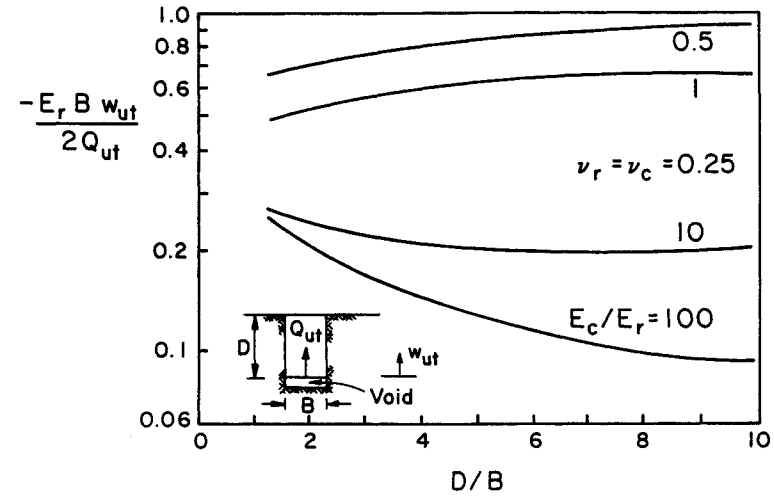

Figure 4-8. Elastic Uplift Displacement of Tip of Shaft Pulled Upward from Tip

bottom of the socket hole (Figure 4-2c). This case is of interest because this type of loading arrangement has been used for test loading of sockets in the field (e.g., 9) and for improving the performance of prototype shafts carrying compressive working loads (e.g., 8). Although there is no net load applied to the shaft-rock mass system, the shaft tip will move and its displacement can be considered as the resultant of two components: (1) an upward displacement because

of the upward jacking force applied to the shaft tip, and (2) a downward displacement because of the jacking force applied to the rock mass beneath the shaft tip. For simplicity, it is assumed that the void occupied by the jack is of infinitesimal thickness, so that the net displacement of the shaft tip is obtained by simple superposition of the two effects described above.

The upward displacement is the same as that predicted by Equation 4-22. To calculate the downward displacement, it is assumed that the underside of the jack acts like a rigid punch on the surface of an elastic half-space with Young's modulus E_b and Poisson's ratio ν_b. When these two components are combined, the resulting displacement of the shaft tip is given by:

$$\frac{E_r B w_{ct}}{2P} = - \left(\frac{1}{\pi}\right) \left(\frac{E_r}{E_c}\right) \left(\frac{2}{\mu B}\right) \left(\frac{\cosh[\mu D]}{\sinh[\mu D]}\right) + \left(\frac{1}{2}\right) \left(\frac{E_r}{E_b}\right) (1 - \nu_b^2) \qquad (4\text{-}23)$$

Similarly, the shaft butt displacement is given by:

$$\frac{E_r B w_c}{2P} = - \left(\frac{1}{\pi}\right) \left(\frac{E_r}{E_c}\right) \left(\frac{2}{\mu B}\right) \left(\frac{1}{\sinh[\mu D]}\right) + \left(\frac{1}{2}\right) \left(\frac{E_r}{E_b}\right) (1 - \nu_b^2) \qquad (4\text{-}24)$$

To illustrate this behavior, the solutions for shaft butt and tip displacement have been plotted in Figures 4-9 and 4-10 for cases where $E_b/E_r = 0.5$, 1, and 2. A negative sign indicates upward vertical displacement. It is evident that, in most practical cases, the net displacement under this form of loading is downward, giving a settlement.

ANALYSIS OF FULL SLIP CONDITION

Consider now the case where slip has occurred along the entire length of the shaft, corresponding to the region beyond point B in Figure 4-3. Within this range, Equations 4-1 and 4-2 are no longer valid. In the following, a shaft subjected to compressive axial load is analyzed first; modification of the analysis for tensile loading then is straightforward.

It is assumed that the shear strength of the interface is given by the Mohr-Coulomb criterion:

$$\tau = c + \sigma_r \tan\phi \qquad (4\text{-}25)$$

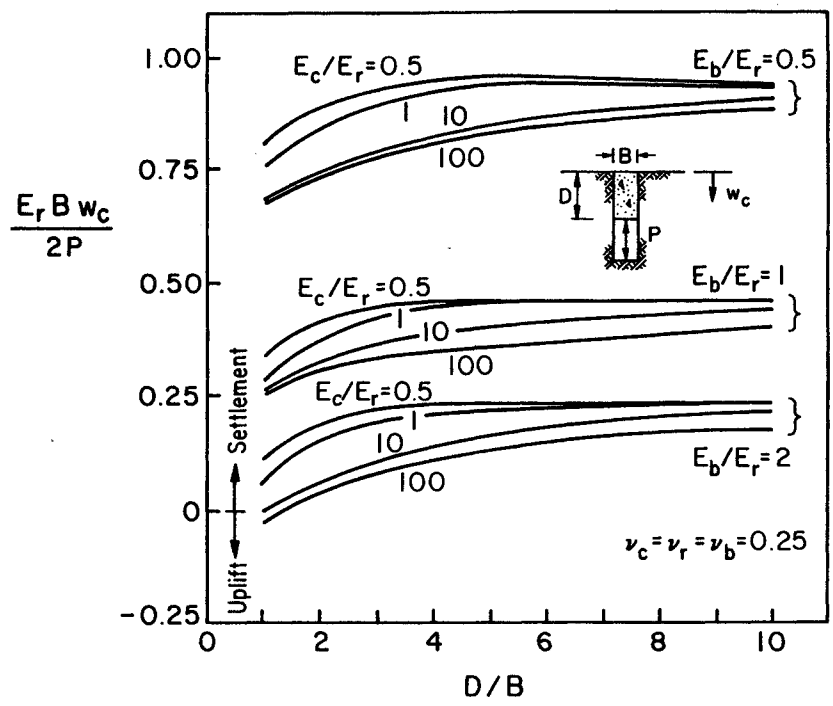

Figure 4-9. Elastic Displacement of Butt of Shaft Jacked at Tip

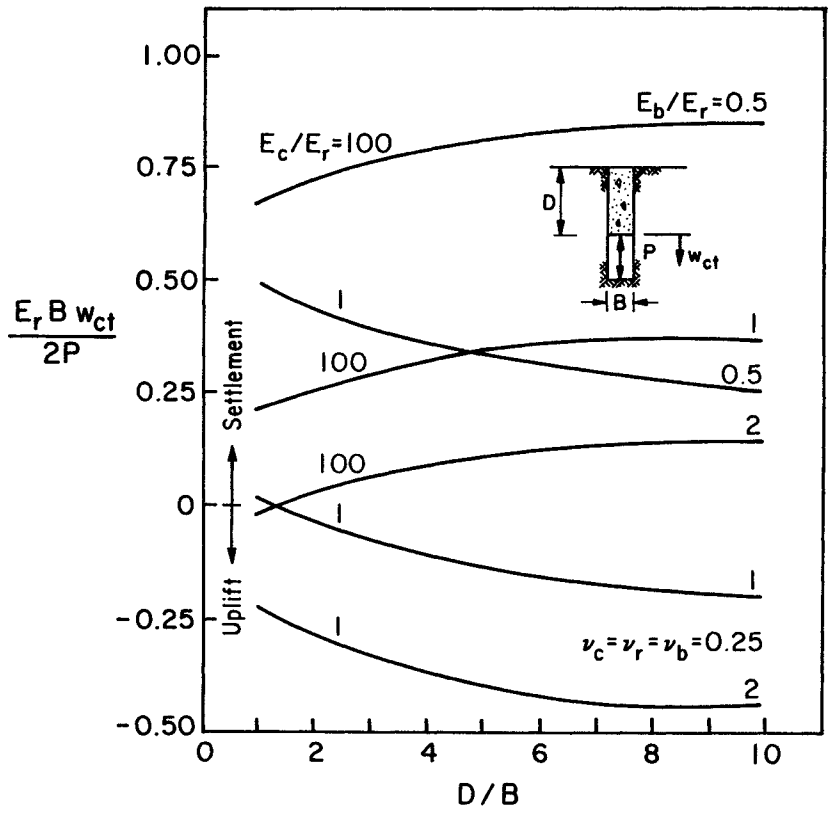

Figure 4-10. Elastic Displacement of Tip of Shaft Jacked at Tip

in which c = interface cohesion and ϕ = interface friction angle. As relative displacement (slip) occurs, the interface may dilate. It is assumed that the displacement components obey the following dilation law:

$$\frac{\dot{u}_c - \dot{u}_r}{\dot{w}_c - \dot{w}_r} = - \tan\psi \tag{4-26}$$

in which ψ = angle of dilation and dot ($\cdot$) = rate of change (28). For this particular problem, it is also possible to write Equation 4-26 in terms of the actual displacement components, so that:

$$\frac{u_c - u_r}{w_c - w_r} = - \tan\psi \tag{4-27}$$

This type of behavior is illustrated in Figure 4-11. As noted in Section 3, the dilation angle may be minimized if a heavy slurry is used during construction.

To determine the radial displacements, conditions of plane strain are assumed independently in the rock mass and in the slipping shaft. The case of compressive radial stress at the interface is considered first; the case where Poisson's ratio effects produce tensile radial stress changes, as in some instances of uplift loading, will be considered later. The assumption of plane strain leads to the following equation for the radial displacement of the rock mass:

$$u_r = \frac{(1 + \nu_r)}{E_r} \frac{B}{2} \sigma_r \tag{4-28}$$

while for the shaft:

$$u_c = - \frac{(1 - \nu_c)}{E_c} \frac{B}{2} \sigma_r + \frac{\nu_c}{E_c} \frac{B}{2} \sigma_z \tag{4-29}$$

The rock mass is considered to behave in a linear elastic manner, even after full slip has taken place, and therefore the vertical displacement at the interface is given, as before, by:

$$w_r = \frac{(1 + \nu_r)}{E_r} B \zeta\tau \tag{4-30}$$

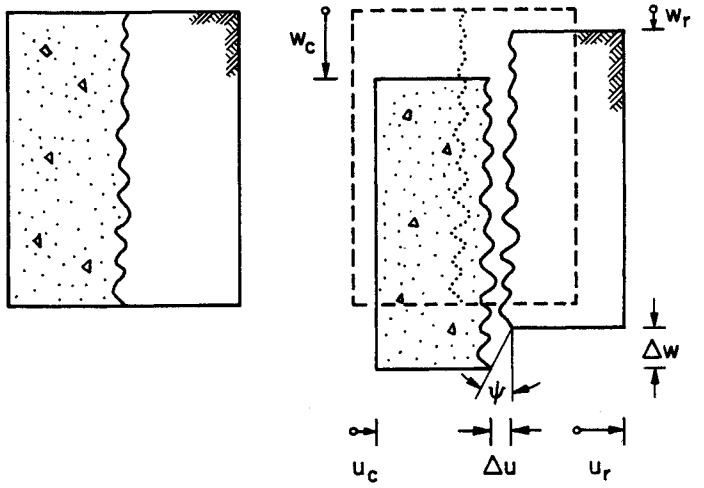

a) Before Shearing b) After Shearing

$$\frac{-\Delta u}{\Delta w} = \frac{u_c - u_r}{w_c - w_r} = -\tan\psi$$

Figure 4-11. Schematic Illustration of Dilatancy at Shaft-Rock Mass Interface

in which, to sufficient accuracy:

$$\zeta = ln[5(1 - \nu_r)D/B] \tag{4-31}$$

If the shaft is considered to be an elastic column, then:

$$\frac{dw_c}{dz} = -\frac{\sigma_z}{E_c} \tag{4-32}$$

and equilibrium of the column requires that:

$$\frac{d\sigma_z}{dz} = -\left(\frac{4}{B}\right)\tau \tag{4-33}$$

When Equations 4-28, 4-29, and 4-30 are substituted into the dilatancy law (Equation 4-27), it is found that:

$$w_c = a_1\tau + a_2\sigma_r - a_3\sigma_z \tag{4-34}$$

where the compliances a_1, a_2, and a_3 are given by:

$$a_1 = \frac{(1 + \nu_r)B\ \zeta}{E_r} \tag{4-35}$$

$$a_2 = \left\{\frac{(1 - \nu_c)B}{2E_c} + \frac{(1 + \nu_r)B}{2E_r}\right\} \left(\frac{1}{\tan\psi}\right) \tag{4-36}$$

$$a_3 = \left(\frac{\nu_c B}{2E_c}\right) \left(\frac{1}{\tan\psi}\right) \tag{4-37}$$

Substitution of Equations 4-25, 4-32, and 4-33 into 4-34 gives the following differential equation which governs the variation of the vertical stress in the shaft:

$$\alpha \frac{d^2\sigma_z}{dz^2} + \beta \frac{d\sigma_z}{dz} - \sigma_z = 0 \tag{4-38}$$

in which

$$\alpha = a_5\left(\frac{E_c B}{4}\right) \tag{4-39}$$

$$\beta = a_3\ E_c \tag{4-40}$$

and

$$a_5 = a_1 + a_4 \tag{4-41}$$

$$a_4 = a_2/\tan\phi \tag{4-42}$$

For a dilatant interface, $\tan\psi$ is greater than zero and therefore the coefficients α and β must be positive.

The solution of Equation 4-38 takes the form:

$$\sigma_z = A\ e^{\lambda_1 z} + C\ e^{\lambda_2 z} \tag{4-43}$$

in which λ_1 and λ_2 are given by:

$$\lambda_1, \lambda_2 = \frac{-\beta \pm (\beta^2 + 4\alpha)^{1/2}}{2\alpha} \tag{4-44}$$

The constants A and C are determined from the boundary conditions. Some particular cases are considered below.

FULL SLIP SOLUTIONS

Shear Socket Under Compression Loading

For a shear socket under compression loading, the appropriate boundary conditions are:

$$\sigma_z = 0 \qquad \text{at } z = D \tag{4-45}$$

and

$$\sigma_z = \sigma_b \qquad \text{at } z = 0 \tag{4-46}$$

and therefore the solution is:

$$\sigma_z = \sigma_b \{C_1 e^{\lambda_1 z} - C_2 e^{\lambda_2 z}\} \tag{4-47}$$

$$\tau = -\left(\frac{\sigma_b}{2}\right) \{C_1 \lambda_1 \frac{B}{2} e^{\lambda_1 z} - C_2 \lambda_2 \frac{B}{2} e^{\lambda_2 z}\} \tag{4-48}$$

$$w_c = -a_3 \sigma_z - a_4 c + a_5 \tau \tag{4-49}$$

in which

$$C_1 = \frac{e^{\lambda_2 D}}{e^{\lambda_2 D} - e^{\lambda_1 D}} \tag{4-50}$$

$$C_2 = \frac{e^{\lambda_1 D}}{e^{\lambda_2 D} - e^{\lambda_1 D}} \tag{4-51}$$

In particular, the shaft butt displacement, w_c, can be calculated by substituting z = 0 into Equations 4-47 to 4-49.

Complete Socket Under Compression Loading

The boundary conditions for this case are:

$$\sigma_z = \sigma_b \qquad \text{at } z = 0 \tag{4-52}$$

and

$$w_c = w_{ct} = \sigma_{tip}\left(\frac{\pi}{2}\right)\left(\frac{1 - \nu_b^2}{E_b}\right)\frac{B}{2} \qquad \text{at } z = D \tag{4-53}$$

in which σ_{tip} is the vertical stress acting at the shaft tip. It has been assumed that the shaft tip acts like a rigid punch, resting on the surface of an elastic half-space with Young's modulus E_b and Poisson's ratio ν_b.

For this case, the solution is found as:

$$\sigma_z = \sigma_b(C_3 e^{\lambda_1 z} + C_4 e^{\lambda_2 z}) + c(C_5 e^{\lambda_1 z} + C_6 e^{\lambda_2 z}) \tag{4-54}$$

$$\tau = -\left(\frac{\sigma_b}{2}\right)(C_3\lambda_1\frac{B}{2}e^{\lambda_1 z} + C_4\lambda_2\frac{B}{2}e^{\lambda_2 z}) - \left(\frac{c}{2}\right)(C_5\lambda_1\frac{B}{2}e^{\lambda_1 z} + C_6\lambda_2\frac{B}{2}e^{\lambda_2 z}) \tag{4-55}$$

$$w_c = -a_3\sigma_z - a_4 c + a_5\tau \tag{4-56}$$

in which

$$C_3 = -\left(\frac{1}{\Phi_2}\right)\left[\frac{\pi}{4}(1 - \nu_b^2)\left(\frac{B}{E_b}\right) + a_3 + \frac{1}{4}a_5\lambda_2 B\right]e^{\lambda_2 D} \tag{4-57}$$

$$C_4 = \left(\frac{1}{\Phi_2}\right)\left[\frac{\pi}{4}(1 - \nu_b^2)\left(\frac{B}{E_b}\right) + a_3 + \frac{1}{4}a_5\lambda_1 B\right]e^{\lambda_1 D} \tag{4-58}$$

$$C_5 = -\frac{a_4}{\Phi_2} \tag{4-59}$$

$$C_6 = \frac{a_4}{\Phi_2} \tag{4-60}$$

The proportion of load transmitted to the tip, σ_{tip}/σ_b, is given by:

$$\frac{\sigma_{tip}}{\sigma_b} = \frac{\Phi_1}{\Phi_2} + \frac{\Phi_3}{\Phi_2}\left(\frac{c}{\sigma_b}\right) \tag{4-61}$$

in which

$$\Phi_1 = \frac{1}{4}\, a_5(\lambda_1 - \lambda_2)B\, e^{(\lambda_1 + \lambda_2)D} \tag{4-62}$$

$$\Phi_2 = \left[\frac{\pi}{4}\,(1-\nu_b{}^2)\left(\frac{B}{E_b}\right) + a_3 + \frac{1}{4}\, a_5\lambda_1 B\right]e^{\lambda_1 D} - \left[\frac{\pi}{4}\,(1-\nu_b{}^2)\left(\frac{B}{E_b}\right) + a_3 + \frac{1}{4}\, a_5\lambda_2 B\right]e^{\lambda_2 D} \tag{4-63}$$

$$\Phi_3 = a_4(e^{\lambda_2 D} - e^{\lambda_1 D}) \tag{4-64}$$

Again, the settlement of the butt can be calculated by substitution of z = 0 into Equations 4-54 and 4-56.

Uplift Loading Applied to Shaft Butt in Shear Socket

In this case (Figure 4-2a), the axial stresses in the shaft are tensile and the Poisson's ratio effects induce tensile changes in the radial stress acting at the interface between the shaft and rock mass. The solution for this case can be obtained by an analysis similar to that for compression loading and is:

$$\sigma_z = \sigma_b\{C_7\, e^{\lambda_3 z} - C_8\, e^{\lambda_4 z}\} \tag{4-65}$$

$$\tau = \left(\frac{\sigma_b}{2}\right)\{C_7\,\lambda_3\,\frac{B}{2}\,e^{\lambda_3 z} - C_8\,\lambda_4\,\frac{B}{2}\,e^{\lambda_4 z}\} \tag{4-66}$$

$$w_u = a_3\,\sigma_z + a_4 c - a_5\tau \tag{4-67}$$

in which

$$C_7 = e^{\lambda_4 D}/(e^{\lambda_4 D} - e^{\lambda_3 D}) \tag{4-68}$$

$$C_8 = e^{\lambda_3 D}/(e^{\lambda_4 D} - e^{\lambda_3 D}) \tag{4-69}$$

and

$$\lambda_3,\ \lambda_4 = \frac{\beta \pm (\beta^2 + 4\alpha)^{1/2}}{2\alpha} = -\lambda_2,\ -\lambda_1 \qquad (4\text{-}70)$$

In this case of uplift loading, the applied axial stress σ_b is tensile and should be input in Equations 4-65 and 4-66 as a negative quantity. It also should be noted carefully that this analysis is strictly valid only as long as the radial stress σ_r remains compressive. For this condition to be satisfied, the tensile stress changes produced by the effect of Poisson's ratio of the shaft must be offset by the compressive changes induced by dilation and any initial in-situ compressive horizontal stress at the interface.

Uplift Loading Applied to Shaft Tip in Shear Socket

In this case, a compressive vertical stress, σ_{tip}, is applied to the shaft tip while the shaft butt is unstressed. The solution is:

$$\sigma_z = \sigma_{tip}\ C_9\{e^{\lambda_3 z} - e^{\lambda_4 z}\} \qquad (4\text{-}71)$$

$$\tau = \left(\frac{\sigma_{tip}}{2}\right) C_9\ \{\lambda_3 \frac{B}{2} e^{\lambda_3 z} - \lambda_4 \frac{B}{2} e^{\lambda_4 z}\} \qquad (4\text{-}72)$$

$$w_u = a_3\sigma_z + a_4 c - a_5\tau \qquad (4\text{-}73)$$

in which

$$C_9 = 1/(e^{\lambda_3 D} - e^{\lambda_4 D}) \qquad (4\text{-}74)$$

and σ_{tip} is a positive (compressive) quantity. The displacement of the shaft butt (w_u) and tip (w_{ut}) may be obtained by substituting z = 0 and z = D, respectively, into Equations 4-71 to 4-73.

Shaft Jacked Upward

This case has been described earlier (Figure 4-2c). After full slip has occurred along the shaft, the rock mass beneath the shaft tip continues to deform elastically, with appropriate deformation parameters E_b and ν_b. For this case, the stress components along the shaft are the same as those given by Equations 4-71 and 4-72, for a shaft loaded in uplift at its tip. However, the displacement of the tip is calculated as the resultant of an upward component from the load applied to

the shaft tip and a downward component from the jacking force loading the rock mass beneath the shaft tip, i.e.:

$$w_u = a_3\sigma_z + a_4 c - a_5\tau + \sigma_{tip}\ (\frac{\pi}{4})\ (\frac{1 - \nu_b^2}{E_b})B \qquad (4\text{-}75)$$

SOME SPECIAL CASES OF FULL SLIP

It is of interest to consider a number of special cases, for which simpler forms of the analytical expressions can be obtained for full slip behavior. The case where no dilatancy occurs at the interface is discussed, and the particular forms of the governing expressions that evolve for purely cohesive and purely frictional interfaces are presented.

No Dilatancy at Interface

For this condition, the dilation angle ψ is zero and $(1/\tan\psi)$ becomes infinite. The governing differential equation for the behavior of the shaft, Equation 4-38, reduces to:

$$\frac{d^2\sigma_z}{dz^2} + (\frac{4F\ \tan\phi}{B})\ \frac{d\sigma_z}{dz} = 0 \qquad (4\text{-}76)$$

in which

$$F = \nu_c/[(1 - \nu_c) + (\frac{E_c}{E_r})\ (1 + \nu_r)] \qquad (4\text{-}77)$$

This equation has the solution:

$$\sigma_z = A\ \exp[-4F\ \tan\phi(z/B)] + C \qquad (4\text{-}78)$$

in which the constants A and C are determined from the boundary conditions. This solution is equivalent to that derived previously for a non-dilatant interface (10).

Shear Socket Under Compression Loading

For this case, the boundary conditions are those presented for Equations 4-45 and 4-46 and the solution for σ_z, τ, and w_c becomes indeterminant, except in the case of a purely cohesive socket, for which only σ_z and τ may be found as:

$$\sigma_z = 4c \left(\frac{D - z}{B}\right) \tag{4-79}$$

and

$$\tau = c \tag{4-80}$$

As σ_b approaches 4c(D/B), the shaft displacements become infinite.

Complete Socket Under Compression Loading

For the case where the shaft rests on an underlying elastic material, the solution is:

$$\sigma_z = \left(\sigma_b + \frac{c}{F \tan\phi}\right) \exp[-4F \tan\phi(z/B)] - \frac{c}{F \tan\phi} \tag{4-81}$$

$$\tau = (\sigma_b F \tan\phi + c) \exp[-4F \tan\phi(z/B)] \tag{4-82}$$

and

$$w_c = w_s + w_{ct} \tag{4-83}$$

where the overall shaft compression, w_s, is given by:

$$w_s = \left(\frac{1}{E_c}\right) \left\{\left(\sigma_b + \frac{c}{F \tan\phi}\right) (1 - \exp[-4F \tan\phi(D/B)]) \left(\frac{B}{4F \tan\phi}\right) - \frac{cD}{F \tan\phi}\right\} \tag{4-84}$$

and the settlement at the tip (z = D) is:

$$w_{ct} = \left(\frac{\pi}{2}\right) \left(\frac{1 - \nu_b^2}{E_b}\right) \left\{\left(\sigma_b + \frac{c}{F \tan\phi}\right) \exp[-4F \tan\phi(D/B)] - \frac{c}{F \tan\phi}\right\} \frac{B}{2} \tag{4-85}$$

The proportion of load transmitted to the tip is given by:

$$\frac{\sigma_{tip}}{\sigma_b} = \frac{Q_{tip}}{Q_c} = \left(1 + \frac{c}{\sigma_b F \tan\phi}\right) \exp[-4F \tan\phi(D/B)] - \frac{c}{\sigma_b F \tan\phi} \tag{4-86}$$

For a purely frictional interface, these equations reduce to:

$$\sigma_z = \sigma_b \exp[-4F \tan\phi(z/B)] \tag{4-87}$$

$$\tau = \sigma_b F \tan\phi \exp[-4F \tan\phi(z/B)] \tag{4-88}$$

$$w_s = \left(\frac{\sigma_b}{E_c}\right) \left(\frac{1}{2F \tan\phi}\right) \{1 - \exp[-4F \tan\phi(D/B)]\} \frac{B}{2} \tag{4-89}$$

$$w_{ct} = \left(\frac{\pi}{2}\right) \left(\frac{1 - \nu_b^2}{E_b}\right) \{\sigma_b \exp[-4F \tan\phi(D/B)]\} \frac{B}{2} \tag{4-90}$$

$$\frac{\sigma_{tip}}{\sigma_b} = \frac{Q_{tip}}{Q_c} = \exp[-4F \tan\phi(D/B)] \tag{4-91}$$

For a purely cohesive interface, these equations become:

$$\sigma_z = \sigma_b - 4c(z/B) \tag{4-92}$$

$$\tau = c \tag{4-93}$$

$$w_s = \left\{\left(\frac{\sigma_b}{E_c}\right) - \left(\frac{c}{E_c}\right) \left(\frac{2D}{B}\right)\right\} D \tag{4-94}$$

$$w_{ct} = \left(\frac{\pi}{2}\right) \left(\frac{1 - \nu_b^2}{E_b}\right) \{\sigma_b - 4c\left(\frac{D}{B}\right)\} \frac{B}{2} \tag{4-95}$$

and

$$\frac{\sigma_{tip}}{\sigma_b} = \frac{Q_{tip}}{Q_c} = 1 - 4\left(\frac{c}{\sigma_b}\right) \left(\frac{D}{B}\right) \tag{4-96}$$

Shear Socket in Uplift

In the absence of dilation, the changes in radial normal stress at the interface are entirely because of Poisson's ratio and are tensile. Therefore, if the in-situ normal stresses on the shaft are insignificant (a conservative assumption), then the interface can have no frictional component of strength. This implies that, at slip, the displacements are indeterminant and that σ_z and τ are given by:

$$\sigma_z = -4c \left(\frac{D - z}{B}\right) \tag{4-97}$$

and

$$\tau = c \tag{4-98}$$

Complete Socket in Uplift

For this case, it is prudent to ignore the tensile tip resistance, and therefore the solution is the same as for a shear socket. The displacements are indeterminant and the stresses are given by Equations 4-97 and 4-98.

RIGID SHAFTS

In practice, it is common for the stiffness of the shaft to be larger than that of the host rock ($E_c >> E_r$). Shafts of this type may behave rigidly when subjected to axial loading and, for such cases, the governing equations presented previously may be simplified.

Shear Socket Under Compression Loading

The initial elastic response of this type of foundation is described by Equation 4-20, from which it is clear that the axial stiffness is proportional to $\tan[\mu D]$, with μD given as:

$$(\mu D)^2 = [\frac{4}{\zeta(1 + \nu_r)}] \ (\frac{E_r}{E_c}) \ (\frac{D}{B})^2 \tag{4-99}$$

in which

$$\zeta = ln[5(1 - \nu_r)D/B] \tag{4-100}$$

and

$$\lambda = E_c/G_r \tag{4-101}$$

For small values of μD, the function $\tanh[\mu D]$ is closely approximated by μD, in which case the elastic stiffness of the shear socket can be approximated as:

$$\frac{Q_c}{w_c} = (\frac{\pi}{(1 + \nu_r)\zeta})E_r D \tag{4-102}$$

Equation 4-102 will be accurate to within 10 percent whenever μD is less than about 0.5, or whenever:

$$\left(\frac{E_c}{E_r}\right)\left(\frac{B}{2D}\right)^2 \geq 1 \tag{4-103}$$

For all practical purposes, Equation 4-103 can be considered as the definition of rigidity with respect to axial compression. A further implication of shaft rigidity is that the elastic stress transfer is linear down the shaft, so that the shear stresses developed at the interface are constant with depth.

If it is also assumed that the shear stress distribution remains constant at full slip, and that $E_c >> E_r$, then the load-displacement relationship for the butt of the shaft, for a dilatant, cohesive-frictional interface, can be written simply as:

$$w_c = R_1\left(\frac{Q_c}{\pi E_r D}\right) - R_2\left(\frac{B}{2}\right) \tag{4-104}$$

in which

$$R_1 = (1 + \nu_r)\left(\zeta + \frac{1}{2\ \tan\phi\ \tan\psi}\right) \tag{4-105}$$

and

$$R_2 = \frac{(1 + \nu_r)}{\tan\phi\ \tan\psi}\left(\frac{c}{E_r}\right) \tag{4-106}$$

Complete Socket Under Compression Loading

For a rigid shaft in full contact at the tip, the elastic stiffness is given by:

$$\frac{Q_c}{w_c} = \frac{1}{(1 - \nu_b^2)} E_b B + \left(\frac{\pi}{\zeta}\right)\left(\frac{D}{B}\right)\frac{E_r B}{(1 + \nu_r)} \tag{4-107}$$

and the proportion of the applied loading transmitted to the tip is:

$$\frac{Q_{tip}}{Q_c} = \frac{\left(\frac{4}{1 - \nu_b}\right)\left(\frac{G_b}{G_r}\right)}{\left(\frac{4}{1 - \nu_b}\right)\left(\frac{G_b}{G_r}\right) + \left(\frac{2\pi}{\zeta}\right)\left(\frac{2D}{B}\right)} \tag{4-108}$$

Once full slip of the shaft has occurred, the load-displacement relationship becomes:

$$w_c = R_4\left(\frac{2Q_c}{\pi E_r B}\right) - R_5\left(\frac{B}{2}\right) \tag{4-109}$$

in which

$$R_5 = \frac{R_2 R_3 (2D/B)}{R_3(2D/B) + R_1} \tag{4-110}$$

$$R_4 = \frac{R_3 R_1}{R_3(2D/B) + R_1} \tag{4-111}$$

and

$$R_3 = \left(\frac{\pi}{2}\right)(1 - \nu_b^2)\left(\frac{E_r}{E_b}\right) \tag{4-112}$$

with the load transmitted to the tip given by:

$$\frac{Q_{tip}}{Q_c} = \frac{R_1}{R_1 + R_3(2D/B)} - \left[\frac{R_6(2D/B)}{R_1 + R_3(2D/B)}\right]\left(\frac{\pi B D c}{Q_c}\right) \tag{4-113}$$

in which

$$R_6 = (1 + \nu_r)/(2 \tan\phi \tan\psi) \tag{4-114}$$

Uplift Loading Applied to Shaft Butt in Shear Socket

In this case, the elastic response of the shaft butt is given by Equation 4-102. Once full slip has occurred, the displacement is given by:

$$w_u = R_1\left(\frac{Q_u}{\pi E_r D}\right) + R_2\left(\frac{B}{2}\right) \tag{4-115}$$

For this case, Q_u should be given as a negative quantity. A negative value of w_u indicates an upward displacement.

Uplift Loading Applied to Shaft Tip in Shear Socket

The uplift displacement at the shaft butt in this case can be calculated from:

$$\frac{Q_u}{w_u} = -\left(\frac{\pi}{(1 + \nu_r)\zeta}\right) E_r D \tag{4-116}$$

in which the negative sign indicates an upward displacement. Q_u is the compressive load applied to the shaft tip to cause the uplift and is assigned a positive value.

After full slip has occurred, the load-displacement relationship becomes:

$$w_u = -R_1\left(\frac{Q_u}{\pi E_r D}\right) + R_2\left(\frac{B}{2}\right) \tag{4-117}$$

in which R_1 and R_2 have been defined previously (Equations 4-105 and 4-106). Again, a negative sign indicates upward displacement.

Shaft Jacked Upward

The elastic displacement at the butt of a rigid shaft loaded in this manner can be calculated from:

$$\frac{w_u}{P} = \left[\left(\frac{E_r}{E_b}\right) \frac{(1 - \nu_b^2)}{2} \left(\frac{2D}{B}\right) - \frac{(1 + \nu_r)\zeta}{\pi}\right] \frac{1}{E_r D} \tag{4-118}$$

in which P is the load applied by the jack at the shaft tip. Once full slip occurs, the displacement becomes:

$$w_u = \left[\frac{(1 - \nu_b^2)}{2} \left(\frac{E_r}{E_b}\right) \left(\frac{2D}{B}\right) - \frac{R_1}{\pi}\right] \left(\frac{P}{E_r D}\right) + R_2\left(\frac{B}{2}\right) \tag{4-119}$$

General Remarks on Rigid Shafts

It is worth noting that, for rigid shafts, the effects of Poisson's ratio of the

shaft concrete, ν_c, are negligible. This can be demonstrated by examining the relationship between the radial and vertical stresses in the shaft at the interface. It can be shown from Equations 4-28 and 4-29 that, during the elastic behavior of the shaft, the radial stress is:

$$\sigma_r = [\frac{(E_r/E_c)\ \nu_c}{(1 + \nu_r) + (1 - \nu_c)\ (E_r/E_c)}]\sigma_z \qquad (4\text{-}120)$$

For a rigid shaft, $E_c >> E_r$ and therefore $\sigma_r << \sigma_z$, which shows that the radial stress acting on the interface is negligible. This fact has several important implications. First, it means that the strength mobilized at the initiation of slip of the shaft is almost entirely cohesive in nature, because at this stage there is almost no normal stress acting to generate frictional resistance. Second, as the shaft slips, the changes in σ_r occur almost entirely because of dilation at the interface. For these reasons, the response of a shaft, employing side resistance only, is essentially the same in uplift as it is under compression loading.

By definition, a rigid shaft will not shorten from the applied axial loading, and therefore the vertical displacements of the butt and tip of the shaft will be the same.

COMPARISONS WITH FINITE ELEMENT SOLUTIONS

The adequacy of the equations presented above can be demonstrated by comparing them with chart solutions, obtained using a nonlinear finite element analysis (17, 18). Comparisons are made for two different cases: the first uses parameters selected to represent a low relative stiffness of the shaft-rock mass system (D/B = 10, E_c/E_r = 10, E_b/E_r = 1), while the second represents a large relative stiffness (D/B = 2, E_c/E_r = 100, E_b/E_r = 1). In all cases, the Poisson's ratio of the rock mass was 0.3 and that of the shaft was 0.15. The interface is assumed to be purely cohesive and non-dilatant. The predictions of the load-displacement response are presented in Figures 4-12 and 4-13, and the predictions of the tip load are given in Figures 4-14 and 4-15. The overall agreement between the simple equations presented herein and the numerical solutions from finite element analysis is very good. However, a few points are worthy of further mention.

In the strictest sense, the simple Equations 4-17 and 4-83 to 4-85 contain no means for predicting the load-displacement response between the occurrence of first slip and full slip of the shaft, but the numerical results indicate that the progression

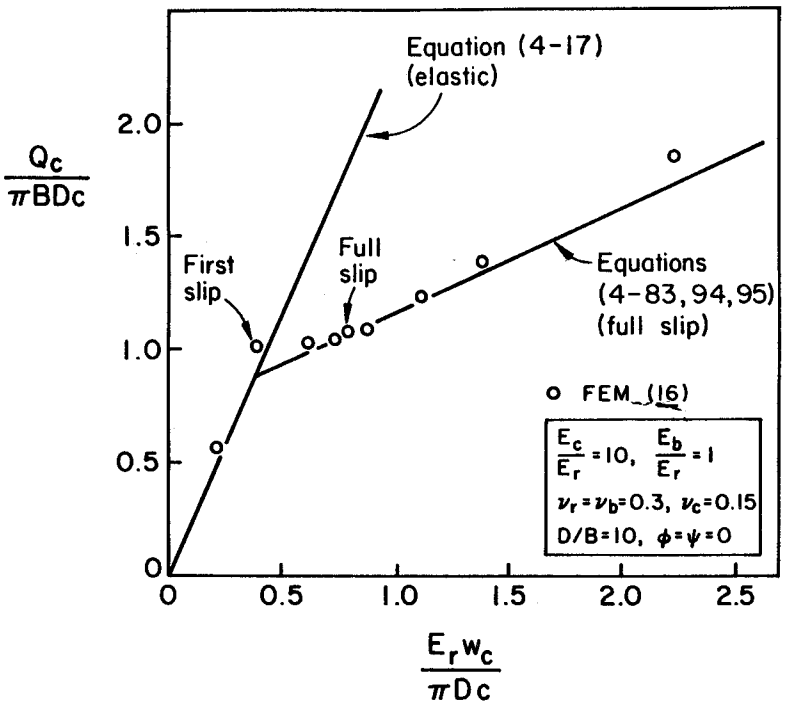

Figure 4-12. Dimensionless Load-Settlement Relationships for Cohesive Socket (Example 1)

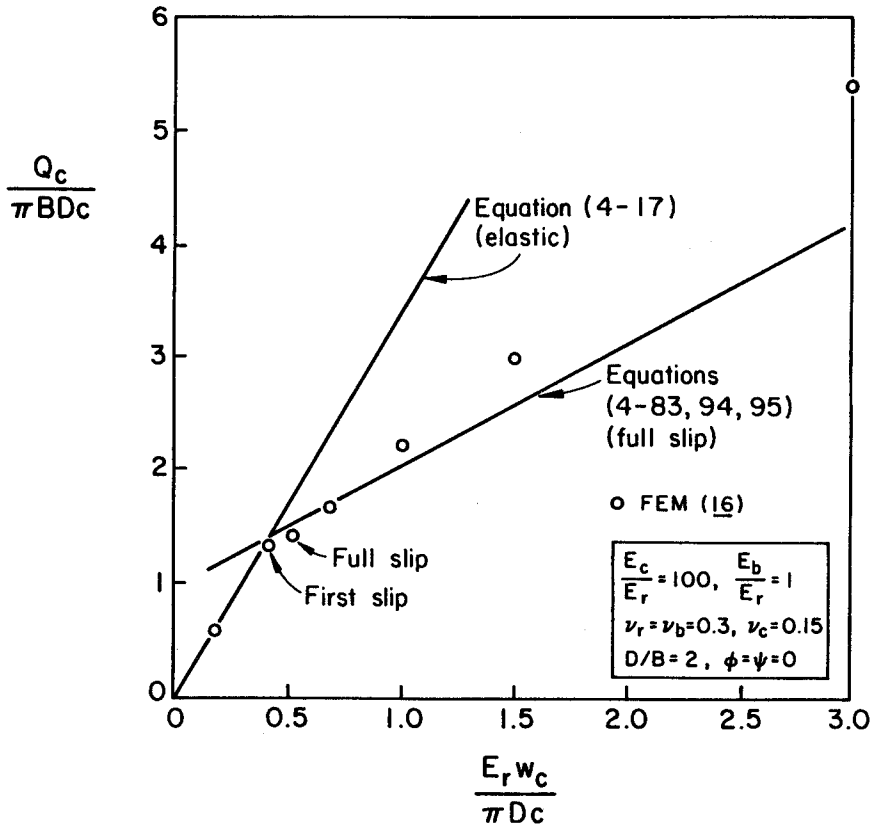

Figure 4-13. Dimensionless Load-Settlement Relationships for Cohesive Socket (Example 2)

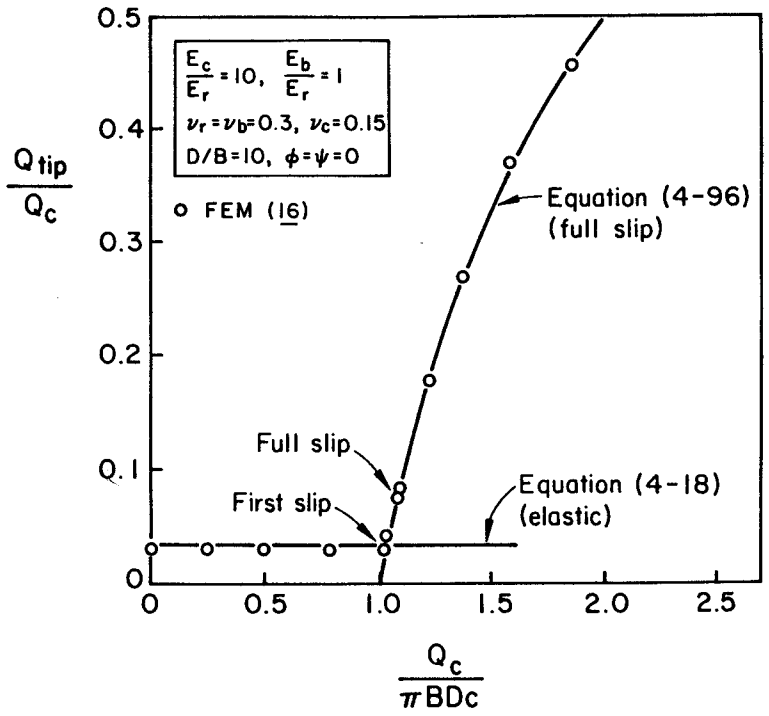

Figure 4-14. Load Transmitted to Tip of Shaft for Cohesive Socket (Example 1)

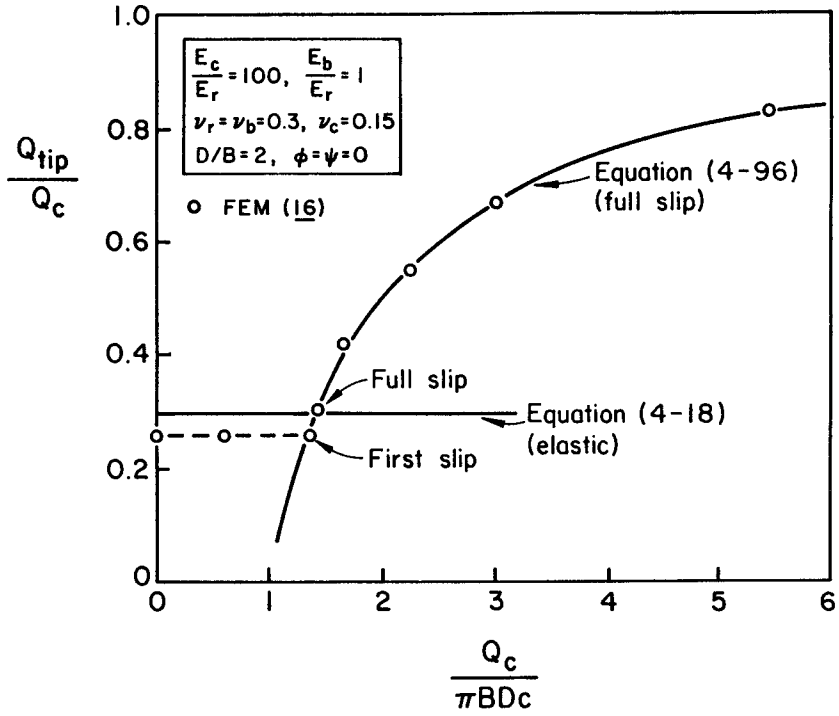

Figure 4-15. Load Transmitted to Tip of Shaft for Cohesive Socket (Example 2)

of slip along the socket takes place over a relatively small interval of displacement. (Finite element predictions of first slip and full slip have been indicated on Figures 4-12 through 4-15). Therefore it seems reasonable, at least for most practical cases, to ignore the small region of the curves corresponding to progressive slip and to assume that the load-displacement relationship is bilinear, with the slope of the initial portion given by Equation 4-17 and the slip portion given by Equation 4-83. This is a simplification, but Figures 4-12 and 4-13 indicate that it is reasonably accurate for a wide range of shaft types.

Figures 4-12 and 4-13 also indicate that Equation 4-83 tends to overpredict the settlement once full slip has occurred. The discrepancies are not large and, from a design point of view, it is fortunate that Equation 4-83 appears to be conservative. The overprediction of settlement is worse for the case of a relatively stiff, stubby shaft (Figure 4-13), and reasons for this can be suggested. In the derivation of Equation 4-83, it was assumed that the shaft and its tip could be considered separately. With regard to the structural stiffness of the overall system, this assumption is likely to lead to greater errors in the case of stiffer, stubbier shafts because greater interaction may take place between the shaft and the tip. This interaction will give rise to the transfer of significant shear stresses on the horizontal plane in the rock mass at the shaft tip. These shear stresses will tend to constrain the rock mass beneath the shaft tip and reduce the settlement component of the tip to a value smaller than that predicted for a rigid punch acting on the surface of an otherwise stress-free half-space.

For design purposes, the simple equations presented above should give a reasonable first approximation for many shaft-rock mass systems, and therefore should prove to be convenient in design for carrying out preliminary studies of the effects of variations in a number of the key parameters. In the following, consideration of some of these effects is presented.

TRENDS IN BEHAVIOR

The comparisons made above between the finite element and closed form solutions were for cases where the strength of the interface could be regarded as purely cohesive and non-dilatant, and where the shear strength was unchanged by any slip produced at the interface. These conditions rarely occur in the field. The initial "bond" strength along the interface may have both cohesive and frictional components. Once rupture occurs, it is likely that the cohesive component of the strength may diminish, dilation will occur, and after sufficient slip has taken place, the interface shear resistance will become purely frictional and dilation

can cease.

Purely Frictional Sockets in Compression Loading

Consider the hypothetical case where the resistance along the interface is purely frictional, with an angle of friction ϕ that remains constant throughout the loading, and where the shaft tip rests directly on the bottom of the socket. Such a model will produce conservative predictions, because it corresponds to a shaft which fits perfectly into the socket in the rock mass, but nowhere along the shaft is there any bonding between the rock mass and the shaft. It also will be conservative to assume that initially there is no transfer of normal stress across the interface between the shaft and the rock and, at least for shallow sockets, this will closely model reality. Under these circumstances, the entire shaft will be on the verge of slipping as soon as compression loading is applied to the shaft butt. A shaft in this kind of socket will exhibit no elastic behavior, but will slip from the commencement of loading. The load-settlement relationship in this case is obtained by substituting z = 0 and c = 0 into Equations 4-54 to 4-56. Some typical solutions have been plotted in Figures 4-16 and 4-17 for cases where E_c/E_r = 10, E_b/E_r = 1, $\nu_r = \nu_b = 0.3$, $\nu_c = 0.15$, $\phi = 30°$, and c = 0. Solutions are plotted for a range of values of D/B and for a number of values of the dilation angle ψ. Dimensionless settlements are plotted in Figure 4-16 and the proportion of the applied compression loading transmitted to the tip, Q_{tip}/Q_c, is plotted in Figure 4-17. Also shown is the elastic solution for a perfectly bonded (no slip) interface. These results indicate that only a small rate of dilation is required to cause a marked increase in stiffness of the shaft under compression loading. A dilatancy angle of $\psi = 30°$ produces behavior approaching the stiffness of a fully bonded (elastic) socket.

If no dilatancy occurs as interface slip takes place ($\psi = 0$), the response of the shaft also is linear, but its stiffness is less than that for a fully bonded socket. The response of this type of shaft to compression loading is predicted by Equations 4-87 to 4-91, from which the butt displacement, w_c, is given by:

$$\frac{E_r w_c}{\sigma_b B} = \left(\frac{E_r}{E_c}\right)\left(\frac{1}{4F\tan\phi}\right)\{1 - \exp[-4F\tan\phi\,(D/B)]\}$$

$$+ \left(\frac{\pi}{4}\right)(1 - \nu_b^2)\left(\frac{E_r}{E_b}\right)\exp[-4F\tan\phi\,(D/B)] \qquad (4\text{-}121)$$

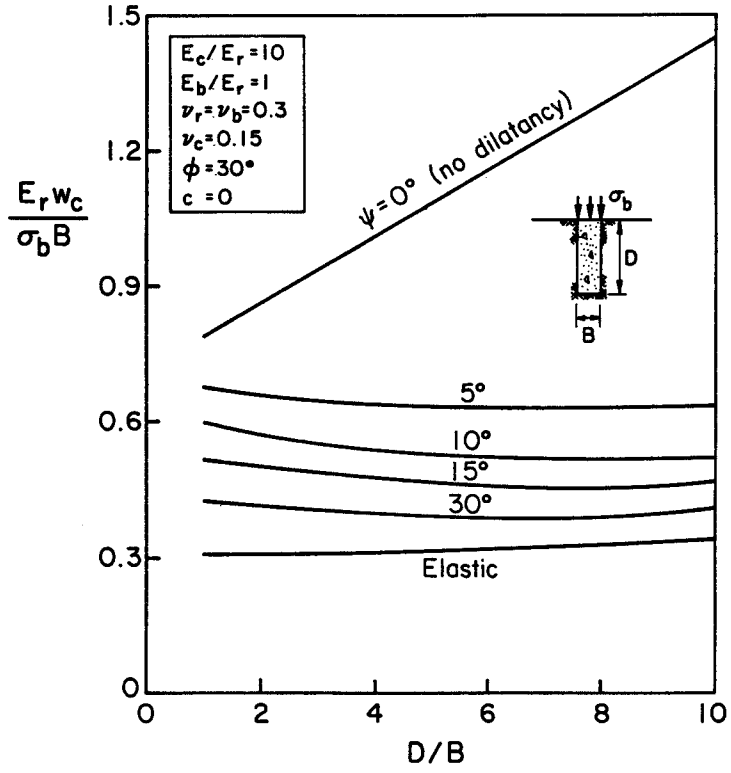

Figure 4-16. Settlement of Purely Frictional Socket with Dilatancy

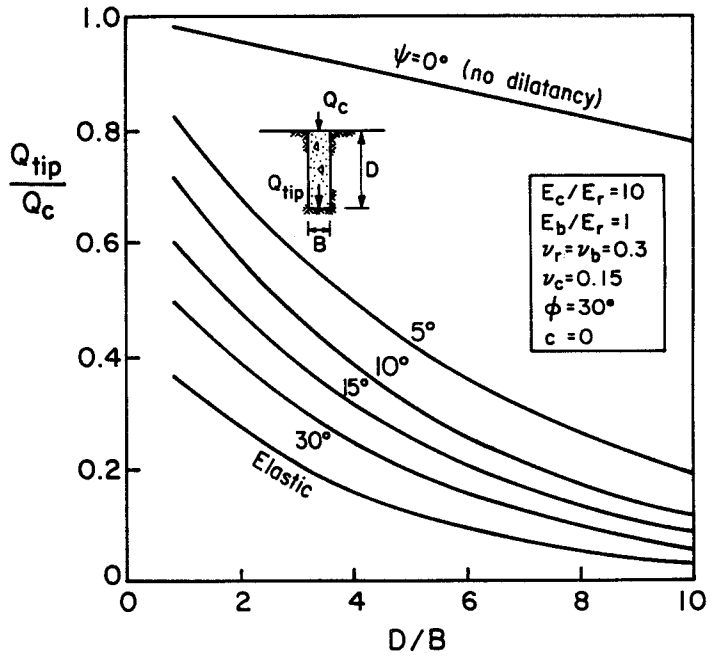

Figure 4-17. Load Distribution in Purely Frictional Socket with Dilatancy

This equation is plotted in Figure 4-18 for a number of sockets having the following properties: $E_c/E_r = 10$, $E_b/E_r = 1$, $\nu_b = \nu_r = 0.3$ and $\nu_c = 0.15$. Results are given for three different values of the interface friction angle, ϕ, and for a range of slenderness ratios (D/B). It can be seen that the stiffness of most of these frictional, but non-dilatant, sockets is in the range from about 20 to 40 percent of the stiffness for an equivalent, perfectly bonded, elastic socket. It is also interesting (and perhaps surprising) to note that there is only a minor dependence of the stiffness of the non-dilatant, frictional shaft on the interface friction angle. This behavior can be understood better when the load distributions predicted by Equation 4-91 are plotted, as in Figure 4-19. For the typical case of $E_c/E_r = 10$ and $\nu_c = 0.15$, a large proportion of the shaft loading is actually transmitted to the shaft tip, regardless of the friction angle, and therefore the predominant contribution to the overall settlement comes from displacement of the rock mass below the shaft tip. It should be remembered also that the load transferred to the tip is a function of the modulus ratio, E_c/E_r, and the Poisson's ratio of the shaft material, ν_c. Increasing E_c/E_r will cause a greater proportion of the load to be transmitted to the tip, while increasing ν_c will cause less because the radial normal stress transmitted across the shaft-rock interface increases, and therefore the greater will be the proportion of loading carried in side shear. A comparison of Figures 4-17 and 4-19 demonstrates the significance of interface dilation on the load transfer in a socket, because the lower the rate of dilatancy, the more compressive load is transmitted to the shaft tip.

Cohesive-Frictional Interface in Compression Loading

Consider now those cases where cohesion is assumed at the interface, and where the cohesion remains constant as slip takes place, but no dilation occurs at the interface ($\psi = 0$).

Some predictions of the load-displacement response of complete sockets subjected to compression loading are given in Figure 4-20. The case where $E_c/E_r = 100$ and D/B = 5 is considered, and typical values of the various parameters that might occur in practice have been used to add dimensions to the predictions. Curves have been plotted for sockets in which c = 0, 0.5, and 1 MN/m^2 (0, 71, and 143 psi) and ϕ = 30° and $\psi = 0°$. For the sockets where c > 0, the response is bilinear, following first the predictions for a linear elastic (fully bonded) socket and then the prediction based on the full slip analysis. For the full slip condition, Equations 4-83, 4-94, and 4-95 predict a linear relationship between load and settlement, with the slope of this line the same as that predicted for a purely frictional interface (Equations 4-89 and 4-90). This slope is independent of the value of the

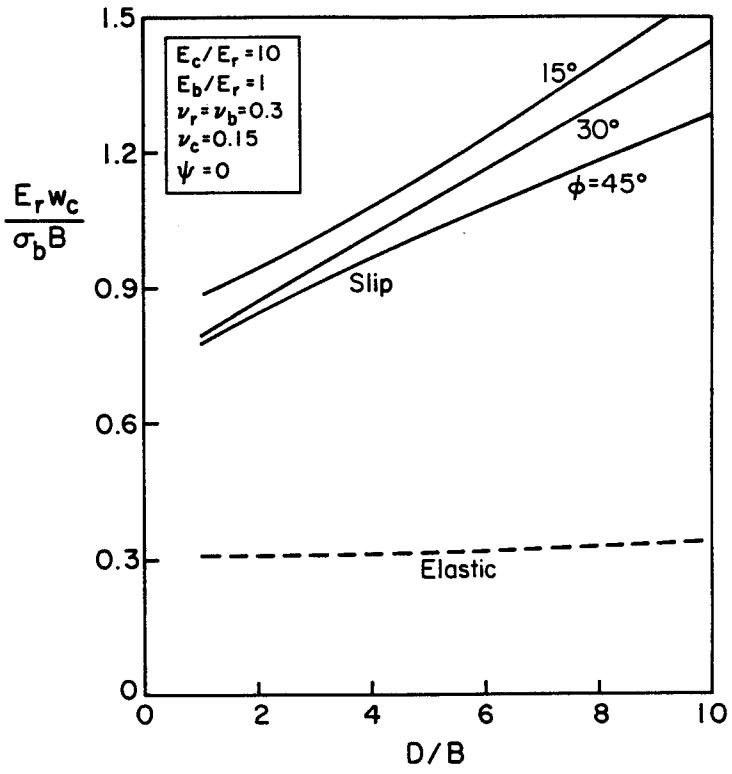

Figure 4-18. Settlement of Purely Frictional Socket without Dilatancy

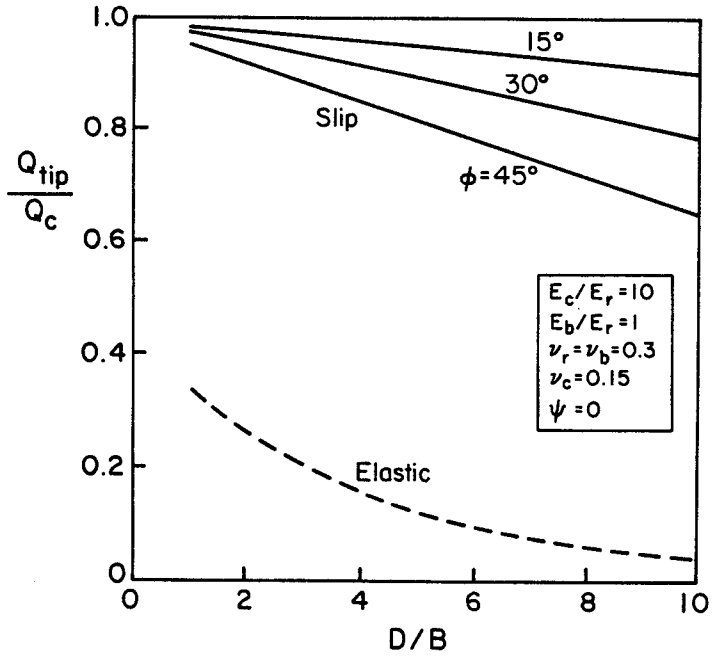

Figure 4-19. Load Distribution in Purely Frictional Socket without Dilatancy

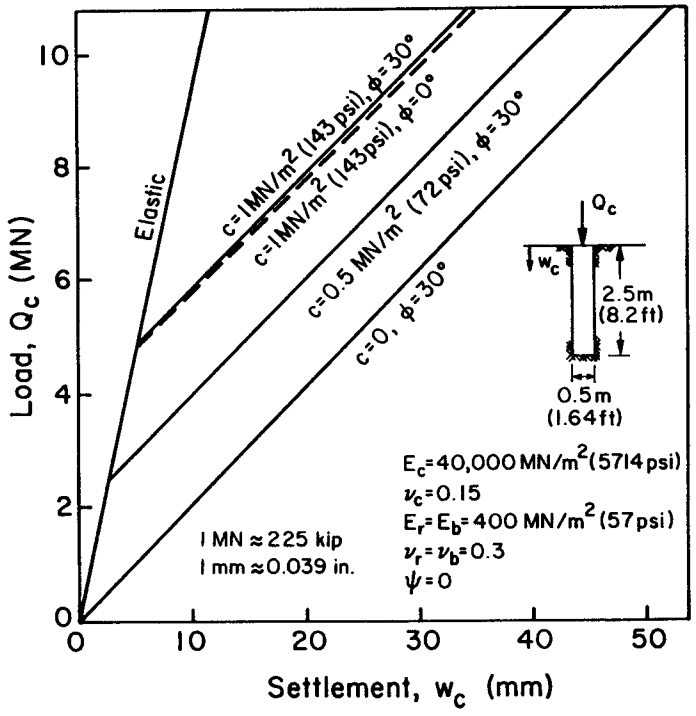

Figure 4-20. Typical Behavior of Cohesive-Frictional Socket

interface cohesion, and therefore the curves corresponding to the three c values are all parallel.

Also plotted on Figure 4-20 is the curve predicted for the case where c = 1 MN/m^2 (143 psi) and $\phi = 0°$. It can be seen that this purely cohesive socket has almost the same load-settlement relationship as that of a socket with c = 1 MN/m^2 (143 psi) and $\phi = 30°$, i.e., the behavior once slip has occurred is almost independent of the value of ϕ. It should be noted, however, that this is true only for very stiff sockets, such as those with $E_c/E_r = 100$ and D/B = 5, because as the ratio E_c/E_r becomes large and the slenderness ratio D/B becomes small, the curves for cohesive-frictional and purely cohesive interfaces are practically the same, i.e., the cohesive effects tend to dominate the frictional effects for very stiff, stubby sockets.

Bounds on Real Behavior in Compression Loading

The analytical solutions presented herein, for the load-settlement response of socketed shafts in compression loading, assume a cohesive-frictional shear strength at the socket walls with the possibility of dilatancy contributing to the shear

resistance. The analysis can only be applied to cases in which the strength parameters and the dilatancy are considered constant, independent of the magnitude of the relative shear displacement at the interface. These assumptions are reasonable for small slip displacements, but they will tend to be unrealistic as larger slip displacements occur. In particular, it is probable that the cohesive component of the strength will be diminished after the bond between the concrete and rock is ruptured. Similarly, it is likely that the tendency for the interface to dilate with shearing will abate as the shearing progresses. With the present analysis, it is not possible to model this gradual reduction of cohesive strength and dilatancy exactly. However, it is possible to use the analysis to produce bounds on the likely load-settlement response, as illustrated schematically in Figure 4-21. The analysis assuming $c = 0$ and $\psi = 0$ should provide a lower bound on the mobilized socket strength and an upper bound on the shaft displacements. Conversely, with the selection of appropriate values of c, ϕ, and ψ, the curve corresponding to the c, ϕ, ψ analysis should provide an upper bound on mobilized strength and a lower bound on the settlements. The actual load-settlement curve is likely to fall between these limits; exactly where it falls depends on the brittleness and the dilatancy of the interface. In an extreme case, if the loss of cohesive strength is rapid, then a curve like OABC could be observed. If the interface exhibits a plastic or work-hardening shear response (which is more likely in well-constructed, dilatant sockets), then the shaft behavior may be more like that respresented by the curve OAF. At larger displacements, the sockets should tend toward a purely frictional, non-dilatant behavior.

Cohesive-Frictional Sockets in Uplift

When the shaft is subjected to uplift loads, the tensile tip resistance normally is ignored. The behavior in this case is illustrated in Figure 4-22 for a relatively rigid shaft with $D/B = 5$, $\nu_r = 0.25$, and interface friction angle $\phi = 30°$. It can be seen that the load-displacement response is initially linear elastic. Full slip of the shaft occurs when $\tau = c$ and therefore $Q_u = -\pi BDc$. A negative value of Q_u denotes tensile load, and a negative value of w_u denotes an upward displacement. For uplift conditions, the load to commence full slip is independent of the angle of friction, because tensile normal stresses are induced at the shaft-rock interface from Poisson's ratio effects, and therefore the interface initially has no frictional resistance.

Once slip has commenced, the stiffness of the shaft is a function of the interface dilation angle, ψ, as illustrated for typical values in Figure 4-22. According to this simple model, the stiffness corresponding to full slip is constant, which

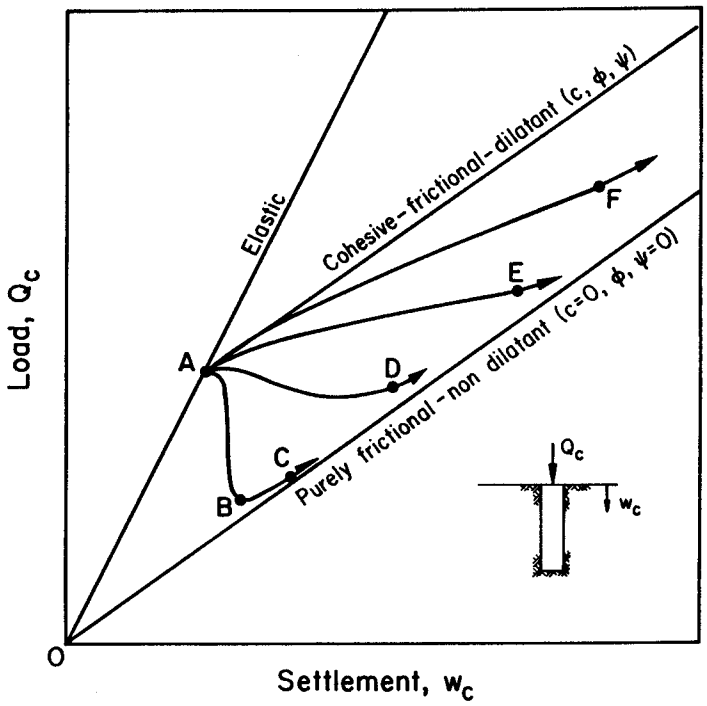

Figure 4-21. Schematic Representation of Socket Behavior

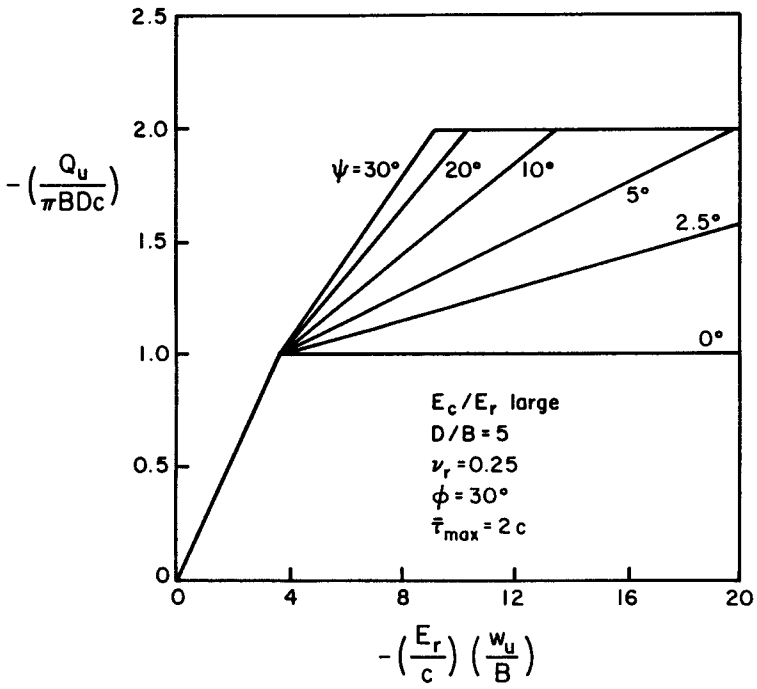

Figure 4-22. Uplift of Relatively Rigid Shaft in Cohesive-Frictional Socket

follows from the assumption of constant c, ϕ, and ψ. The slip response is stiffer for larger values of ψ. In reality, the dilation must cease after sufficient slip displacement has occurred, and ultimately a maximum uplift load will be reached. The value of this ultimate load is given by $Q_u = \pi BD\bar{\tau}_{max}$, in which $\bar{\tau}_{max}$ is the peak unit side shear resistance. In Figure 4-22, the case of $\bar{\tau}_{max} = 2c$ is given.

OVERLYING SOIL LAYER

Consider now the case where a layer of soil overlies the rock and the axial loading is defined at the surface of the soil, as in Figure 4-23a. To be explicit, only the case of compression loading will be dealt with here. However, the same principles would also apply to the case of uplift loading.

In this analysis, it is assumed that the complete distribution of soil shearing resistance on the shaft is known. The axial displacement, w_c, at the groundline then may be determined after a suitable structural decomposition of the shaft and its loading, as shown in Figure 4-23b. The portion of the shaft lying within the soil can be analyzed as a free-standing column subjected to known loading, and the displacements of point A at the groundline relative to point B at the soil-rock interface, w_{AB}, can be determined simply. The axial load Q_o transmitted to the level of the rock surface can be computed from statics, and the displacement at this level, w_o, can be computed by the methods described previously in this section. The groundline displacement then can be calculated by superposition as:

$$w_c = w_o + w_{AB} \tag{4-122}$$

If Equation 4-122 is to be used successfully, the distribution of shear stress acting along the shaft-soil interface must be known. As a worst case, the presence of the soil could be ignored completely, and then it would be assumed that the full applied loading, Q_c, is transmitted to the level of the rock surface ($Q_o = Q_c$). For this condition, the displacement w_{AB}, is given by:

$$w_{AB} = \frac{4\ Q_c\ D_s}{\pi B^2\ E_c} \tag{4-123}$$

This approach may be considered overly conservative, and therefore two further cases are discussed below. In both, it is assumed that a limiting soil shear resistance has developed along the shaft. For relatively shallow soil deposits and relatively large axial loads, the assumption of a limiting soil resistance is

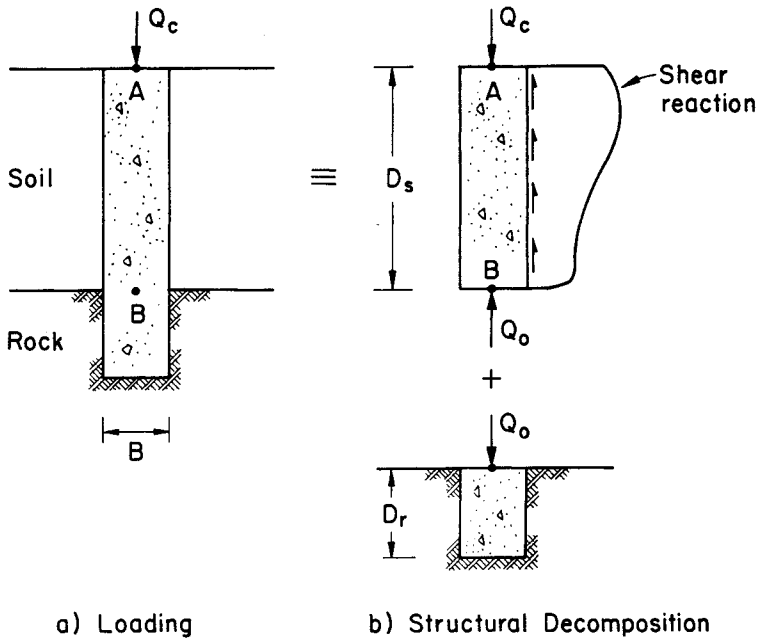

Figure 4-23. Rock Socketed Shaft in Compression with Overlying Soil Layer

likely to be realistic.

Constant Soil Resistance

Consider first the case where the soil shearing resistance is constant with depth, so that a shear stress τ_f is developed along the shaft. For shafts through cohesive soil layers, a total stress approach can be adopted and therefore τ_f can be written as:

$$\tau_f = \alpha \, s_u \tag{4-124}$$

in which s_u = undrained shear strength of the soil and α = adhesion factor. Recommendations for α have been given elsewhere (29).

For this form of shearing resistance, the axial load transmitted to the surface of the rock is given by:

$$Q_o = Q_c - \pi B D_s \tau_f \tag{4-125}$$

and the relative displacement, w_{AB}, is:

$$w_{AB} = \left(\frac{4}{\pi B^2 E_c}\right)\left(Q_c D_s - \pi \frac{B}{2} D_s^2 \tau_f\right) \quad (4\text{-}126)$$

Soil Resistance Increasing Linearly with Depth

Consider now the case where the soil shearing resistance τ_f increases linearly with depth below the soil surface as:

$$\tau_f = \rho z \quad (4\text{-}127)$$

This form of variation may be applicable in cohesionless soils. For example, in a dry, frictional soil of unit weight γ, the shearing resistance along the interface can be written as:

$$\tau_f = K\,\bar{\sigma}_v \tan\delta = K\,\gamma\,z\,\tan\delta \quad (4\text{-}128)$$

so that:

$$\rho = K\gamma \tan\delta \quad (4\text{-}129)$$

In these equations, $\bar{\sigma}_v$ = vertical effective stress, K = coefficient of horizontal soil stress acting on the shaft interface, and δ = interface friction angle. Suggested values of K have been given elsewhere (29, 30).

For this form of shearing resistance, the axial load transmitted to the surface of the rock is:

$$Q_o = Q_c - \pi \frac{B}{2} D_s^2 \rho \quad (4\text{-}130)$$

and the relative displacement is:

$$w_{AB} = \left(\frac{4}{\pi B^2 E_c}\right)\left[Q_c D_s - \left(\frac{\pi}{6}\right) B D_s^3 \rho\right] \quad (4\text{-}131)$$

SUMMARY

Analyses have been presented which allow the prediction of the load-displacement behavior of shafts socketed into rock and subjected to either axial uplift or

compression loading. The analyses are based on a simple model of an elastic shaft embedded in an elastic rock mass, where the behavior at the interface between the two materials may be elasto-plastic. Relatively simple closed form expressions have been derived for the cases of: (1) no slip at the interface and (2) slip occurring along the entire length of the socket (the so-called "full slip" condition).

Equations have been presented to describe the behavior for many of the possible combinations of material parameters and loading cases. For reference, the equation numbers corresponding to the various cases presented have been summarized in Figures 4-24 and 4-25.

Comparisons have been made between the predictions of the closed form expressions and previously published solutions obtained using the finite element method. Agreement was found between the analytical and numerical solutions for both the no slip and full slip cases. The agreement is satisfactory for design purposes, with the closed form solution having the attraction of ease of use.

Indications also have been given of how the predictions of the load-displacement response of the shaft should be altered to allow for the presence of a soil layer overlying the rock mass.

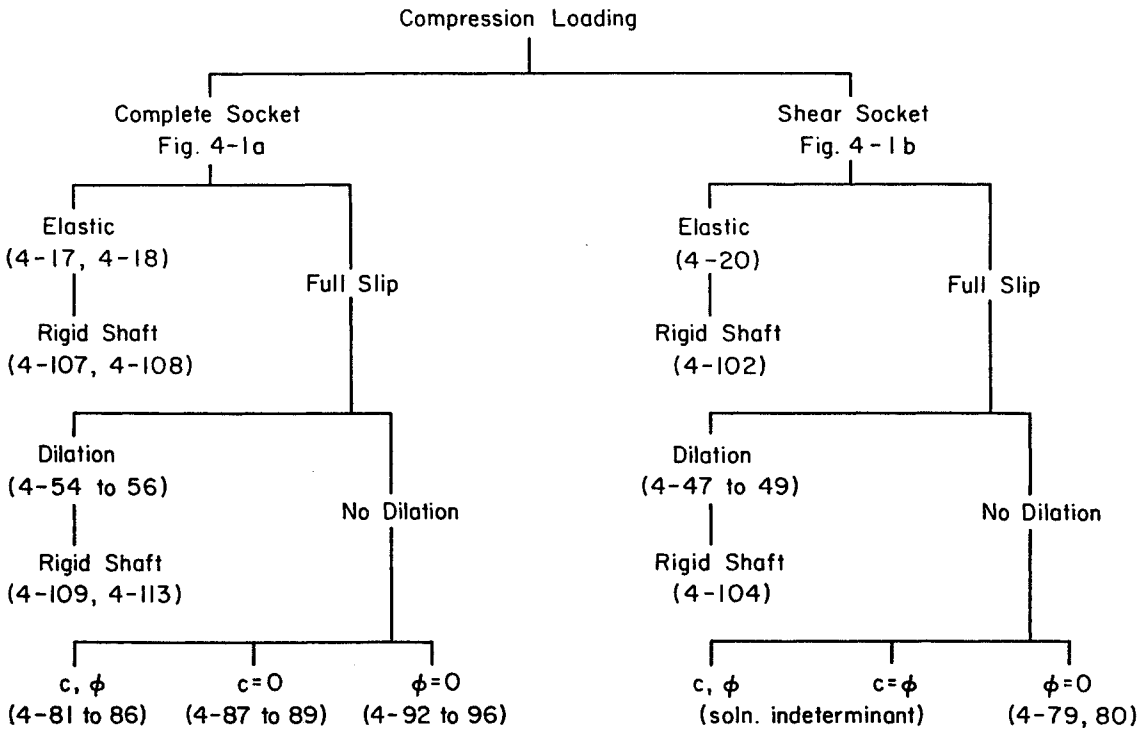

Figure 4-24. Summary of Solutions for Sockets in Compression Loading

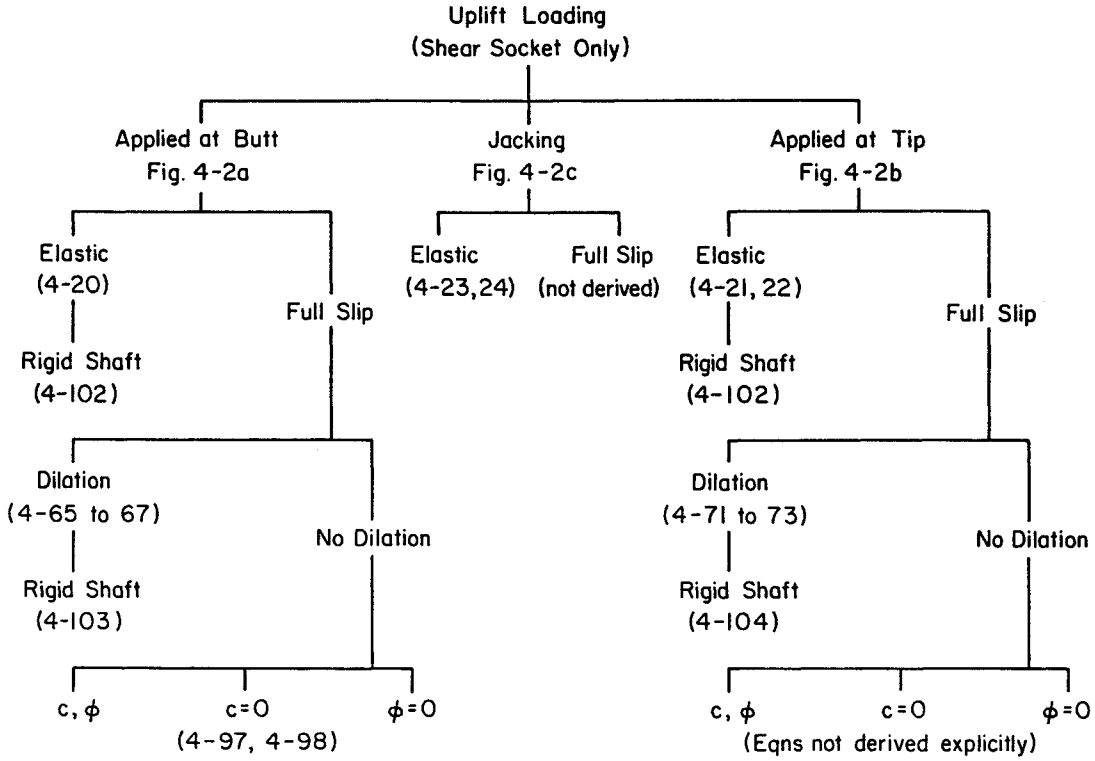

Figure 4-25. Summary of Solutions for Shear Sockets in Uplift Loading

REFERENCES

1. Donald, I. B., Sloan, S. W. and Chiu, H. K., "Theoretical Analyses of Rock Socketed Piles", Proceedings, International Conference on Structural Foundations on Rock, Vol. 1, Sydney, 1980, pp. 303-316.

2. Horvath, R. G., "Field Load Test Data on Concrete-to-Rock Bond Strength for Drilled Pier Foundations", Publication No. 78-07, University of Toronto, Toronto, 1978, 97 p.

3. Horvath, R. G., "Research Project Report on Load Transfer System for Rock-Socketed Drilled Pier Foundations", For the National Research Council of Canada, DSS File No. 10X5.31155-9-4420, Contract Serial No. 1SX79.000531, 1980.

4. Horvath, R. G., "Behaviour of Rock-Socketed Drilled Pier Foundations", Ph.D Dissertation, University of Toronto, Toronto, 1982.

5. Horvath, R. G., "Rock Sockets in Soft Rock: Discussion", Journal of the Geotechnical Engineering Division, ASCE, Vol. 110, No. GT10, Oct. 1984, pp. 1525-1528.

6. Horvath, R. G. and Kenney, T. C., "Shaft Resistance of Rock-Socketed Drilled Piers", Proceedings, Symposium of Deep Foundations, ASCE, New York, 1979, pp. 182-214.

7. Horvath, R. G. and Kenney, T. C., "Caissons Socketed in Sound Mica Schist: Discussion", Journal of the Geotechnical Engineering Division, ASCE, Vol. 108, No. GT7, July 1982, pp. 991-993.

8. Horvath, R. G., Kenney, T. C., and Kozicki, P., "Methods of Improving the Performance of Drilled Piers in Weak Rock", Canadian Geotechnical Journal, Vol. 20, No. 4, Nov. 1983, pp. 758-772.

9. Johnston, I. W., Donald, I. B., Bennet, A. G., and Edwards, J. W., "The Testing of Large Diameter Pile Rock Sockets with a Retrievable Test Rig", Proceedings, 3rd Australia-New Zealand Conference on Geomechanics, Vol. 1, Wellington, 1980, pp. 105-108.

10. Kulhawy, F. H. and Goodman, R. E., "Design of Foundations on Discontinuous Rock", Proceedings, International Conference on Structural Foundations on Rock, Vol. 1, Sydney, 1980, pp. 209-220.

11. Kulhawy, F. H. and Goodman, R. E., "Foundations in Rock", Chapter in Ground Engineers Reference Book, Ed. F. G. Bell, Butterworths, London, in press.

12. Ladanyi, B., "Friction and Endbearing Tests on Bedrock for High Capacity Socket Design: Discussion", Canadian Geotechnical Journal, Vol. 14, No. 1, Feb. 1977, pp. 153-155.

13. Pells, P. J. N. and Rowe, R. K., "A Design Method for Rock Socketed Piles", Symposium on Socketed Foundations on Weak Rock, Institution of Engineers, Australia, Canberra, 1981, pp. 1-12.

14. Pells, P. J. N., Rowe, R. K., and Turner, R. M., "An Experimental Investigation into Sideshear for Socketed Piles in Sandstone", Proceedings, International Conference on Structural Foundations on Rock, Vol. 1, Sydney, 1980, pp. 291-302.

15. Pells, P. J. N. and Turner, R. M., "Elastic Solutions for the Design and Analysis of Rock-Socketed Piles", Canadian Geotechnical Journal, Vol. 16, No. 3, Aug. 1979, pp. 481-487.

16. Rowe, R. K. and Armitage, H. H., "The Design of Piles Socketed into Weak Rock", Report GEOT-11-84, University of Western Ontario, London, 1984, 365 p.

17. Rowe, R. K. and Armitage, H. H., "Theoretical Solutions for Axial Deformation of Drilled Shafts in Rock", Report GEOT-3-86, University of Western Ontario, London, 1986, 27 p.

18. Rowe, R. K. and Armitage, H. H., "A Design Method for Drilled Piers in Soft Rock", Report GEOT-5-86, University of Western Ontario, London, 1986, 41 p.

19. Rowe, R. K. and Pells, P. J. N., "A Theoretical Study of Pile-Rock Socket Behavior", Proceedings, International Conference on Structural Foundations on Rock, Vol. 1, Sydney, 1980, pp. 253-264.

20. Williams, A. F., "The Design and Performance of Piles Socketed Into Weak Rock", Ph.D. Dissertation, Monash University, Melbourne, 1980.

21. Williams, A. F., Donald, I. B., and Chiu, H. K., "Stress Distributions in Rock Socketed Piles", Proceedings, International Conference on Structural Foundations on Rock, Vol. 1, Sydney, 1980, pp. 317-325.

22. Williams, A. F., Johnston, I. W., and Donald, I. B., "The Design of Sockets in Weak Rock", Proceedings, International Conference on Structural Foundations on Rock, Vol. 1, Sydney, 1980, pp. 327-347.

23. Williams, A. F. and Pells, P. J. N., "Side Resistance Sockets in Sandstone, Mudstone and Shale", Canadian Geotechnical Journal, Vol. 18, No. 4, Nov. 1981, pp. 502-513.

24. Randolph, M. F. and Wroth, C. P., "Analysis of Deformation of Vertically Loaded Piles", Journal of the Geotechnical Engineering Division, ASCE, Vol. 104, No. GT12, Dec. 1978, pp. 1465-1488.

25. Farmer, I. W., "Stress Distribution Along a Resin Grouted Anchor", International Journal of Rock Mechanics and Mining Sciences, Vol. 12, No. 11, Nov. 1975, pp. 347-351.

26. Randolph, M. F., "A Theoretical Study of the Performance of Piles", Ph.D. Dissertation, University of Cambridge, Cambridge, 1977, 260 p.

27. Poulos, H. G. and Davis, E. H., Elastic Solutions for Soil and Rock Mechanics, John Wiley and Sons, New York, 1974, 411 p.

28. Davis, E. H., "Theories of Plasticity and the Failure of Soil Masses", Ch. 6 in Soil Mechanics: Selected Topics, Butterworths, London, 1968, pp. 341-380.

29. Stas, C. V. and Kulhawy, F. H., "Critical Evaluation of Design Methods for Foundations Under Axial Uplift and Compression Loading", Report EL-3771, Electric Power Research Institute, Palo Alto, Nov. 1984, 198 p.

30. Kulhawy, F. H., Trautmann, C. H., Beech, J. F., O'Rourke, T. D., McGuire, W., Wood, W. A., and Capano, C., "Transmission Line Structure Foundations for Uplift-Compression Loading", Report EL-2870, Electric Power Research Institute, Palo Alto, Feb. 1983, 412 p.

Section 5

LOAD-DISPLACEMENT RESPONSE OF LATERALLY LOADED SHAFTS

Drilled shaft foundations are employed often to transmit lateral (horizontal) forces and overturning moments to the ground. As in most design, an adequate margin of safety against failure must be ensured, and the displacements resulting from this form of loading must be tolerable. In this section, some of the existing methods for predicting the lateral displacements of deep foundations will be reviewed briefly, and then some new and simple closed form solutions for the response of rock-socketed drilled shafts will be presented.

RECENT METHODS

The authors are unaware of any published method of analysis specifically for use in predicting the response of rock-socketed shafts subjected to lateral loading. To date, it has been customary practice to adopt the techniques developed for laterally loaded piles in soil to the problem of a laterally loaded rock socket. There is some justification for this approach, but what is lacking is a complete set of solutions covering the ranges of material and geometric parameters encountered in rock sockets. The solutions that have been developed for laterally loaded piles generally cover the cases of long slender piles where the ratio of the stiffness of the pile material to that of the soil is large. Shafts in rock are usually much stubbier than their counterpart piles in soil, and the ratio of the deformation modulus of a reinforced concrete shaft to that of the surrounding rock mass is usually much lower than the modulus ratio for piles in soil.

In recent years, theoretical approaches for predicting the lateral displacements of piles have been developed extensively. Two main approaches generally have been employed. In the simplest approach, known as the subgrade reaction method, the laterally loaded pile is idealized as an elastic beam loaded transversely and restrained by uniform linear springs acting along the length of the beam. The effect of this idealization is to ignore the continuous nature of the soil medium. Closed form solutions for this idealization are available for a variety of loading conditions and end restraints on the pile (1). This model has been improved by allowing the spring stiffness to vary along the length of the pile (2, 3) and,

subsequently, by replacing the linear springs by nonlinear p-y curves (4, 5, 6, 7). For these extended forms of the subgrade-reaction approach, numerical solution techniques are required and, from a design point of view, the method loses some of its attraction. In addition, there are further limitations to this approach. First, difficulties exist in choosing appropriate p-y curves for a given combination of pile or shaft size and soil or rock type. Second, replacement of the soil or rock continuum by discrete springs precludes the extension of the analysis to groups, because interaction between neighboring piles or shafts will not be taken into account.

The second major development in the analysis of laterally loaded piles was made by modeling the soil as an elastic continuum and the pile as an elastic beam. Numerical solutions were developed, first with the use of the integral equation (or boundary element) method (e.g., 8, 9, 10, 11) and second with the use of the finite element method (e.g., 12, 13, 14, 15). Most of these elastic solutions were presented in the form of charts. Until about 1981, the designer had to choose between the succinct solutions available using the simple idealization of subgrade reaction and the more cumbersome solutions available in the form of charts provided by the elastic continuum analysis. In 1981, closed form expressions for the response of flexible piles to lateral loading were presented (16). The description "flexible" was applied to piles in which the induced displacements and bending moments are confined to the upper part of the pile and the overall length of the pile does not significantly affect its response. The expressions are only approximate, but they provide a close fit to the more rigorous solutions obtained by the finite element method.

The designer of laterally loaded piles in soil now has available solutions for the pile response that are very simple to use. Unfortunately for the designer of laterally loaded, rock-socketed shafts, these solutions do not cover all cases occurring in practice. In the following, new solutions are developed to cover the case of stubby rigid shafts socketed into rock.

PROBLEM IDEALIZATION

Consider the problem shown in Figure 5-1, which represents the cases where either rock is at the ground surface or the lateral loading on the shaft at the level of the rock surface can be specified completely. The shaft is idealized as a cylindrical elastic inclusion, with an equivalent Young's modulus E_e and Poisson's ratio $\nu_e = \nu_c$, depth D, and diameter B. For a solid shaft having an actual bending rigidity $(EI)_c$, the equivalent Young's modulus is given by:

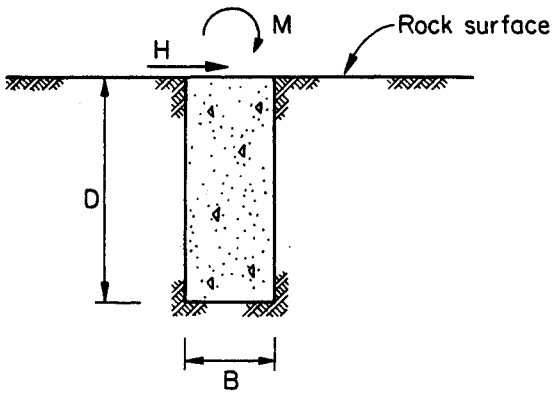

Figure 5-1. Lateral Loading at Rock Surface

$$E_e = (EI)_c/(\pi B^4/64) \qquad (5\text{-}1)$$

The elastic shaft is embedded in a homogeneous, isotropic elastic rock mass, with properties E_r and ν_r, and at the surface of the rock mass it is subjected to a known lateral (horizontal) force H and an overturning moment M.

The analysis of the problem shown in Figure 5-1 will be considered first. The more general case of lateral loading of a shaft socketed into a rock mass, with an overlying soil layer, will be considered subsequently.

ANALYSIS

As described previously, lateral loading predictions have been made using a number of different analytical techniques. In the following, some simple closed form equations are presented for both relatively flexible and relatively rigid shafts subjected to lateral loading. These equations are applicable for most of the rock-socketed shafts encountered in practice. They have been derived from the results of a finite element study of the behavior of axisymmetric bodies subjected to nonsymmetric loading. The technique has been described in the literature (17) and is similar to that used for lateral loading of "flexible" piles (13, 14, 15, 16) and for the study of the effects of surface loadings on pile behavior (18). Eight-noded, isoparametric, quadrilateral elements, with 3 × 3 Gaussian integration, were used in the present study.

An extensive parametric study was performed for socketed shafts covering a large range of relative stiffnesses, and it was found that the effects of variations in Poisson's ratio of the rock mass, ν_r, could be represented approximately by considering an equivalent shear modulus of the rock mass, G*, defined by:

$$G^* = G_r(1 + 3\nu_r/4) \tag{5-2}$$

in which

$$G_r = \frac{E_r}{2(1 + \nu_r)} \tag{5-3}$$

is the actual shear modulus of the elastic rock mass. The use of the parameter G^* was suggested previously for the case of relatively flexible piles (16), and the present study has verified that it also provides an adequate representation of the behavior of relatively rigid shafts in elastic rock masses with a range of values of ν_r.

For a homogeneous rock mass, it was found that the horizontal displacement, u, and rotation, θ, of the shaft at the level of the rock surface depends on the relative moduli of the shaft and rock mass, E_e/G^*, and on the geometry of the shaft, D/B. The finite element predictions are presented in Figures 5-2 to 5-4. Figure 5-2 shows the lateral load-displacement relationships; Figure 5-3 shows the relationships between moment and rotation; and Figure 5-4 indicates the load-rotation and moment-displacement relationships. Two types of plot of the same data are provided in each figure. These show the dimensionless displacements plotted against the modulus ratio, E_e/G^*, and slenderness ratio, D/B. The finite element results have been plotted as the dashed curves on all figures.

It was suggested (16) that a shaft would behave as if it were infinitely long where:

$$(D/B) \geq (E_e/G^*)^{2/7} \tag{5-4}$$

For these cases, the shaft response is dependent only on the modulus ratio E_e/G^* and Poisson's ratio of the rock mass ν_r. Dotted curves corresponding to the equality condition in Equation 5-4 have been plotted on Figures 5-2, 5-3, and 5-4, from which it can be seen that the finite element predictions are independent of D/B whenever Equation 5-4 holds. Such a shaft is "flexible", and the following

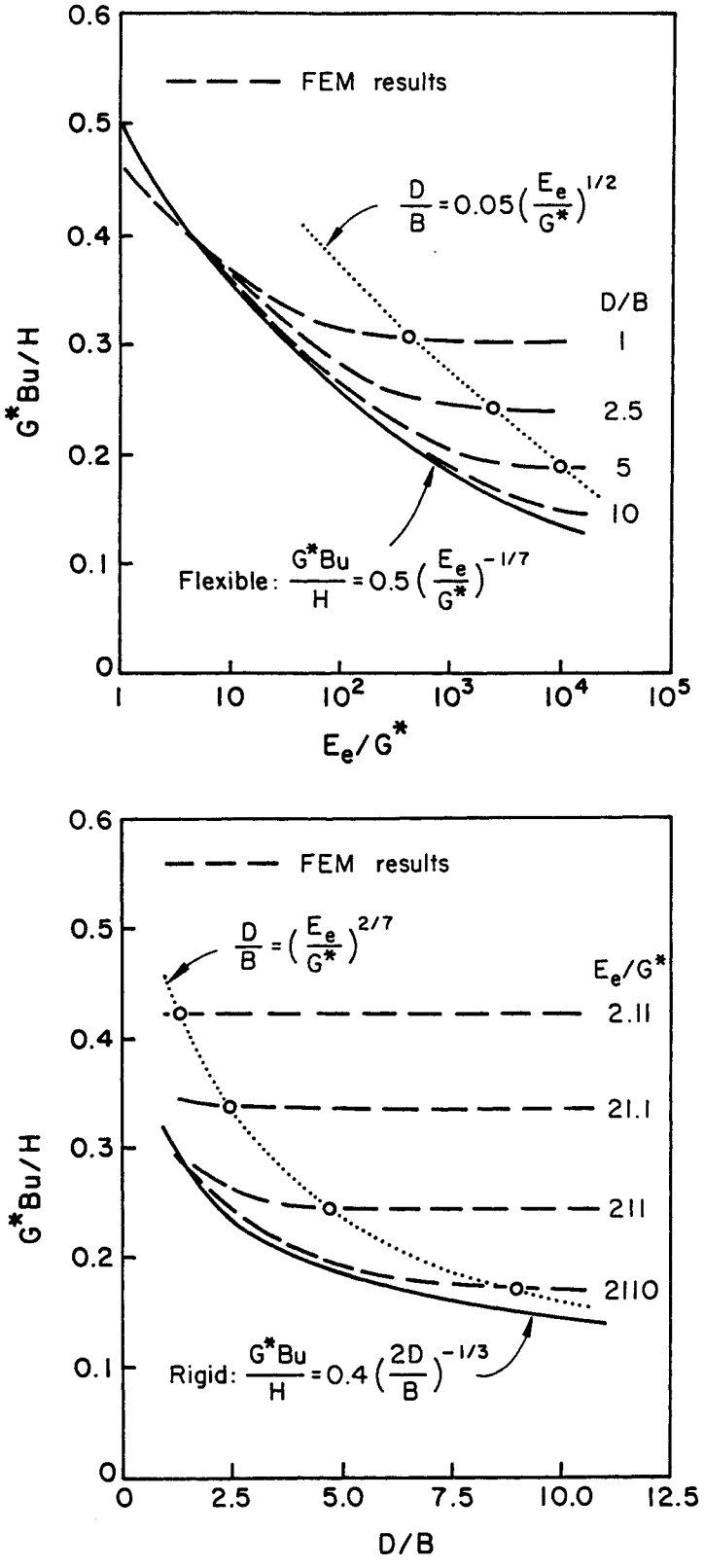

Figure 5-2. Lateral Load-Displacement Relationships

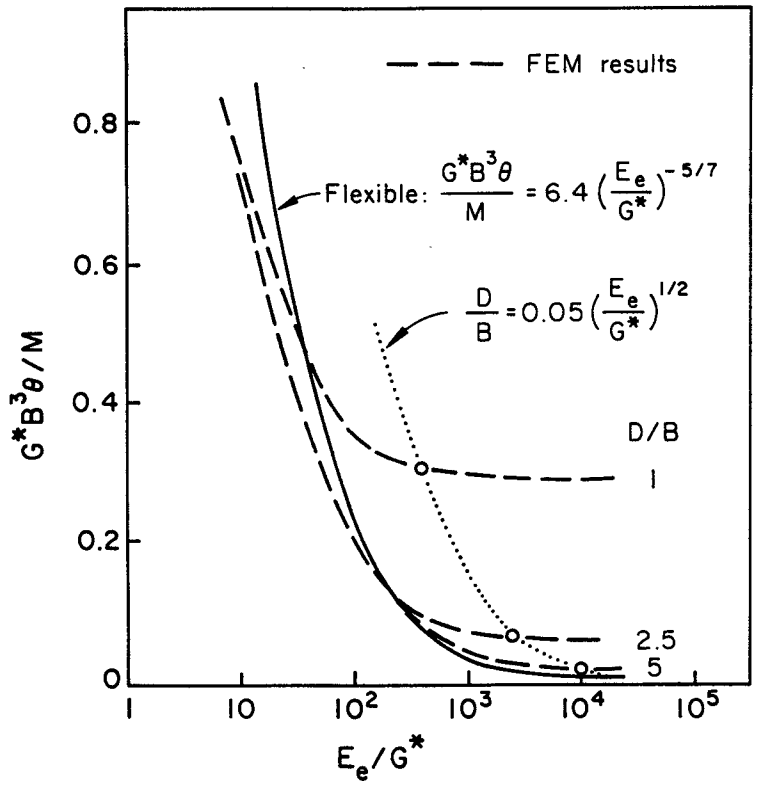

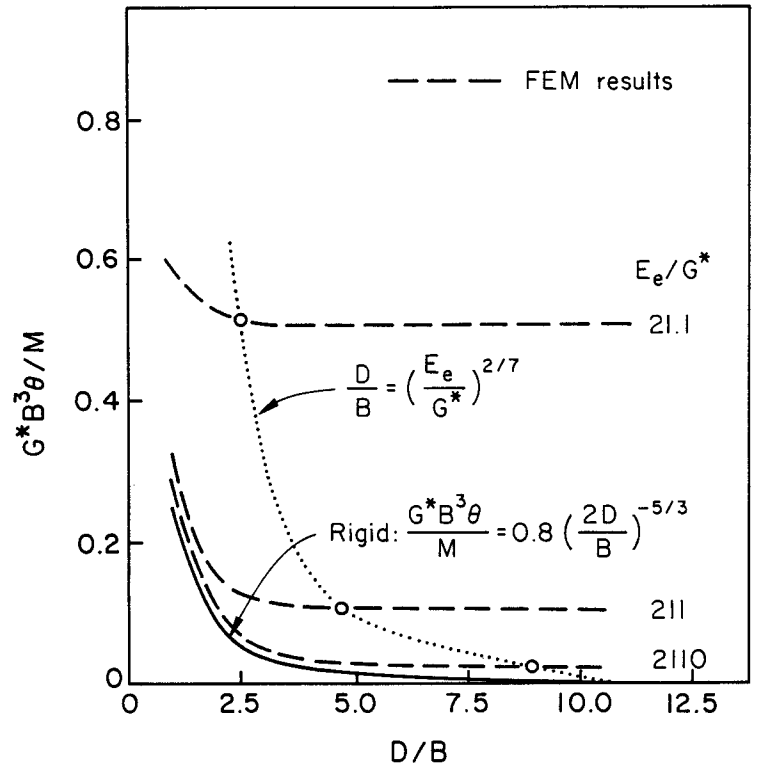

Figure 5-3. Moment-Rotation Relationships

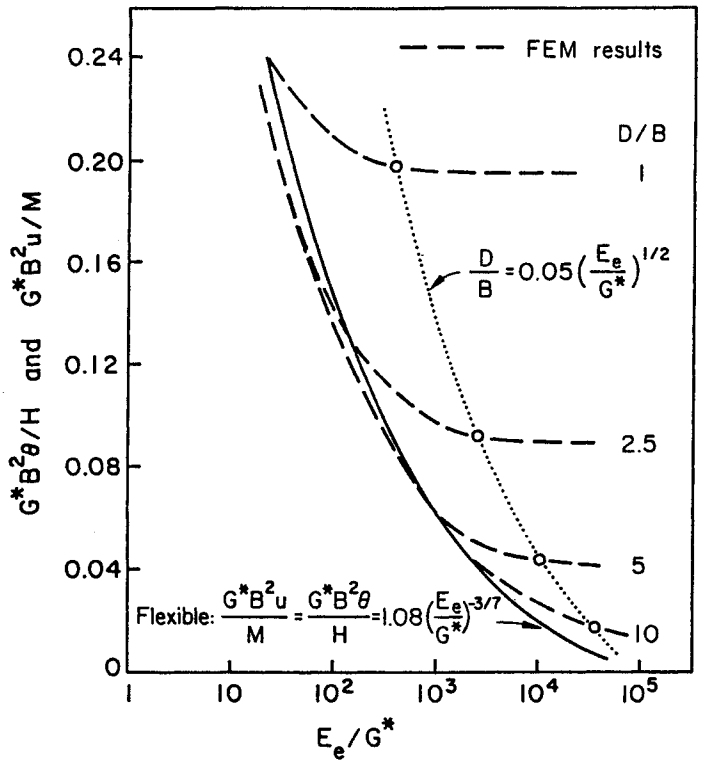

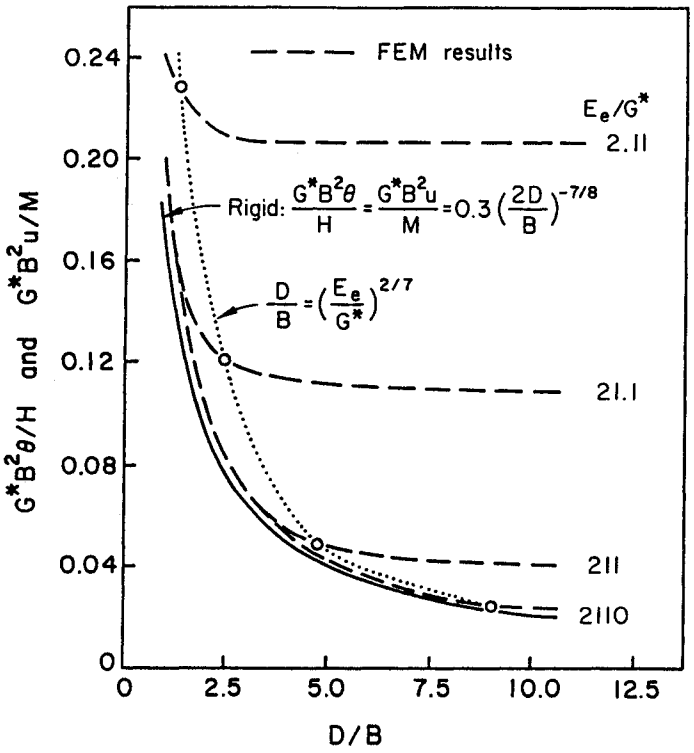

Figure 5-4. Lateral Load-Rotation and Moment-Displacement Relationships

closed form expressions provide accurate approximations for the deformations (16):

$$u = 0.5 \frac{H}{G^*B} \left(\frac{E_e}{G^*}\right)^{-1/7} + 1.08 \frac{M}{G^*B^2} \left(\frac{E_e}{G^*}\right)^{-3/7} \quad (5\text{-}5)$$

$$\theta = 1.08 \frac{H}{G^*B^2} \left(\frac{E_e}{G^*}\right)^{-3/7} + 6.4 \frac{M}{G^*B^3} \left(\frac{E_e}{G^*}\right)^{-5/7} \quad (5\text{-}6)$$

The appropriate forms of these equations have been plotted on Figures 5-2, 5-3, and 5-4. It is clear from these figures that Equations 5-5 and 5-6 provide adequate predictions of the behavior of "flexible" shafts socketed into elastic rock masses. The accuracy of these equations was verified (16) for the following ranges of parameters: $10^2 \leq E_e/E_r \leq 10^6$ and $D/B \geq 10$. The present study has shown that the range of applicability can be extended to $1 \leq E_e/E_r \leq 10^6$ and $D/B \geq 1$.

When short stubby shafts are socketed into weak rock, the shafts will behave as rigid structural members. In these cases, the displacements of the shaft will be independent of the modulus ratio, E_e/E_r, and will depend only on the slenderness ratio, D/B, and Poisson's ratio of the rock mass, ν_r. This type of behavior can be contrasted to that of a "flexible" shaft.

The dotted curves in Figures 5-2, 5-3, and 5-4 indicate that a shaft will behave as a rigid member where:

$$D/B \leq 0.05(E_e/G^*)^{1/2} \quad (5\text{-}7)$$

The present study showed that the displacements of these rigid shafts can be expressed, to sufficient accuracy, by the simple closed form expressions below:

$$u = 0.4 \frac{H}{G^*B} \left(\frac{2D}{B}\right)^{-1/3} + 0.3 \frac{M}{G^*B^2} \left(\frac{2D}{B}\right)^{-7/8} \quad (5\text{-}8)$$

$$\theta = 0.3 \frac{H}{G^*B^2} \left(\frac{2D}{B}\right)^{-7/8} + 0.8 \frac{M}{G^*B^3} \left(\frac{2D}{B}\right)^{-5/3} \quad (5\text{-}9)$$

Appropriate forms of these equations have been plotted as solid curves on Figures 5-2, 5-3, and 5-4, where satisfactory agreement with the finite element solutions can be seen. Because the shaft displaces as a rigid body in the elastic rock mass,

the depth beneath the surface to its center of rotation can be computed as:

$$z_c = \left\{\frac{0.4\ (\frac{2D}{B})^{-1/3} + 0.3\ (\frac{e}{B})\ (\frac{2D}{B})^{-7/8}}{0.3\ (\frac{2D}{B})^{-7/8} + 0.8\ (\frac{e}{B})\ (\frac{2D}{B})^{-5/3}}\right\} B \qquad (5\text{-}10)$$

in which $e = M/H$ is the vertical eccentricity of the applied horizontal force H. When applying Equations 5-8, 5-9, and 5-10, it should be noted that their accuracy has been verified only for the following ranges of parameters: $1 \leq D/B \leq 10$ and $E_e/E_r \geq 1$.

Traditionally, the influence factors for laterally loaded piles and shafts have been presented in the form of numerous charts (e.g., 8, 9, 10, 11). The approximate Equations 5-5, 5-6, 5-8, 5-9, and 5-10 are more attractive for design because they are in closed form.

Shafts can be described as having "intermediate" stiffness whenever the slenderness ratio is bounded approximately as follows:

$$0.05(E_e/G^*)^{1/2} \leq D/B \leq (E_e/G^*)^{2/7} \qquad (5\text{-}11)$$

Figures 5-2 to 5-4 show that, in these cases, the finite element predictions are almost always larger than the predictions from Equations 5-5 and 5-6 for flexible shafts and Equations 5-8 and 5-9 for rigid shafts. Typically, the displacements for an intermediate case exceed the maximum of the predictions for corresponding rigid and flexible shafts by no more than about 25 percent, and often by much less. For the sake of simplicity, without the sacrifice of much accuracy, it is suggested that the displacements in the intermediate case be taken as 1.25 times the maximum of either: (a) the predicted displacement of a rigid shaft with the same slenderness ratio (D/B) as the actual shaft, or (b) the predicted displacement of a flexible shaft with the same modulus ratio (E_e/G^*) as the actual shaft. Values calculated in this manner should, in most cases, be slightly larger than those given by the more rigorous finite element analysis for a shaft of intermediate stiffness.

RANGE OF APPLICATION

In practice, shafts which are socketed into rock normally will have a slenderness ratio falling within the range 1 to 10. Furthermore, the modulus ratio E_e/E_r

generally will lie in the range of 1 to 10,000. The combinations of modulus and slenderness ratios which produce flexible, intermediate, and rigid shafts are shown in Figure 5-5 for $\nu_r = 0.25$. It can be seen that each case covers a significant portion of those likely to occur in practice.

SOIL OVERLYING ROCK

Consider now a layer of soil overlying rock as shown in Figure 5-6a. In this problem, it is assumed that the complete distribution of soil reaction on the shaft is known. The groundline horizontal displacement u and rotation θ then can be determined after structural decomposition of the shaft and its loading, as shown in Figure 5-6b. The portion of the shaft within the soil may be analyzed as a determinant beam subjected to known loading. The displacement and rotation of point A relative to point B can be determined by established techniques of structural analysis (e.g., the slope-deflection method). The horizontal shear force, H_o, and bending moment, M_o, acting in the shaft at the rock surface level can be computed from statics and the displacement and rotation at this level can be computed by the methods described previously in this section. The overall groundline displacements then can be calculated by superposition of the appropriate parts.

The key to successful use of this method lies in determining the distribution of the soil reaction. As a worst case, the soil could be ignored completely, allowing the portion of the shaft in soil to be treated as a free standing cantilever. This case may be overly conservative. For simplicity, it will be assumed that the magnitude of the lateral loading applied is sufficient to cause yielding within the soil and for limiting soil reaction stresses to develop along the leading face of the shaft. Furthermore, it is assumed that this limiting condition is reached at all points down the shaft, from the ground surface to the interface with the underlying rock mass.

These assumptions may represent an oversimplification, because some loading conditions may not be large enough to develop this limiting state. In these cases, the predictions of groundline displacements will overestimate the true values. However, the decision to socket the shafts into rock commonly is made because the soil can not provide adequate restraint. In these circumstances, the assumption of a limiting soil reaction distribution is likely to be sufficient.

The determination of the limiting soil reactions is discussed below for the limiting cases of purely cohesive soil and purely frictional soil. It should be

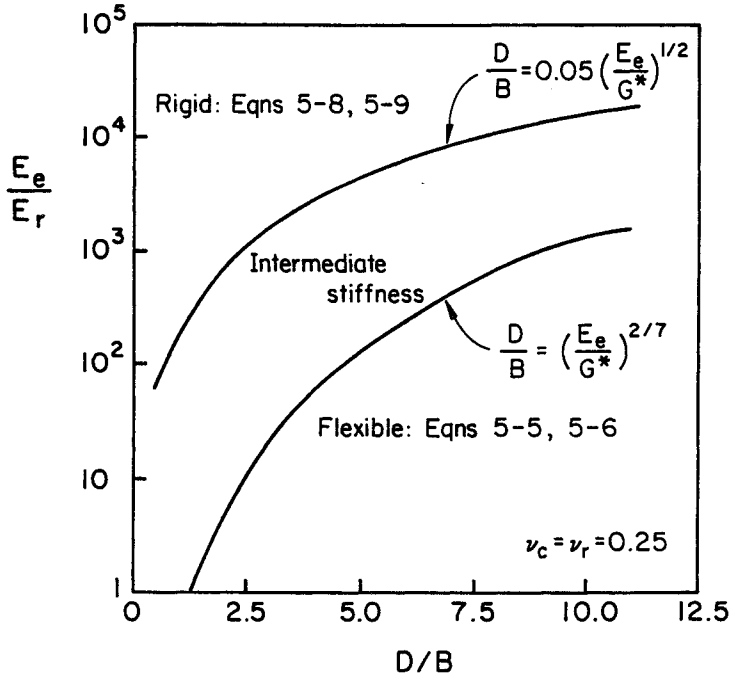

Figure 5-5. Ranges of Application

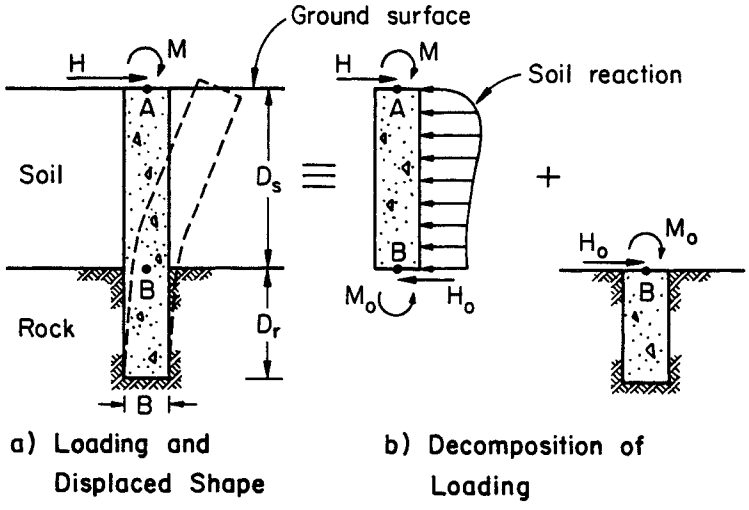

Figure 5-6. Rock Socketed Shaft under Lateral Loading with Overlying Soil Layer

noted that these cases represent simple models for soil behavior, and therefore they may not be appropriate for all field situations. They are intended to be used where the rock socket dominates the overall behavior and provides the large majority of the resistance to load. In these cases, simplifications of the actual soil behavior will have a minor effect on the overall shaft performance.

Shafts Through Cohesive Soil

It is often accepted that the ultimate soil resistance for piles and shafts in purely cohesive soil increases with depth from about 2 s_u at the surface (s_u = undrained shear strength of the soil) up to about 8 to 12 s_u at a depth of about 3 foundation diameters below the surface. One commonly used simplified distribution of soil resistance ranges from zero at the ground surface to a depth of 1.5B and has a constant value of 9 s_u below this depth (19). This distribution is illustrated in Figure 5-7 and assumes that the shaft movements will be sufficient to generate this reaction distribution.

For this case, the lateral displacement, u_{AB}, and rotation, θ_{AB}, of point A at the shaft butt, relative to point B at the soil-rock interface, can be determined by structural analysis of the shaft, treating it as a beam subjected to known loading, which gives:

$$(EI)_e\, u_{AB} = \frac{1}{3} HD_s^3 + \frac{1}{2} MD_s^2 - \frac{9}{8} s_u(D_s - 1.5B)^3 (D_s + B/2)B \qquad (5\text{-}12)$$

$$(EI)_e\, \theta_{AB} = \frac{1}{2} HD_s^2 + MD_s - \frac{3}{2} s_u(D_s - 1.5B)^3 B \qquad (5\text{-}13)$$

in which D_s = depth of soil layer and $(EI)_e$ = bending rigidity of the shaft section.

The shear force, H_o, and bending moment, M_o, acting at point B can be determined from statics as:

$$H_o = H - 9\, s_u(D_s - 1.5B)B \qquad (5\text{-}14)$$

$$M_o = M + HD_s - 4.5\, s_u(D_s - 1.5B)^2 B \qquad (5\text{-}15)$$

Equations 5-12 to 5-15 and the assumed soil reaction stress are valid only if $H_o > 0$ and $M_o > 0$.

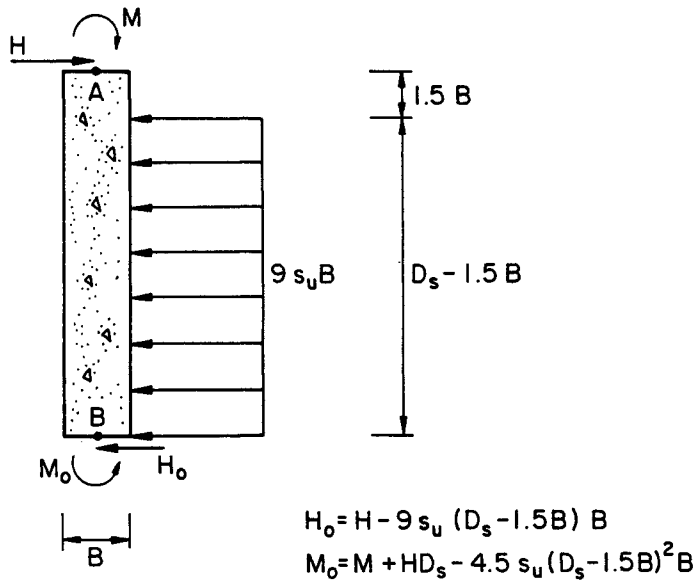

Figure 5-7. Idealized Loading of Socketed Shaft through Cohesive Soil

The contribution to the groundline displacement from the loading transmitted to the rock mass now can be computed by analyzing a rock-socketed shaft of embedded length D_r, subjected to a horizontal force H_o and moment M_o applied at the level of the rock surface. This procedure has been described previously. These components of displacement should be added to the displacement and rotation calculated using Equations 5-12 and 5-13 to determine the overall groundline response.

Shafts Through Cohesionless Soil

This case can be analyzed using the reaction distribution suggested for a cohesionless soil shown in Figure 5-8 (20). The following assumptions have been made in deriving this distribution.

1. The active soil stress acting on the back of the shaft is neglected.
2. The distribution of soil stress along the projected front of the shaft is equal to three times the Rankine maximum passive stress.
3. The shape of the shaft section has no influence on the distribution of ultimate soil stress or the magnitude of the ultimate lateral resistance.
4. The full lateral resistance is mobilized at the displacement being considered.

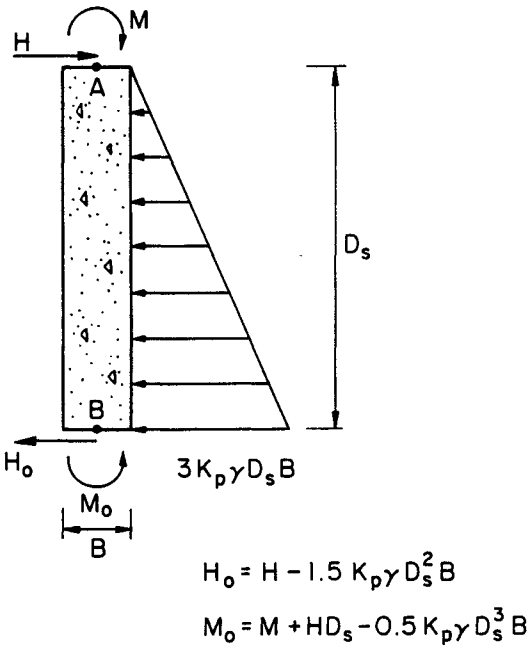

Figure 5-8. Idealized Loading of Socketed Shaft through Cohesionless Soil

The distribution of soil resistance, p_u, is given by:

$$p_u = 3\ K_p\ \bar{\sigma}_v \tag{5-16}$$

in which $\bar{\sigma}_v$ = vertical effective stress, $K_p = (1 + \sin\bar{\phi})/(1 - \sin\bar{\phi})$, and $\bar{\phi}$ = soil effective stress friction angle.

The simplifying assumption of an ultimate soil resistance equal to three times the Rankine maximum passive stress is based on limited empirical evidence from comparisons between predicted and observed ultimate loads (20). These comparisons suggest that the assumed value of 3 may, in some cases, be conservative. Further discussion on this assumed stress distribution, and a comparison with the lateral resistance factors suggested by Hansen (21), are given in (22).

For a dry cohesionless soil, with unit weight γ, the relative displacement and rotation, u_{AB} and θ_{AB}, can be determined from structural analysis as:

$$(EI)_e\ u_{AB} = \frac{1}{3}\ HD_s^3 + \frac{1}{2}\ MD_s^2 - \frac{1}{10}\ K_p\gamma D_s^5 B \tag{5-17}$$

$$(EI)_e \theta_{AB} = \frac{1}{2} HD_s^2 + MD_s - \frac{1}{8} K_p \gamma D_s^4 B \quad (5\text{-}18)$$

The shear force and bending moment at the level of the rock surface are given by:

$$H_o = H - 1.5K_p \gamma D_s^2 B \quad (5\text{-}19)$$

$$M_o = M + HD_s - 0.5K_p \gamma D_s^3 B \quad (5\text{-}20)$$

As before, this analysis will only be valid if $H_o > 0$ and $M_o > 0$.

The displacements at the groundline can be computed by assuming that the loading given in Equations 5-19 and 5-20 acts on a rock-socketed shaft and then by adding the resulting displacements to those given by Equations 5-17 and 5-18.

SUMMARY

A general approach has been presented to predict the displacements of laterally loaded shafts in rock. This approach includes the horizontal groundline displacements and rotation of the shaft resulting from the application of both a horizontal force and overturning moment at the ground surface. Simple solutions, expressible in closed form, have been presented for a shaft embedded directly in rock and a shaft penetrating an overlying soil layer before being embedded in the underlying rock. The solutions cover the full range of relative shaft to rock mass stiffness and shaft geometries encountered in practice. The approximate closed form expressions are in good agreement with solutions obtained using the finite element method.

REFERENCES

1. Hetenyi, M., Beams on Elastic Foundations, University of Michigan Press, Ann Arbor, 1946, 255 p.

2. Reese, L. C. and Matlock, H., "Non-Dimensional Solutions for Laterally Loaded Piles with Soil Modulus Proportional to Depth," Proceedings, 8th Texas Conference on Soil Mechanics and Foundation Engineering, 1956, pp. 1-41.

3. Matlock, H. and Reese, L. C., "Generalized Solutions for Laterally Loaded Piles," Journal of the Soil Mechanics and Foundations Division, ASCE, Vol. 86, No. SM5, Oct. 1960, pp. 63-91.

4. Matlock, H. and Ripperger, E. A., "Measurements of the Soil Pressure on a Laterally Loaded Pile," Proceedings, ASTM, Vol. 58, 1958, pp. 1245-1259.

5. Gill, H. L. and Demars, K. R., "Displacement of Laterally Loaded Structures in Nonlinearly Responsive Soil," Technical Report R670, Naval Civil Engineering Laboratory, Port Hueneme, 1970.

6. Matlock, H., "Correlations for Design of Laterally Loaded Piles in Soft Clay," Proceedings, 2nd Offshore Technology Conference, Vol. 1, Houston, 1970, pp. 577-594.

7. Reese, L. C., Cox, W. R., and Koop, R. D., "Field Testing and Analysis of Laterally Loaded Piles in Stiff Clay," Proceedings, 7th Offshore Technology Conference, Vol. 2, Houston, 1975, pp. 473-483.

8. Poulos, H. G., "Behavior of Laterally Loaded Piles: I - Single Piles," Journal of the Soil Mechanics and Foundations Division, ASCE, Vol. 97, No. SM5, May 1971, pp. 711-731.

9. Poulos, H. G., "Behavior of Laterally Loaded Piles: II - Pile Groups," Journal of the Soil Mechanics and Foundations Division, ASCE, Vol. 97, No. SM5, May 1971, pp. 733-751.

10. Poulos, H. G., "Behavior of Laterally Loaded Piles: III - Socketed Piles," Journal of the Soil Mechanics and Foundations Division, ASCE, Vol. 98, No. SM4, Apr. 1972, pp. 341-360.

11. Banerjee, P. K. and Davies, T. G., "The Behavior of Axially and Laterally Loaded Single Piles Embedded in Nonhomogeneous Soils," Geotechnique, Vol. 28, No. 3, Sept. 1978, pp. 309-326.

12. Carayannacou-Trezos, S., "Comportement des Pieux Sollicites Horizontalement," Dr. Ing. Dissertation, Universitie Paris VI, 1977.

13. Randolph, M. F., "A Theoretical Study of the Performance of Piles," Ph.D. Dissertation, University of Cambridge, Cambridge, 1977, 260 p.

14. Kuhlemeyer, R. L., "Static and Dynamic Laterally Loaded Floating Piles," Journal of the Geotechnical Engineering Division, ASCE, Vol. 105, No. GT2, Feb. 1979, pp. 289-304.

15. Kuhlemeyer, R. L., "Bending Element for Circular Beams and Piles," Journal of the Geotechnical Engineering Division, ASCE, Vol. 105, No. GT2, Feb. 1979, pp. 325-330.

16. Randolph, M. F., "The Response of Flexible Piles to Lateral Loading," Geotechnique, Vol. 31, No. 2, June 1981, pp. 247-259.

17. Wilson, E. L., "Structural Analysis of Axisymmetric Solids," Journal of the American Institute for Aeronautics and Astronautics, Vol. 3, 1965, pp. 2269-2274.

18. Carter, J. P., "A Numerical Method for Pile Deformations Due to Nearby Surface Loadings," Proceedings, 4th International Conference on Numerical Methods in Geomechanics, Vol. 2, Edmonton, 1982, pp. 811-817.

19. Broms, B. B., "Lateral Resistance of Piles in Cohesive Soils," Journal of the Soil Mechanics and Foundations Division, ASCE, Vol. 90, No. SM2, Mar. 1964, pp. 27-63.

20. Broms, B. B., "Lateral Resistance of Piles in Cohesionless Soils," Journal of the Soil Mechanics and Foundations Division, ASCE, Vol. 90, No. SM3, May 1964, pp. 123-156.

21. Hansen, J. B., "The Ultimate Behavior of Rigid Piles Against Transversal Forces," Bulletin 12, Danish Geotechnical Institute, Copenhagen, 1961.

22. Poulos, H. G. and Davis, E. H., Pile Foundation Analysis and Design, John Wiley and Sons, New York, 1980, 397 p.

Section 6

LOAD-DISPLACEMENT RESPONSE OF TORSIONALLY LOADED SHAFTS

Almost all laterally loaded drilled shaft foundations will be subjected to some degree of torsion because of the eccentricity of the applied loading. In addition, single pole transmission line structures subjected to unbalanced line loading will transmit torsional loads directly to the foundation.

Theoretical investigations of the torsional response of piles embedded in an elastic soil have been made (1, 2). A numerical analysis yielded solutions to this problem in the form of charts of torsional flexibility plotted as a function of pile geometry and relative stiffness (1). Also, an approximate analysis has been presented which is based on a simple assumption about the stress field in the soil surrounding a pile undergoing torsion and leads to a closed form solution for the torsional stiffness of the pile (2).

In this section, it will be shown that the approximate analysis is not restricted to slender piles in soil, but is also applicable to cylindrical foundations having geometric and material properties typical of those for shafts socketed into rock. This approximate solution is in good agreement with the more rigorous solutions. Because of its simple algebraic form, the approximate solution is attractive for design purposes.

The analysis of rock-socketed shafts subjected to torsion then is extended to the case where a relatively shallow soil layer overlies the rock.

PROBLEM DEFINITION

For completeness, solutions to the torsion problem will be developed for the cases of a cylindrical shaft in a "complete" rock socket and in a "side shear only" socket. For the complete socket (Figure 6-1a), it is assumed that perfect contact is maintained between the shaft and the rock socket so that torque may be transmitted to the rock mass along both the side and tip interfaces. For the "side shear" socket (Figure 6-1b), perfect contact is maintained only along the side interface, and no bonding or torsional restraint is assumed at the shaft tip.

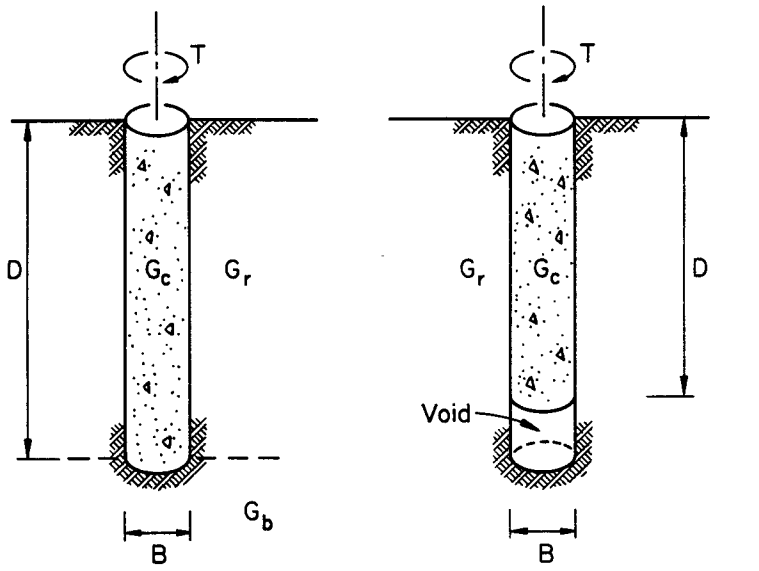

a) "Complete" Socket b) "Side Shear Only" Socket

Figure 6-1. Shafts Subjected to Torsion Loading

In either case, the shaft is regarded as an elastic inclusion of depth D and diameter B, with torsional rigidity $(GJ)_c$, embedded in an elastic rock mass. J is the polar moment of inertia of the circular shaft section and, for convenience, an equivalent shear modulus of the pier G_e is defined as:

$$G_e = (GJ)_c/(\pi B^4/32) \qquad (6\text{-}1)$$

The rock mass surrounding the shaft, from the surface of the rock mass to the shaft tip, has an elastic shear modulus G_r, while below this level the modulus is G_b. A torque T is applied at the level of the rock surface.

LINEAR ELASTIC BEHAVIOR

The analysis presented here follows closely that published for the torsional response of piles in soil (2). A simplifying assumption was made concerning the stress field in the material surrounding the shaft, which enabled a closed form solution to be determined. The assumption is that the magnitude of circumferential shear stress induced on horizontal planes ($\tau_{z\theta}$ in polar coordinates) is negligible compared to the shear stress induced on cylindrical surfaces ($\tau_{r\theta}$). If the component $\tau_{z\theta}$ is ignored completely, then the displacements in the rock mass

surrounding the shaft can be imagined as an infinite number of cylinders twisting inside each other. From symmetry, there can be no variation of the field quantities in the circumferential direction and, under the above assumption, the equilibrium equation for the circumferential direction can be written in terms of polar coordinates as:

$$\frac{\partial}{\partial r} (r^2 \tau_{r\theta}) = 0 \tag{6-2}$$

Upon integration, the variation of shear stress with radius, r, is given by:

$$\tau_{r\theta} = \frac{\tau_o B^2}{4r^2} \tag{6-3}$$

in which $\tau_o = \tau_{r\theta}$ at r = B/2. The shear strain in the rock mass, $\gamma_{r\theta}$, may be written as:

$$\gamma_{r\theta} = \frac{\tau_{r\theta}}{G_r} = r \frac{\partial}{\partial r} \left(\frac{v}{r}\right) \tag{6-4}$$

in which v = circumferential displacement. Equations 6-3 and 6-4 can be combined to give:

$$\frac{\partial}{\partial r} \left(\frac{v}{r}\right) = \frac{\tau_o B^2}{4G_r r^3} \tag{6-5}$$

Integrating Equation 6-5 and substituting r = B/2 gives the rotation of the shaft, Φ, as:

$$\Phi = \frac{\tau_o}{2G_r} \tag{6-6}$$

The variation of Φ with depth, z, can be determined by considering the relationship between the torque T at depth z and the rate of change of rotation with depth, or:

$$\frac{d\Phi}{dz} = - \frac{T}{(GJ)_c} \tag{6-7}$$

Torque will be transferred gradually to the rock mass with depth, and therefore equilibrium of the shaft requires that:

$$\frac{dT}{dz} = -\pi\ B^2\ \tau_o/2 \tag{6-8}$$

Equations 6-6 to 6-8 can be combined to give:

$$\frac{d^2\Phi}{dz^2} = \frac{\pi B^2 \tau_o}{2(GJ)_c} = \frac{\pi B^2 G_r \Phi}{(GJ)_c} \tag{6-9}$$

Using Equation 6-1, this equation can be simplified further, to give:

$$\frac{d^2\Phi}{dz^2} = \mu^2\Phi \tag{6-10}$$

in which $\mu^2 = 32/(\lambda B^2)$ and $\lambda = G_e/G_r$. It should be noted that, in deriving Equation 6-10, it also has been assumed implicitly that $\partial\tau_{r\theta}/\partial z$ is small compared with $\partial\tau_{r\theta}/\partial r$.

Equation 6-10 has a solution of the form:

$$\Phi = A \cosh \mu z + C \sinh \mu z \tag{6-11}$$

The constants A and C are determined from the boundary conditions of the problem.

Complete Socket

For a complete socket, perfect contact is maintained between the shaft tip and the rock, so torsional restraint is provided by the rock mass below this level. To sufficient accuracy, the shaft tip may be regarded as a rigid punch of diameter B on the surface of a half space, with shear modulus G_b. The punch is subjected to a torque T_{tip} and its stiffness is given by:

$$\frac{T_{tip}}{\Phi_{tip}} = \frac{2}{3} B^3 G_b \tag{6-12}$$

in which Φ_{tip} is the twist of the punch. Although the shaft tip is not at the surface, the rock mass above the shaft tip also is subjected to torsion because of the twisting of the shaft and therefore, to sufficient accuracy, the presence of

the overlying rock may be ignored in the treatment of the tip behavior.

The relevant boundary conditions at the shaft tip, z = D, are therefore:

$$\Phi = \Phi_{tip} = (\frac{3}{2}) \frac{T_{tip}}{G_b B^3} \tag{6-13}$$

and

$$\frac{d\Phi}{dz} = (\frac{d\Phi}{dz})_{tip} = - (\frac{32}{\pi}) \frac{T_{tip}}{\lambda G_b B^4} \tag{6-14}$$

Substitution of these boundary conditions into Equation 6-11 leads eventually to the following equation for the torsional stiffness factor of the shaft foundation:

$$\frac{T}{G_r B^3 \Phi} = \frac{(\frac{2}{3}) (\frac{1}{\xi}) + \pi(\frac{D}{B}) \frac{\tanh[\mu D]}{\mu D}}{1 + (\frac{64}{3\pi\lambda\xi}) (\frac{D}{B}) \frac{\tanh[\mu D]}{\mu D}} \tag{6-15}$$

in which $\xi = G_r/G_b$. Equation 6-15 has been derived for the case of a homogeneous rock mass with $G_b = G_r$ (2).

Also of interest is the torque transmitted to the shaft tip, T_{tip}, which can be calculated from:

$$\frac{T_{tip}}{T} = \frac{\frac{1}{\cosh[\mu D]}}{1 + (\frac{3\pi\xi}{2}) (\frac{D}{B}) \frac{\tanh[\mu D]}{\mu D}} \tag{6-16}$$

The solutions given by Equations 6-15 and 6-16 are plotted in Figures 6-2 and 6-3 for a homogeneous rock mass with $\xi = 1$. In Figure 6-2, the dimensionless stiffness factor is plotted as a function of both the stiffness ratio, $\lambda = G_e/G_r$, and the slenderness ratio, D/B. The ranges selected correspond to shafts in rock that are commonly encountered in practice. Equation 6-15 has been plotted as the broken curves, and these have been compared with the numerical solutions (1) plotted as solid curves. The agreement between the two solutions is close for all values investigated. The approximate analysis basically ignored the shear stress component $\tau_{z\theta}$ (circumferential shear stress exerted between horizontal planes).

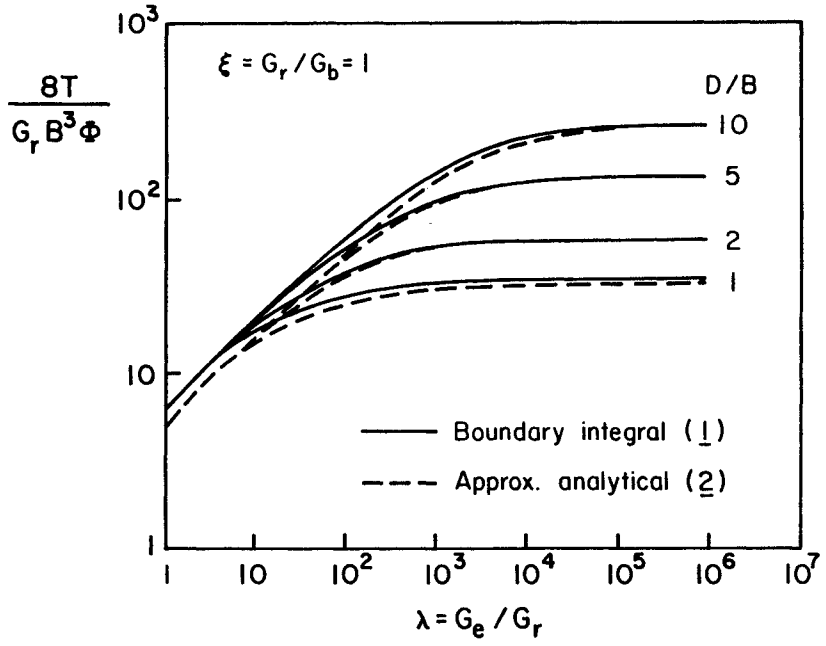

Figure 6-2. Torsional Stiffness Factors for Shafts in Rock ($G_r/G_b = 1$)

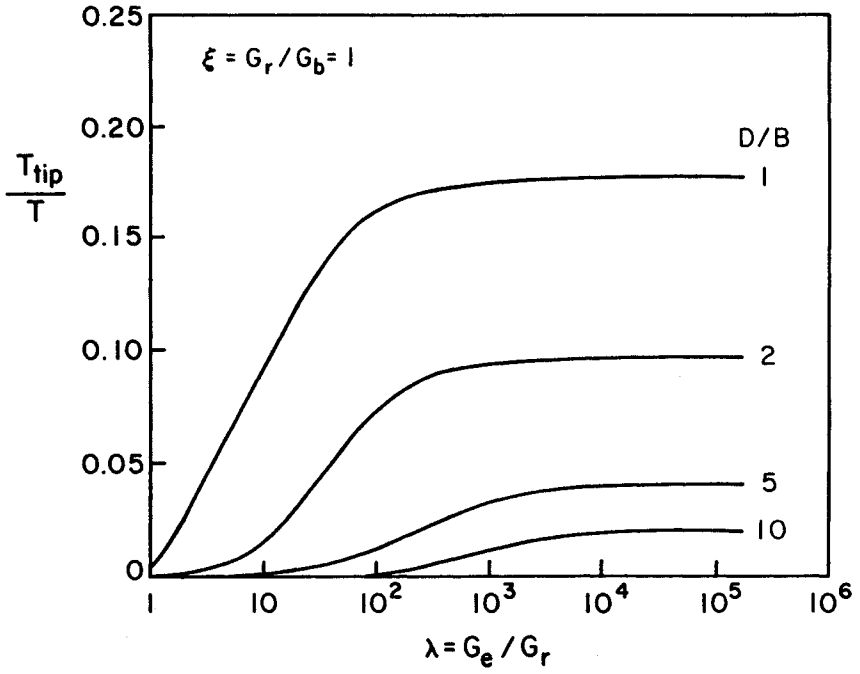

Figure 6-3. Torque Transmitted to Shaft Tip ($G_r/G_b = 1$)

The more rigorous solution indicates a slightly stiffer response of the foundation. The differences, however, are small and could be ignored for almost all practical cases. The solution for the torsional stiffness given by Equation 6-15 has the attraction of being expressed in algebraic form.

The solution given by Equation 6-16 for the proportion of the applied torque transmitted to the tip has been plotted in Figure 6-3. It can be seen that, in all cases, the torque transmitted to the tip is relatively small. For a rigid shaft (small D/B and large λ) making perfect contact at its tip, the parameter μD approaches 0 and in the limit:

$$\frac{T_{tip}}{T} = \frac{1}{1 + (\frac{3\pi\xi}{2})\ (\frac{D}{B})} \tag{6-17}$$

For a stubby, rigid shaft with D/B = 1 in a homogeneous rock mass (ξ = 1), the maximum torque transmitted to the tip is only about 17.5 percent of the applied torque and, for more slender shafts, it is much less. Therefore, most of the restraint against twisting of the foundation is provided by circumferential side shear.

Side Shear Socket

From the preceding comments, it can be concluded that the torsional behavior of a shaft in a "complete" socket will be very similar to a "side shear only" socket. For the latter case, the stiffness can be predicted by setting the ratio $\xi = G_r/G_b$ to approach infinity in Equation 6-15, from which it is found that:

$$\frac{T}{G_r\ B^3\ \Phi} = \pi\ (\frac{\tanh[\mu D]}{\mu D})\ (\frac{D}{B}) \tag{6-18}$$

By definition, the torque at the shaft tip, T_{tip}, is zero. If the shaft is rigid, μD approaches 0 and:

$$\frac{T}{G_r\ B^3\ \Phi} = \pi(\frac{D}{B}) \tag{6-19}$$

The response for shafts with D/B = 2 in "side shear only" sockets is plotted in

Figure 6-4. Solutions for a range of values of relative stiffness, $\lambda = G_e/G_r$, are given. For purposes of comparison, the results for "complete" sockets in which ξ = 0.1 and 1, also are plotted on this figure. It is clear that, when a shaft makes perfect contact with a much stiffer material below the tip (e.g., $\xi = G_r/G_b = 0.1$), the torsional stiffness of the foundation element is not increased proportionally. Also, the stiffness of a shaft in a "complete" socket in a homogeneous rock mass is only slightly greater than the stiffness of a shaft with the same dimensions in a "side shear only" socket. Therefore, the conditions at and below the tip of most rock-socketed shafts have only a minor influence on the torsional stiffness, despite the fact that they can have a significant influence on the proportion of the applied torque transmitted to the tip, as shown in Figure 6-5.

SOIL OVERLYING ROCK

Consider now the case where a layer of soil overlies the rock, and the applied torque, T, is defined at the surface of the soil as shown in Figure 6-6. In this problem, it is assumed that the complete distribution of circumferential shear stress on the portion of the shaft within the soil layer is known. The total twist of the shaft at the surface then may be determined after analyzing separately the portions of the shaft in soil and in rock and applying superposition (Figure 6-6b).

The success of this method depends on the correct determination of the soil reaction to the applied torsion. It is assumed here that the soil layer is relatively shallow, of depth D_s, and that the reason the shaft is socketed into rock is because of the inability of the soil alone to provide adequate resistance to the applied loading. In these circumstances, it appears reasonable to assume that a limiting distribution of circumferential shear stress acts between the soil and the shaft.

To determine the effect of the soil layer on the torsional response of the shaft, a number of assumptions are possible. Three of these are discussed below.

First, the presence of the soil layer could be ignored completely, in which case zero shear stress would be considered at the face of the shaft. Therefore, the full applied torque would be considered to be transmitted to the level of the rock surface. In this, the most conservative approach, the twist, Φ_{AB}, of the shaft butt, A, relative to a point in the shaft at the interface between soil and rock, B, is given by:

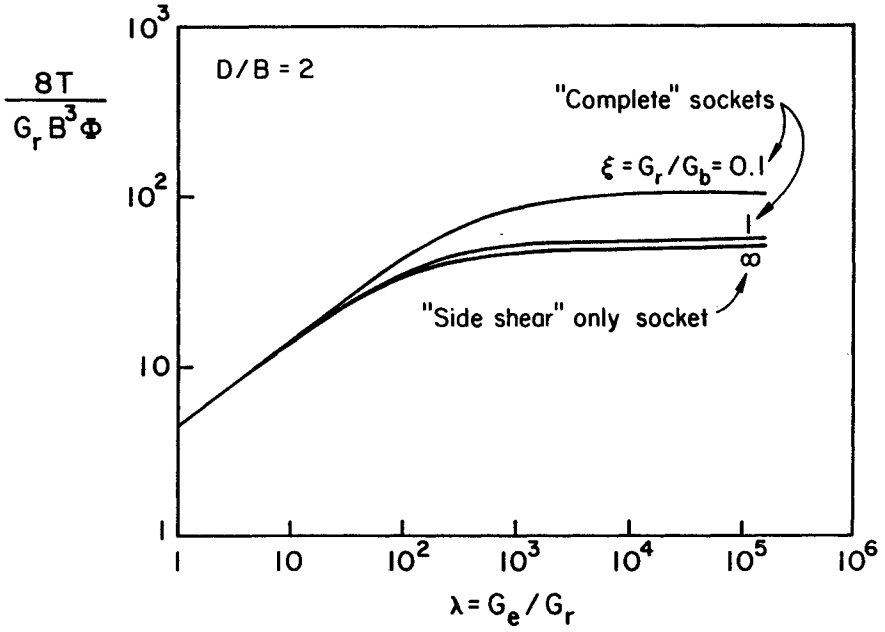

Figure 6-4. Torsional Stiffness Factors for Shafts in Rock (D/B = 2)

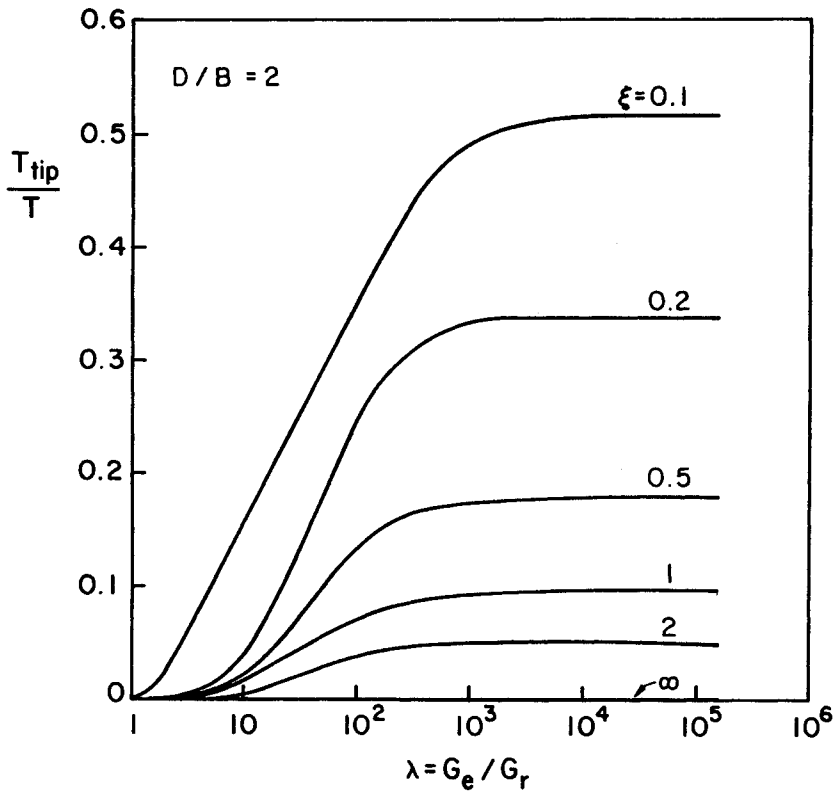

Figure 6-5. Torque Transmitted to Shaft Tip (D/B = 2)

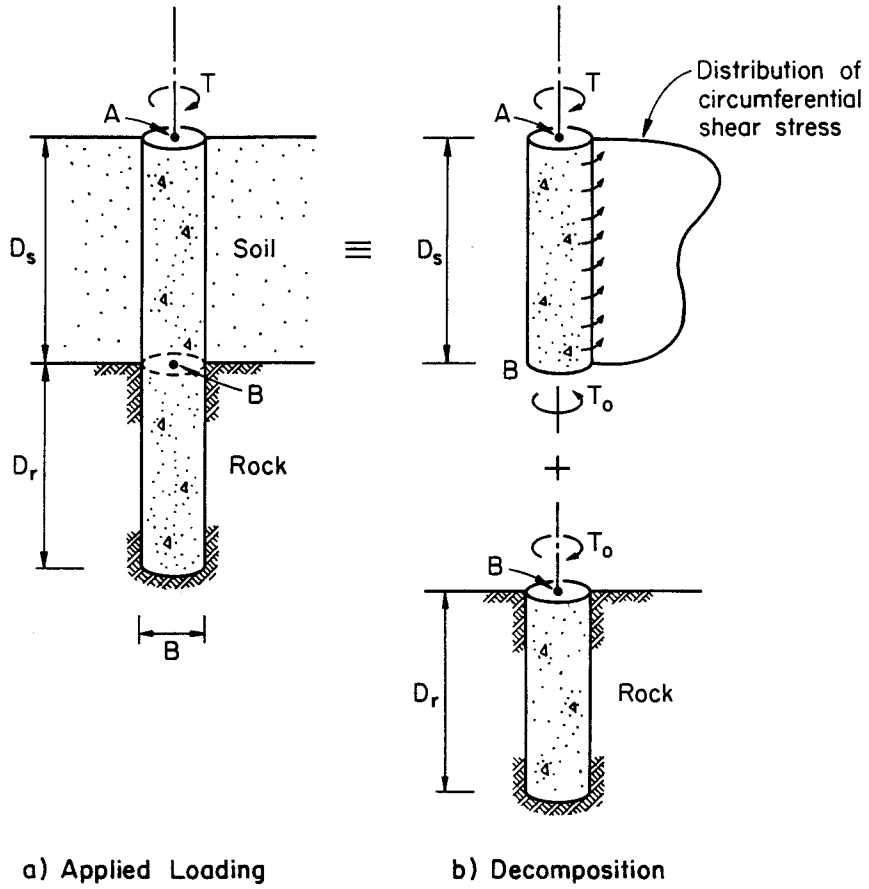

a) Applied Loading b) Decomposition

Figure 6-6. Rock Socketed Shaft under Torsional Loading with Overlying Soil Layer

$$\Phi_{AB} = \frac{T D_s}{(GJ)_c} \tag{6-20}$$

This quantity should be added to the twist of the lower portion of the shaft embedded in the rock to give the overall twist at the groundline, Φ. The contribution from the depth embedded in rock can be calculated by the techniques described previously.

Second, it could be assumed that some resistance to torque is provided by the soil and, in particular, that a constant value of shear stress, τ_f, is developed along the entire interface between the shaft and soil. This assumption appears reasonable for a shallow layer of perhaps residual clay overlying rock, where a total stress approach to the soil behavior can be adopted and τ_f is given by:

$$\tau_f = \alpha\, s_u \tag{6-21}$$

in which s_u = undrained shear strength of the clay (considered constant with depth), and α = empirical adhesion factor.

Suggested values for α have been given elsewhere (3) for axially loaded shafts, and the same values ought to provide reasonable first estimates of the maximum adhesion developed under torsional loading. For this case, the torque transmitted to the level of the rock surface, T_o, is given by:

$$T_o = T - \pi B^2 D_s \tau_f/2 \tag{6-22}$$

and the twist of point A relative to B is given as:

$$\Phi_{AB} = \frac{1}{(GJ)_c}\,(TD_s - \pi B^2 D_s{}^2 \tau_f/4) \tag{6-23}$$

A third possibility is to assume that the torsional resistance of the soil increases linearly with depth, z, so that:

$$\tau_f = \rho z \tag{6-24}$$

This form of resistance is likely to be more realistic for sands where, for a dry sand of unit weight γ, ρ can be written as:

$$\rho = K\gamma \tan\delta \tag{6-25}$$

in which K = coefficient of horizontal soil stress and δ = interface friction angle. Suggested values for K have been presented elsewhere (3, 4). For this case, the torque at the level of the rock surface is:

$$T_o = T - \pi B^2 D_s{}^2 \rho/4 \tag{6-26}$$

and the relative twist of the length of the shaft in the soil is:

$$\Phi_{AB} = \frac{1}{(GJ)_c}\,(TD_s - \frac{\pi}{12}\, B^2 D_s{}^3 \rho) \tag{6-27}$$

It should be noted that these cases represent simple models for soil behavior, and

therefore they may not be appropriate for all field situations. They are intended to be used where the rock socket dominates the overall behavior and provides the large majority of the resistance to load. In these cases, simplifications of the actual soil behavior will have a minor effect on the overall shaft performance.

SUMMARY

An analysis of the response of shafts socketed into rock and subjected to torsion has been presented. Simple, closed form predictions have been made of the rotation of the shaft at the ground level for shafts embedded in an elastic rock mass. For most shafts encountered in practice, the contact conditions at the shaft tip and the nature of the material underlying the tip have only a minor influence on the torsional behavior. Modifications to those solutions have been presented for the case where the shaft first penetrates a soil layer before being embedded in the underlying rock mass.

REFERENCES

1. Poulos, H. G., "Torsional Response of Piles", Journal of the Geotechnical Engineering Division, ASCE, Vol. 101, No. GT10, Oct. 1975, pp. 1019-1035.

2. Randolph, M. F., "Piles Subjected to Torsion", Journal of the Geotechnical Engineering Division, ASCE, Vol. 107, No. GT8, Aug. 1981, pp. 1095-1111.

3. Stas, C. V. and Kulhawy, F. H., "Critical Evaluation of Design Methods for Foundations Under Axial Uplift and Compression Loading", Report EL-3771, Electric Power Research Institute, Palo Alto, 1984, 198 p.

4. Kulhawy, F. H., Trautmann, C. H., Beech, J. F., O'Rourke, T. D., McGuire, W., Wood, W. A., and Capano, C., "Tranmission Line Structure Foundations for Uplift-Compression Loading", Report EL-2870, Electric Power Research Institute, Palo Alto, 1983, 412 p.

Section 7

INTERPRETATION OF FIELD TESTS

In this section, a number of reported field load tests on rock-socketed shafts are examined, and the data are interpreted in terms of the simple analytical models presented in previous sections. The procedures outlined and used herein are quite general and can be used to interpret a wide range of load tests on model-scale and prototype shafts. The simple models have been fitted to the test data to evaluate and identify the key parameters involved. Some of these parameters, in turn, have been correlated against more commonly used engineering properties of the rock mass.

AXIAL LOAD TESTS

The majority of field data from test loading of rock sockets has been obtained for axial loading conditions. These tests include both vertical compression and uplift loading of complete and shear-only socketed shafts. In many cases, the full load-displacement curve was reported, which allows a more detailed interpretation of the field behavior than simply estimating the maximum average side shear resistance. A number of these tests were selected for study and, in particular, the simple model for the load-displacement behavior presented in Section 4 was fitted to the test data by back-calculation of the parameter values. By this approach, some of the more important aspects of the mechanical behavior of the socketed shafts have been highlighted, and the key parameters of the model have been identified for practical cases. The cases selected for study are listed in Table 7-1, which also includes details of each test configuration and the interpretation that has been made.

Rigid Shafts

In Table 7-1, modulus values of the rock mass surrounding the shaft (E_r), and in some cases the rock beneath the base (E_b), are listed together with the geometric details of each shaft (D and B). The values of E_r and E_b have been back-calculated using the methods described below, and the values of D and B have been obtained from the source references. In all cases, it has been assumed that the equivalent modulus of the concrete shaft is $E_c = 35$ GN/m^2 (5×10^6 psi). For rigid shafts, the precise value of E_c is unimportant, since it is not used directly in any of the back-calculation procedures. However, an approximate value for E_c is required to

Table 7-1

DETAILS OF AXIAL LOAD TESTS

Test[a] I.D.	Reference	Rock Type	q_u[b] (MN/m^2)	D (m)	B (m)	S_1 (MN/m)	S_2 (MN/m)	S_3 (MN/m)	ν_r[c] and ν_b	E_r (MN/m^2)
Shear Sockets - Compression Loading										
P1	1	Shale	6.75	1.37	0.71	661	61	-	0.22	378
P3	1	Shale	6.75	1.37	0.71	447	244	-	0.22	256
Bay St.	2	Shale	41.0	0.686	0.838	649	250	-	0.22	426
S3	3	Mudstone	0.55	2.51	1.17	1613	294	-	0.26	535
S5	3	Mudstone	0.59	2.59	1.12	1478	221	-	0.26	491
A2	4	Sandstone	6.0	0.92	0.21	121	8	-	0.25	146
A3	4	Sandstone	6.0	0.40	0.316	119	14	-	0.25	184
Voided Toe	5	Chalk	0.8	8.59	1.146	730	130	-	0.25	113
A3	8	Siltstone	0.3	8.90	0.45	500	23	-	0.25	96
Complete Sockets - Compression Loading										
P2	1	Shale	6.75	1.37	0.71	630	229	172	0.22	360
P4	1	Shale	6.75	1.37	0.71	880	563	194	0.22	392
M8	3	Mudstone	2.0	1.80	0.66	1250	60	60	0.26	613
Solid Toe	5	Chalk	0.8	8.50	1.146	825	236	-	0.25	128[g]
A1	8	Siltstone	0.3	8.95	0.45	1000	20	-	0.25	176[g]
Shear Sockets - Uplift Loading										
1A	6	Sandstone	2.5	1.08	0.472	1500	92	-	0.25	1188
1B	6	Sandstone	2.5	1.75	0.45	341	76	-	0.25	208
1C	6	Sandstone	2.5	2.77	0.45	1000	167	-	0.25	451
2B	6	Sandstone	2.5	0.90	0.45	125	8	-	0.25	111
2C	6	Sandstone	2.5	1.30	0.536	208	36	-	0.25	141
2F	6	Sandstone	2.5	1.67	0.464	385	65	-	0.25	239
3B	6	Sandstone	18.0	0.80	0.45	1333	478	-	0.25	1258
3C	6	Sandstone	18.0	1.60	0.45	2400	469	-	0.25	1551
24-2	7	Limestone	-	1.20	0.60	712	17	-	0.25	468
24-3	7	Limestone	-	1.32	0.60	356	140	-	0.25	226
A4	8	Siltstone	0.2	3.95	0.45	425	19	-	0.25	150

a - As designated in source reference

b - Average values quoted in source reference

c - Either assumed (0.25) or as quoted in source reference

d - E_c = 35 GN/m^2 assumed

e - Measured ψ = 4.3°

f - Measured ψ = 5.7°

g - $E_b = E_r$ assumed

h - Indeterminant

i - Estimate only, direct measurement not made

j - Cast under bentonite

Table 7-1 Continued

E_b (MN/m^2)	$(\frac{E_c}{E_r})(\frac{B}{2D})^{2d}$	c (MN/m^2)	$\tan\phi \cdot \tan\psi$	$\psi°$ (ϕ = 30°)	$\psi°$ (ϕ = 45°)	$\bar{\tau}_{max}$ (MN/m^2)	$c/\bar{\tau}_{max}$	Roughness Class
-	6.2	1.10	0.0252	2.5	1.4	-	-	R4
-	9.2	1.20	0.2978	27.3	16.6	2.09	0.57	R4
-	30.7	1.66	0.2698	25.1	15.1	-	-	R4[i]
-	3.6	0.30	0.0537	5.3[e]	3.1[e]	0.57	0.53	R4
-	3.3	0.28	0.0409	4.1[f]	2.3[f]	0.46	0.61	R4
-	3.1	0.75	0.0126	1.2	0.7	1.12	0.67	R2
-	29.7	1.02	0.0428	4.2	2.5	1.41	0.72	R3
-	1.4	0.039	0.0324	3.2	1.9	-	-	j
-	0.2	0.077	0.0056	0.6	0.3	-	-	-
230	6.5	0.82	0.0352	3.5	2.0	-	-	R3
260	6.0	0.92	0.2884	26.5	16.1	-	-	R4
85	1.9	h	-	-	-	-	-	-
128[g]	1.2	0.066	0.0194	1.9	1.1	-	-	j
176[g]	0.1	-	-	-	-	-	-	-
-	1.4	0.25	0.0150	1.5	0.9	0.85	0.29	-
-	2.8	0.43	0.0535	5.3	3.1	1.80	0.24	-
-	0.5	0.29	0.0318	3.2	1.8	-	-	-
-	19.7	0.10	0.0170	1.7	1.0	0.80	0.13	-
-	10.5	0.22	0.0474	4.7	2.7	0.47	0.47	-
-	2.8	0.59	0.0390	3.9	2.2	0.90	0.66	-
-	2.2	0.83	0.1473	14.3	8.4	3.18	0.26	-
-	0.4	1.24	0.0469	4.6	2.7	2.26	0.55	-
-	4.7	0.15	0.0061	0.6	0.3	-	-	-
-	8.0	0.071	0.0097	1.0	0.6	-	-	-
-	0.8	0.066	0.0067	0.7	0.4	-	-	-

1 m = 3.28 ft

1 MN/m^2 = 145 psi = 10.44 tsf

1 GN/m^2 = 145 ksi = 10,440 tsf

1 MN/m = 68.5 kip/ft

determine whether each shaft will behave as a rigid member.

In Section 4, it was shown that, to sufficient accuracy, a shaft loaded axially will behave rigidly whenever the stiffness ratio, $(E_c/E_r)/(2D/B)^2$, is greater than about 1. In all but five of the cases listed in Table 7-1, this condition has been met, and therefore the interpretation of rigid shaft behavior is justified. Although some shafts have values of the stiffness ratio less than 1, their behavior has been interpreted under the assumption that they also are rigid. The errors following from this assumption are small, and the minimum observed stiffness ratio of about 0.1 still indicates an extremely stiff shaft.

Interpretation of Rigid Shaft Behavior

It was shown in Section 4 that the elastic response of a rigid shaft in a side shear-only socket can be described by:

$$w_c = \frac{(1 + \nu_r)\zeta}{\pi E_r D} Q_c \tag{7-1}$$

in which

$$\zeta = ln[5(1 - \nu_r)\ D/B] \tag{7-2}$$

For a rigid shaft, the side shear distribution is uniform, and the shaft will slip whenever the shear stress reaches a magnitude of $\tau = c$.

Once full slip occurs along the dilatant, cohesive-frictional interface, the load-displacement relationship becomes:

$$w_c = R_1 \left(\frac{Q_c}{\pi E_r D}\right) - R_2\left(\frac{B}{2}\right) \tag{7-3}$$

in which

$$R_1 = (1 + \nu_r)\ \left(\zeta + \frac{1}{2\ \tan\phi\ \tan\psi}\right) \tag{7-4}$$

and

$$R_2 = \left(\frac{1 + \nu_r}{\tan\phi \ \tan\psi}\right) \left(\frac{c}{E_r}\right) \tag{7-5}$$

During compression load testing of a socket, the slopes of the load-displacement curves can be measured, and the behavior may be idealized as shown in Figure 7-1. If the shaft is rigid, then the measured slopes theoretically are related to the model parameters by:

$$S_1 = \frac{\pi E_r D}{(1 + \nu_r)\zeta} \tag{7-6}$$

and

$$S_2 = \frac{\pi E_r D}{R_1} \tag{7-7}$$

Equation 7-6 can be inverted and then the rock mass modulus E_r can be determined directly from the measured slope S_1 (of the initial portion of the curve) and the dimensions of the shaft, as long as a value for ν_r is assumed. Equations 7-3 to 7-5 show that the slope of the idealized curve, corresponding to full slip, is a function of the two interface strength parameters, c and ϕ, and the interface dilation angle, ψ. A maximum of only two parameter values may be determined from a straight line fit to the experimental data, and therefore it is not possible to determine c, ϕ, and ψ independently. However, the separate determination of ϕ and ψ is unnecessary, because these parameters always appear in combination in the equation describing the load-displacement response. Therefore, the quantity $(\tan\phi \cdot \tan\psi)$ can be obtained from the measured slopes S_1 and S_2 as follows:

$$\tan\phi \cdot \tan\psi = \left(\frac{1}{2\zeta}\right) \left(\frac{S_2}{S_1 - S_2}\right) \tag{7-8}$$

The cohesion c then can be calculated from:

$$c = (2\zeta \ \tan\phi \ \tan\psi + 1) \ \frac{Q_i}{\pi DB} \tag{7-9}$$

in which Q_i is the intercept on the vertical axis ($w_c = 0$) of the straight line

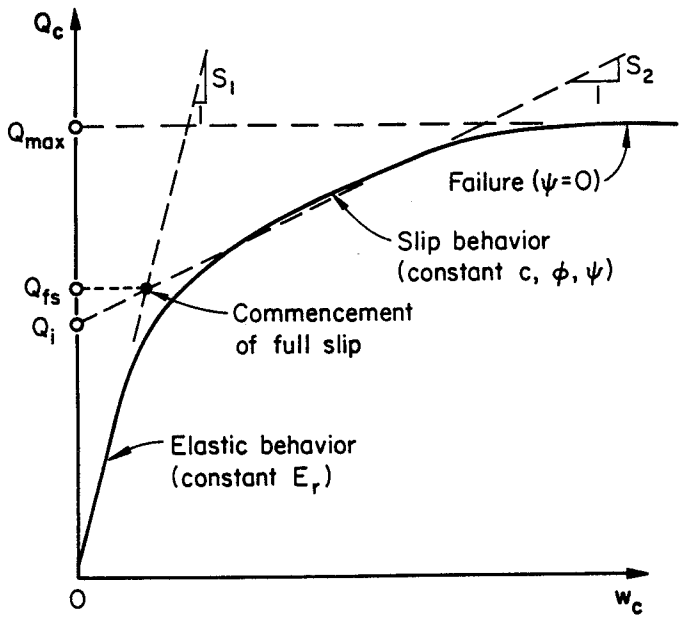

Figure 7-1. Interpretation of Side-Shear-Only Test

fitted to the full-slip portion of the load-displacement curve. Alternatively, c can be computed from:

$$c = \frac{Q_{fs}}{\pi DB} \tag{7-10}$$

in which Q_{fs} is the load at the initiation of full slip (Figure 7-1). Equation 7-10 can be considered as a useful check on the curve fitting procedure.

In many field tests on shear sockets, an ultimate load is observed after relatively large slip displacement has occurred. The schematic load-displacement curve in Figure 7-1 shows this behavior. In reality, the dilation occurring at the shaft-rock interface will not continue indefinitely. There also may be degradation of the strength parameters c and ϕ as slip takes place, but this is not considered in the present simple model of interface behavior. Once the dilation ceases, there can be no further increase in the radial normal stress acting on the shaft and therefore no further increase in frictional strength. At this stage, the shaft load reaches its ultimate value. For the simple model to account for this behavior, a third (horizontal) linear portion of the load-deflection curve is assumed (Figure 7-1). The average shear stress acting on the interface at this

stage, $\bar{\tau}_{max}$, is often termed the unit side shear resistance. Typical values of $\bar{\tau}_{max}$ measured in field loading tests have been given in Figure 3-7.

The measured response during test loading of a complete socket may be interpreted similarly. In this case, additional information might be available, such as the relationship between the settlement of the shaft butt and the load transmitted to the tip, as shown in Figure 7-2. For this case, the slope S_1 is related to the elastic and geometric parameters by:

$$S_1 = \left(\frac{B}{1 - \nu_b^2}\right) E_b + \left(\frac{\pi}{\zeta}\right) \left(\frac{D}{B}\right) \left(\frac{B}{1 + \nu_r}\right) E_r \qquad (7\text{-}11)$$

It is obvious from this equation that the measurement of S_1 alone is insufficient to determine both E_b and E_r, unless a value for the ratio E_b/E_r is determined independently or assumed. If measurements are made of the tip load, and it is also assumed that $\nu_r = \nu_b$, then enough information is available to determine both E_r and E_b. For a relatively rigid shaft, it is sufficient to ignore the shortening of the shaft. Therefore, the measured slope, S_3, of the curve of the tip load versus butt displacement is related to the elastic modulus E_b by:

$$S_3 = \left(\frac{B}{1 - \nu_b^2}\right) E_b \qquad (7\text{-}12)$$

Substitution of Equation 7-12 into 7-11 allows the determination of E_r.

Once full slip of the shaft has occurred, the load-displacement relationship for the complete socket becomes:

$$w_c = R_4 \left(\frac{2Q_c}{\pi E_r B}\right) - R_5 \frac{B}{2} \qquad (7\text{-}13)$$

in which

$$R_5 = \frac{R_2 \, R_3(2D/B)}{R_3(2D/B) + R_1} \qquad (7\text{-}14)$$

$$R_4 = \frac{R_3 \, R_1}{R_3(2D/B) + R_1} \qquad (7\text{-}15)$$

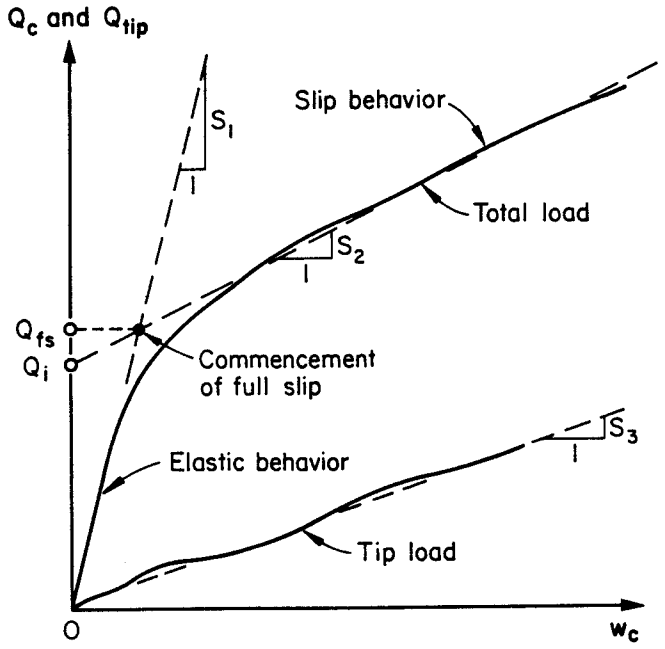

Figure 7-2. Interpretation of Complete Socket Test

$$R_3 = \left(\frac{\pi}{2}\right)\ (1 - \nu_b^2)\ \left(\frac{E_r}{E_b}\right) \tag{7-16}$$

As with a shear socket, the slopes S_1, S_2, and S_3 can be used to determine the quantity $(\tan\phi \cdot \tan\psi)$ and, for the complete socket, the appropriate relationship is:

$$\tan\phi \cdot \tan\psi = \left(\frac{1}{2\zeta}\right)\ \left(\frac{S_2 - S_3}{S_1 - S_2}\right) \tag{7-17}$$

For this case, the cohesion c can be obtained from

$$c = (2\zeta\ \tan\phi\ \tan\psi + 1)\ \frac{Q_i}{\pi BD} \tag{7-18}$$

in which Q_i is the intercept of the "full slip" line on the vertical axis (Figure 7-2).

For convenience, the equations used to back-calculate E_r, E_b, c, and $(\tan\phi \cdot \tan\psi)$ for the compression load cases have been summarized in Table 7-2. It should be

Table 7-2

INTERPRETATION OF AXIAL LOAD TESTS ON RIGID SHAFTS

(a) Shear Socket - Compression or Uplift

$$E_r = \left[\frac{(1 + \nu_r)\zeta}{\pi D}\right] S_1$$

$$\tan\phi \cdot \tan\psi = \left(\frac{1}{2\zeta}\right) \left(\frac{S_2}{S_1 - S_2}\right)$$

$$c = (2\zeta \tan\phi \cdot \tan\psi + 1) \frac{Q_i}{\pi BD}$$

(b) Complete Socket - Compression

$$E_r = \left[\frac{(1 + \nu_r)\zeta}{\pi D}\right] (S_1 - S_3)$$

$$E_b = \left[\frac{(1 - \nu_b^2)}{B}\right] S_3$$

$$\tan\phi \cdot \tan\psi = \left(\frac{1}{2\zeta}\right) \left(\frac{S_2 - S_3}{S_1 - S_2}\right)$$

$$c = (2\zeta \tan\phi \tan\psi + 1) \frac{Q_i}{\pi BD}$$

noted that the behavior of a rigid shaft in uplift loading is essentially the same as that for an identical shaft in a shear socket subjected to compression loading. Only the directions of the displacements and applied loads are reversed.

Back-Analysis

The techniques described above have been applied to 25 axial load tests reported in the literature. The back-calculated values of the model parameters are listed in Table 7-1, and the load-displacement curves are given in Appendix A, in which each figure shows the measured response of the shaft and the interpretation that has been made. In all cases, at least a bilinear fit has been made to the observed behavior, corresponding to an initial elastic response and then to full slip of the shaft. For some tests on shear-only sockets, ultimate failure was observed in the

field. As discussed above, this has required the fitting of a third linear section to the observed load-displacement curve. In such cases, the final horizontal portion of the curve indicates that dilation at the interface has ceased ($\psi = 0$), and the shaft continues to slip in its socket under constant load, with a constant shear stress ($\bar{\tau}_{max}$) acting at the interface. In these cases, the value of $\bar{\tau}_{max}$ has been determined from the observed maximum applied load.

Although values for ϕ and ψ can not be determined separately from the test data, values of ψ corresponding to an assumed $\phi = 30°$ and 45° have been listed in Table 7-1 for reference purposes. In several of the tests (3), dilation at the interface was measured. Plots of dilation versus shear displacement for these cases are included in Appendix A, and the measured values of ψ are given in Table 7-1.

Comments and General Observations

The complete interpretation of some tests required the making of some additional assumptions. It was necessary to assume that Poisson's ratio (ν_r and ν_b) was equal to 0.25, whenever specific data were not provided in the source references. For the "solid toe" shaft (5), a value of S_3 was not measured directly, but an estimate was made on the basis of data from plate load tests in the chalk. In determining E_r for shaft P2 (1), it was assumed that no load was transmitted to the tip until the shaft began to slip (Figure A-10). While this assumption is not in complete agreement with the observations, it is considered reasonable for the purposes of the present interpretation.

Quite a wide range of values of ($\tan\phi \cdot \tan\psi$), from 0.0024 to 0.30, was deduced from the test results. This parameter is very sensitive to the value of S_2, which is determined by some subjective interpretation. Large values of S_2 (relative to S_1) yield large values for ($\tan\phi \cdot \tan\psi$). On the other hand, the deduced cohesion, c, is less sensitive to S_2 (unless S_2 is close to S_1) but more sensitive to Q_i. E_r and E_b are directly proportional to S_1 and S_3, respectively.

It is also interesting to note the observed values of the ratio $c/\bar{\tau}_{max}$. For a rigid shaft, this value is equal to the ratio of the shaft load at first slip and the ultimate shaft load. A wide range was observed, from 0.13 to 0.72, indicating that shaft slip may commence well before the maximum load is reached.

Correlations with Roughness and Strength

Correlations were made between the deduced values, c and ($\tan\phi \cdot \tan\psi$), and the

measured interface roughness, where available. Several classes of interface roughness have been defined (4) and these are given in Table 7-3. A continuous measure of roughness, RF, also has been defined (1) as follows:

$$RF = \left(\frac{2\bar{a}}{B}\right)\left(\frac{L_t}{D}\right) \tag{7-19}$$

in which $\bar{a}$ = average height of asperities along the socket, B/2 = nominal socket radius, L_t = total distance traveled up and down the asperities along the socket wall profile, and D = nominal socket depth.

By considering the irregular socket profile as an equivalent set of regular, periodically spaced asperities, it is possible to correlate approximately the roughness factor suggested in Equation 7-19 with the roughness classes given in Table 7-3. Details of the roughness factor corresponding to several regular profiles are given in Figure 7-3, and the approximate equivalence between RF and roughness class is given in Table 7-3.

The roughness class, where provided directly in the source reference or determined from RF, has been listed in Table 7-1. Attempts to correlate c and $(\tan\phi \cdot \tan\psi)$ with roughness class have been made in Figures 7-4 and 7-5, but it is clear that no strong trends can be established. For future tests, it would be useful to quantify socket roughness (either as a class or a value of RF) for axial load tests in rock to allow correlation of strength with roughness.

In many of the cases reported in Table 7-1, values of uniaxial compressive strength for the rock have been recorded. This has allowed correlations between c, $(\tan\phi \cdot \tan\psi)$, $\bar{\tau}_{max}$, and q_u, as shown in Figures 7-6 to 7-8. In all figures, the stresses have been normalized by the atmospheric pressure, p_a. From Figure 7-6, it is clear that a good correlation exists between c and q_u. All data points lie above or on the curve given by:

$$\left(\frac{c}{p_a}\right) = 0.1\left(\frac{q_u}{p_a}\right)^{2/3} \tag{7-20}$$

Figure 7-7 also shows a good correlation between $(\tan\phi \cdot \tan\psi)$ and q_u, although intuitively this may have been less obvious. A reasonable lower bound to most data points is given by:

Table 7-3

APPROXIMATE EQUIVALENCE BETWEEN ROUGHNESS CLASS AND ROUGHNESS FACTOR

Class[a]	Definition[a]	Roughness Factor[b] × Nominal Radius of Socket (RF × B/2) mm
R1	Straight, smooth-sided socket, grooves or indentations less than 1.0 mm (0.04 in) deep	0 to 1
R2	Grooves of depth 1 to 4 mm (0.04 to 0.16 in), width greater than 2 mm (0.08 in), at spacing 50 to 200 mm (2 to 8 in)	1 to 4
R3	Grooves of depth 4 to 10 mm (0.16 to 0.4 in), width greater than 5 mm (0.2 in), at spacing 50 to 200 mm (2 to 8 in)	4 to 14
R4	Grooves or undulations of depth greater than 10 mm (0.4 in), width greater than 10 mm (0.4 in), at spacing 50 to 200 mm (2 to 8 in)	> 14

a - As defined in (4)

b - As defined in (1)

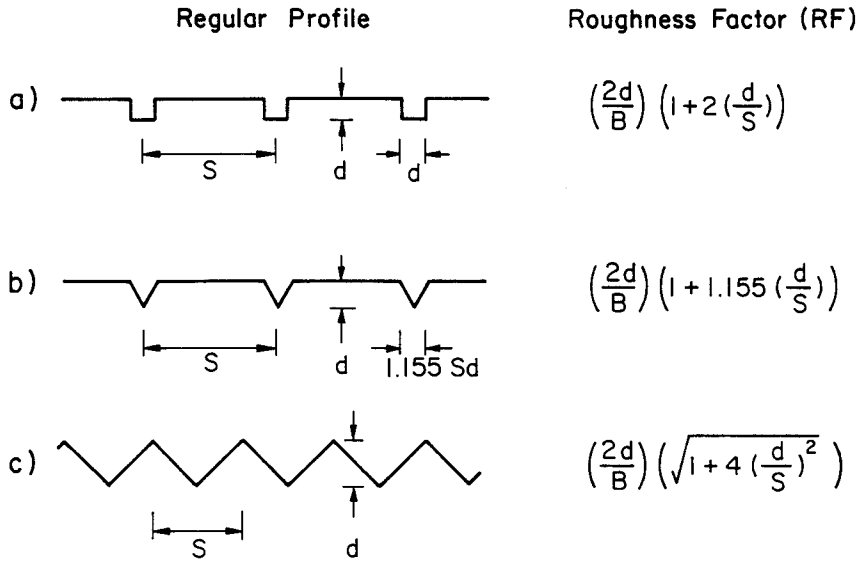

Figure 7-3. Roughness Factors for Selected Regular Profiles

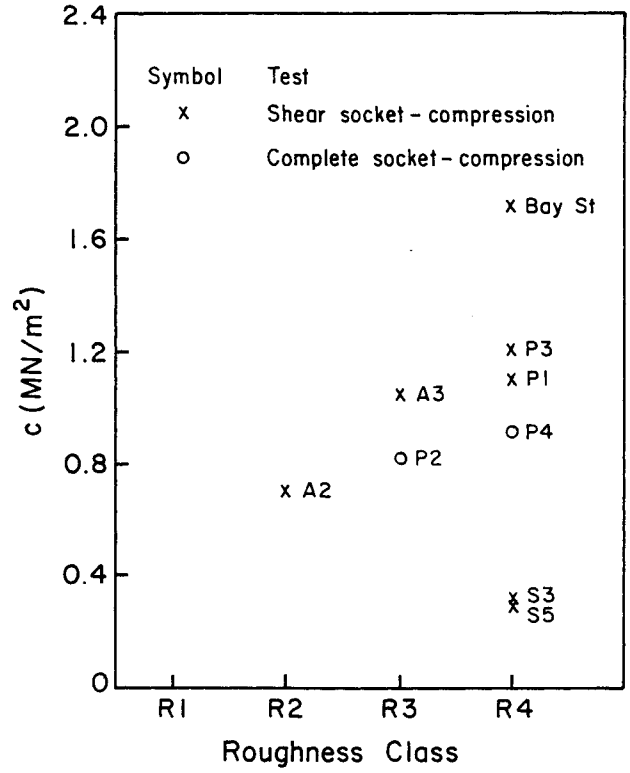

Figure 7-4. Interface Cohesion vs. Socket Roughness Class

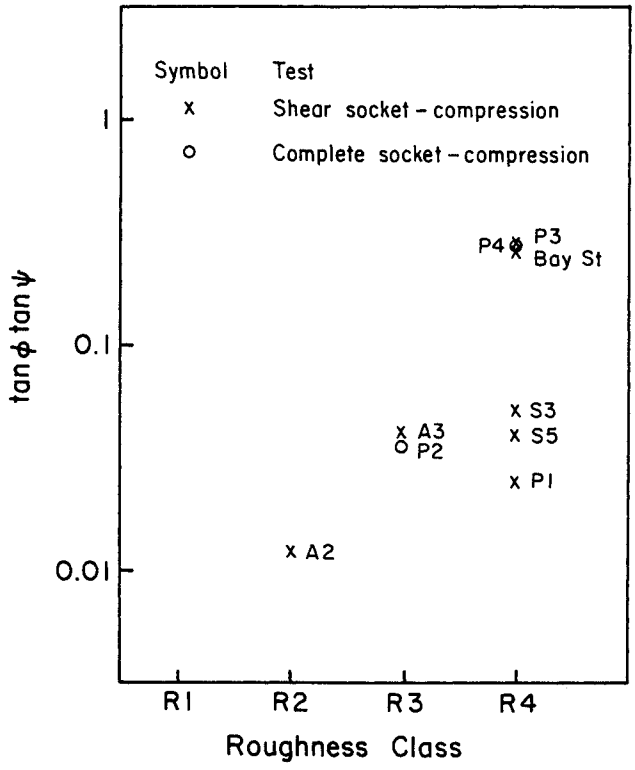

Figure 7-5. Interface Friction-Dilation Parameters vs. Socket Roughness Class

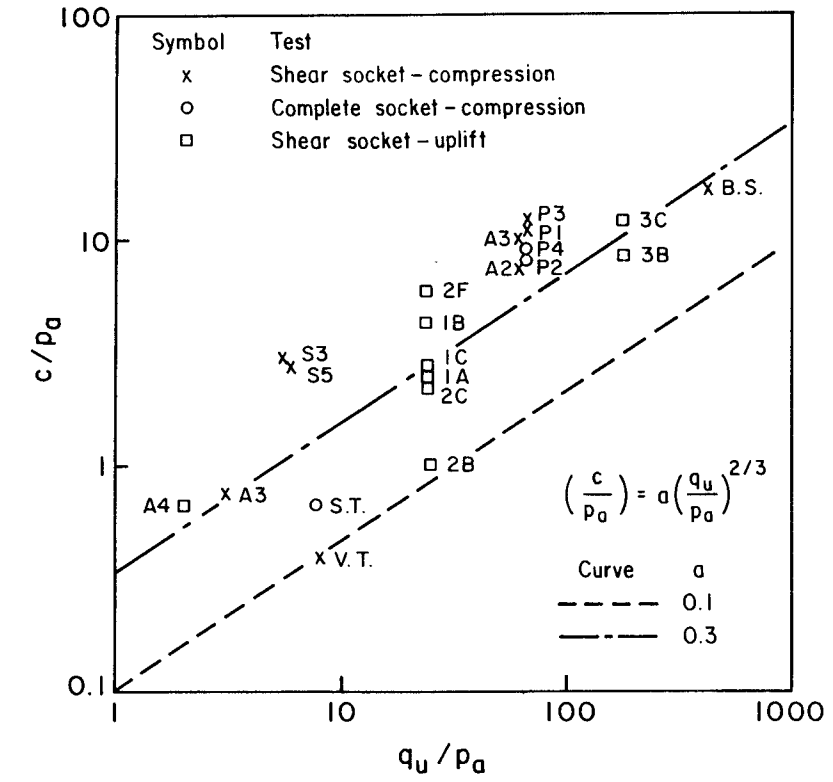

Figure 7-6. Interface Cohesion vs. Uniaxial Compressive Strength of Rock

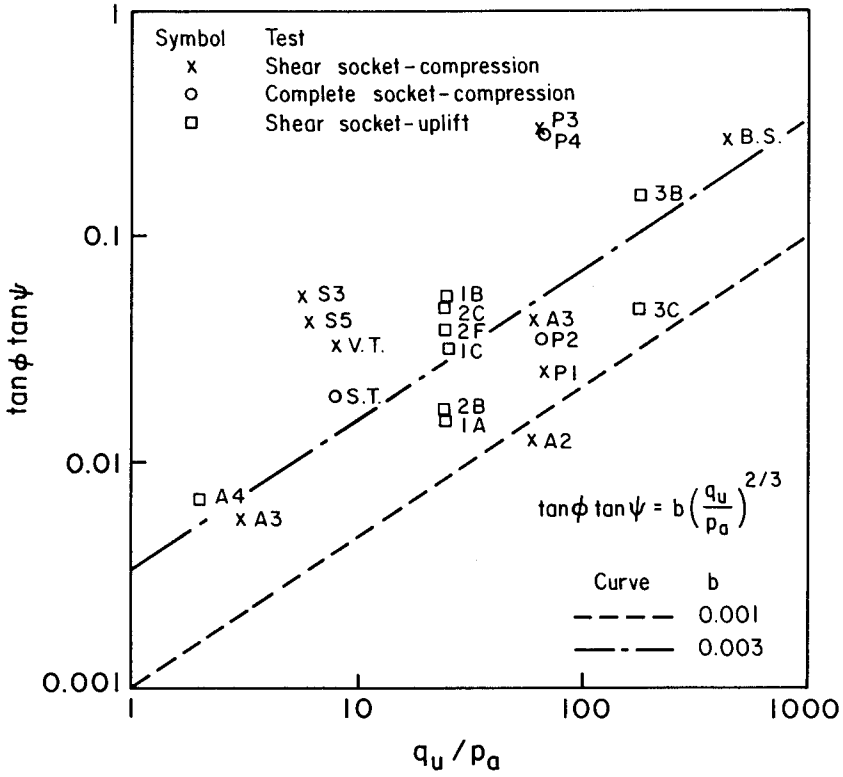

Figure 7-7. Interface Friction-Dilation Parameters vs. Uniaxial Compressive Strength of Rock

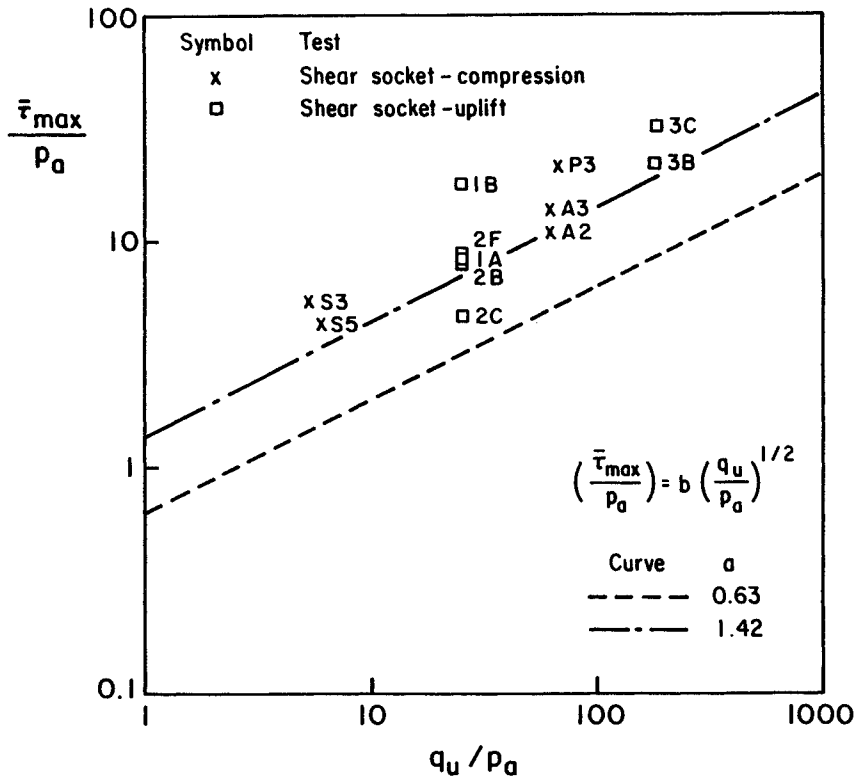

Figure 7-8. Relationships between Peak Side Shear and Uniaxial Compressive Strength of Rock

$$(\tan\phi \cdot \tan\psi) = 0.001\left(\frac{q_u}{p_a}\right)^{2/3} \tag{7-21}$$

The same exponent appearing in both Equations 7-20 and 7-21 may only be fortuitous. Confirmation of these equations must await further corroborating data.

From the cases examined in Table 7-1, only a few values are available for $\bar{\tau}_{max}$, as plotted in Figure 7-8. The design curve suggested in Section 3 and repeated below:

$$\left(\frac{\bar{\tau}_{max}}{p_a}\right) = 0.63\left(\frac{q_u}{p_a}\right)^{1/2} \tag{7-22}$$

also has been plotted on Figure 7-8, and it forms a lower bound to all the data points.

LATERAL LOAD TESTS

There is a dearth of data in the literature on the performance of rock-socketed shafts subjected to lateral loading. Indeed, the authors have found only one reported test in which two shafts embedded in rock over a significant proportion of their length were loaded laterally (10). This load test involved the jacking together of two adjacent shafts, which once formed part of the foundations for an electrical transmission line structure. A schematic cross-section showing the two shafts and the loading arrangement is given in Figure 7-9. Each shaft has a different length and diameter and, in particular, each has a different eccentricity of the loading point above the immediate rock surface. Furthermore, between the shafts, the rock surface slopes at approximately 25 degrees to the horizontal. This last feature has been ignored in the interpretation of the test data, and the immediate surface around each shaft was treated as horizontal. Any structural interaction between the shafts and the fact that shaft 14-U has an enlarged base also have been ignored. However, the eccentricity of loading of each shaft has been taken into account, as has the eccentricity of the heights above the rock surface of the displacement measuring points. In the latter regard, each shaft was assumed to behave rigidly during lateral loading, and the rock mass was assumed to behave elastically, so that horizontal displacements at the groundline may be calculated from the measured horizontal displacements, using the centers of rotation deduced from Equation 5-10. For a rigid shaft, the groundline horizontal displacement and rotation are given by (Section 5):

$$u = 0.4 \frac{H}{G^*B} \left(\frac{2D}{B}\right)^{-1/3} + 0.3 \frac{M}{G^*B^2} \left(\frac{2D}{B}\right)^{-7/8} \tag{7-23}$$

$$\theta = 0.3 \frac{H}{G^*B^2} \left(\frac{2D}{B}\right)^{-7/8} + 0.8 \frac{M}{G^*B^3} \left(\frac{2D}{B}\right)^{-5/3} \tag{7-24}$$

and the center of rigid body rotation is at a depth, z_c, given by:

$$z_c = \left\{ \frac{0.4\left(\frac{2D}{B}\right)^{-1/3} + 0.3\left(\frac{e}{B}\right)\left(\frac{2D}{B}\right)^{-7/8}}{0.3\left(\frac{2D}{B}\right)^{-7/8} + 0.8\left(\frac{e}{B}\right)\left(\frac{2D}{B}\right)^{-5/3}} \right\} B \tag{7-25}$$

In the above equations, H and M are the applied shear and moment at the ground surface, e = M/H is the vertical eccentricity of the applied horizontal force, and

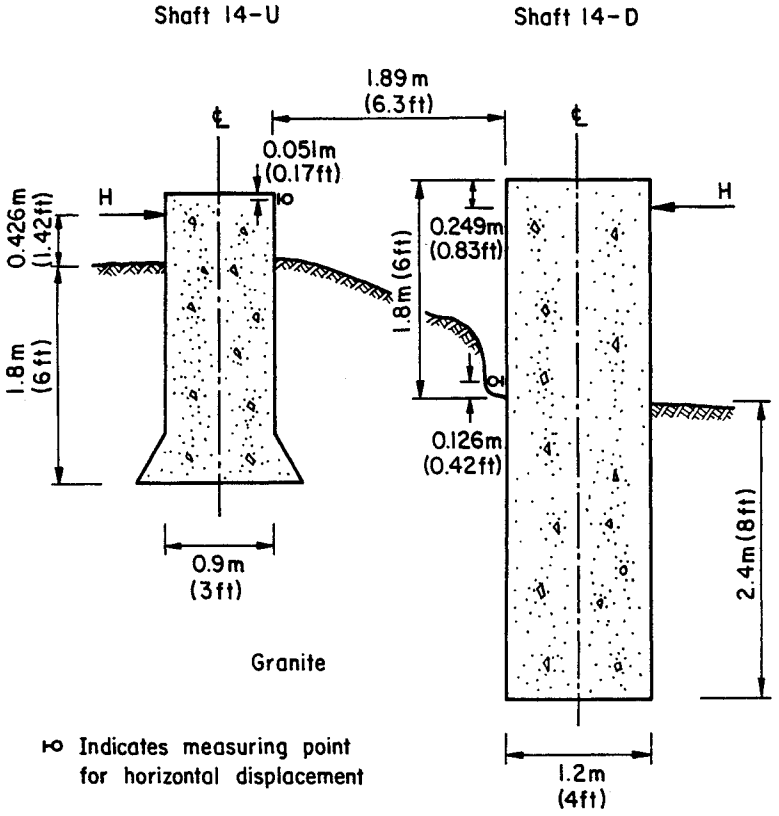

Figure 7-9. Details of Lateral Load Test

G* is related to the elastic properties of the rock mass by:

$$G^* = \left(\frac{1 + 3\nu_r/4)}{1 + \nu_r}\right) \frac{E_r}{2} \tag{7-26}$$

For the assumption of rigid shaft behavior to be valid, the following condition must hold:

$$(E_c/G^*)(B/2D)^2 \geq 100 \tag{7-27}$$

in which $E_e = (EI)_c/(\pi B^4/64)$ is the equivalent Young's modulus of the shaft section, $(EI)_c$ is its actual bending rigidity, and the moment of inertia of a circular section about a diameter is $\pi B^4/64$.

The measured lateral load-horizontal displacement relationship for each of these shafts is given in Figures 7-10 and 7-11. A straight line has been fitted to the

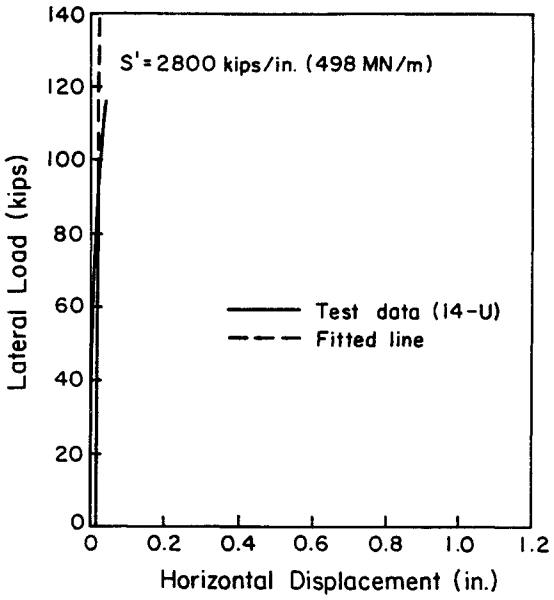

Figure 7-10. Load Test Results for Shaft 14-U

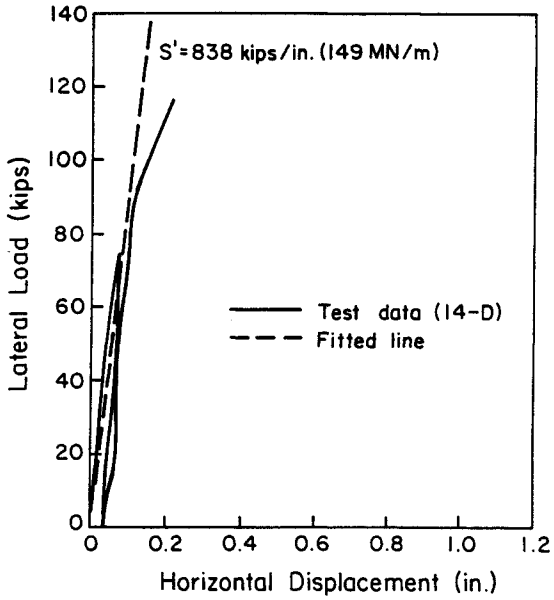

Figure 7-11. Load Test Results for Shaft 14-D

initial portion of each curve, and the slope of the line S' has been reported in Table 7-4 for each case. Also recorded in Table 7-4 are the slopes S of the linear relations between the measured applied load and the deduced horizontal displacements at the groundline. Equation 7-23 has been used to determine values of G* for each case from the slopes, S = H/u, and the known geometries and loading configurations. In each case, a value of $\nu_r = 0.25$ has been assumed for the rock mass, allowing the determination of E_r from Equation 7-26. Deduced values of the Young's modulus for the rock mass immediately surrounding each shaft have also been listed in Table 7-4. It can be seen that the calculated modulus for shaft 14-U is approximately four times that for shaft 14-D. Values of the bending rigidity of the shafts have not been given in the source reference, but assuming typical reinforced concrete details implies that E_e is on the order of 50 GN/m^2 (7×10^6 psi). The relative stiffness, $(E_e/G^*)(B/2D)^2$, has been calculated for each shaft, assuming E_e = 50 GN/m^2, and also is given in Table 7-4. In both cases, the relative stiffness is less than 100, indicating that for each shaft, the assumption of rigid behavior may be slightly inaccurate. However, values of $(E_p/G^*)/(B/2D)^2$ = 16 and 65 still indicate very stiff shafts.

Table 7-4

DETAILS OF LATERAL LOAD TESTS

Shaft I.D.	D (m)	B (m)	e (m)	S' MN/m	S MN/m	G* (MN/m^2)	E_r (MN/m^2)	$(E_c/G^*)(B/2D)^2$
14-U	1.8	0.9	0.426	498	600	196	414	16
14-D	2.4	1.2	1.551	149	157	48	101	65

Source: Data obtained from (10).

TORSION LOAD TESTS

No reported cases of torsional load tests on rock-socketed shafts were found in the literature. Therefore, it is not possible to illustrate the application of the theory developed in Section 7 to the interpretation of a torsional field test.

SUMMARY

Interpretations have been made of reported field load tests on rock-socketed shafts. Twenty-five tests were found in the literature for axial loading (both compression and uplift), but only two were found for lateral loading, and none were found for torsional loading.

For most of the examined cases of axial loading, it was shown that rigid shaft behavior was reasonable. This is largely because of the stubby geometry of the test shafts, but may also result because the data were obtained for shafts in sedimentary rocks. The assumption of rigidity may be less acceptable for shafts in harder rocks where the modulus values for the rock mass and the shaft material are closer.

It is suggested that the simple theoretical model for shaft behavior under axial loading, including slip, provides a reasonable fit to the experimental data, and may be used to back-calculate parameter values from field load tests. By applying this model, good correlations were found between the uniaxial compressive strength of the intact rock and the cohesion, c, the friction-dilation parameter, $(\tan\phi \cdot \tan\psi)$, and the peak unit side shear stress, $\bar{\tau}_{max}$.

For the two shafts in rock subjected to lateral loading, a linear relationship

between horizontal load and displacement was found at working load levels. The analytical model presented in Section 5 was used to calculate the apparent modulus of the rock mass for lateral loading conditions. Further field testing of this type is required to verify the linear model for working load levels in rock, over the common range of shaft geometries and rock types.

REFERENCES

1. Horvath, R. G., Kenney, T. C., and Kozicki, P., "Methods of Improving the Performance of Drilled Piers in Weak Rock," Canadian Geotechnical Journal, Vol. 20, No. 4, Nov. 1983, pp. 758-772.

2. Horvath, R. G., Kenney, T. C., and Trow, W. A., "Results of Tests to Determine Shaft Resistance of Rock-Socketed Drilled Piers", Proceedings, International Conference on Structural Foundations on Rock, Vol. 1, Sydney, 1980, pp. 349-361.

3. Williams, A. F., "The Design and Performance of Piles Socketed into Weak Rock," Ph.D. Dissertation, Monash University, Melbourne, 1980 (as reported in 9).

4. Pells, P. J. N., Rowe, R. K., and Turner, R. M., "An Experimental Investigation into Side Shear for Socketed Piles in Sandstone," Proceedings, International Conference on Structural Foundations on Rock, Vol. 1, Sydney, 1980, pp. 291-302.

5. Mallard, D. J. and Ballantyne, J. L., "The Behavior of Piles in Upper Chalk at Littlebrook D Power Station," Piles in Weak Rock, Institution of Civil Engineers, London, 1977, pp. 47-72.

6. Webb, D. L. and Davies, P., "Ultimate Tensile Loads of Bored Piles Socketed into Sandstone Rock," Proceedings, International Conference on Structural Foundations on Rock, Vol. 1, Sydney, 1980, pp. 265-270.

7. Kulhawy, F. H., O'Rourke, T. D., Stewart, J. P., and Beech, J. F., "Transmission Line Structure Foundations for Uplift-Compression Loading: Load Test Summaries", Report EL-3160, Electric Power Research Institute, Palo Alto, 1983, 729 p.

8. Davies, P., Webb, D. L., Hooley, P., and Yeats, J. A., "Geotechnical Parameters for Design of Bored Piles Founded in Weathered Siltstone Rock," Proceedings, 7th European Conference on Soil Mechanics and Foundation Engineering, Vol. 3, Brighton, 1979, pp. 43-50.

9. Chiu, H. K. and Dight, P. M., "Prediction of the Performance of Rock-Socketed Side-Resistance-Only Piles Using Profiles," International Journal of Rock Mechanics and Mining Sciences, Vol. 20, No. 1, Feb. 1983, pp. 21-32.

10. Tucker, K. D. and Askari, S., "Interim Report on Evaluation of SCE BIPILE Computer Program," Southern California Edison Company, 1986 (privately communicated).

Section 8

DESIGN EXAMPLE OF FOUNDATION FOR LATTICE TOWER

In this section, some of the analytical techniques and empirical data presented earlier will be used for the preliminary design of a drilled shaft foundation for one leg of a lattice tower transmission structure. The calculations illustrate only the preliminary design of a shaft in rock. In general, it is good practice to test load some foundation elements at any new site until sufficient experience with the natural materials and confidence in the design have been gained.

GEOTECHNICAL DATA AND DESIGN CRITERIA

The design loadings for this example are shown in Figure 8-1. The foundation to be used is a drilled shaft in rock, and it is assumed that the rock outcrops at the surface. The rock mass is of good quality, having tightly interlocking, undisturbed rock with rough unweathered joints spaced at about 3 to 9 feet. The rock mass is assumed to have the following properties: Young's modulus (E_r) = 2000 kip/ft^2 and Poisson's ratio (ν_r) = 0.25, and the uniaxial compressive strength of the intact rock (q_u) = 100 kip/ft^2.

The foundation is to be designed according to the following specifications: (1) a minimum factor of safety of 2.5 under axial compression, axial uplift, and lateral loading, (2) maximum axial and lateral displacements under the respective working loads of 1 inch, and (3) maximum groundline rotation under the lateral force of 1 degree.

DESIGN PROCEDURE FOR AXIAL LOADING

The aim of the design exercise is to determine suitable shaft dimensions to meet all the design criteria. For the given loadings, it is likely that axial compression will govern the design, and therefore a suitable starting point for the design process involves an examination of the ultimate condition. In the following, it is assumed that resistance to axial loading is provided only by the side shear. Tip resistance is ignored to simplify the example.

Knowledge of the rock strength, together with the preliminary design Equation 7-22,

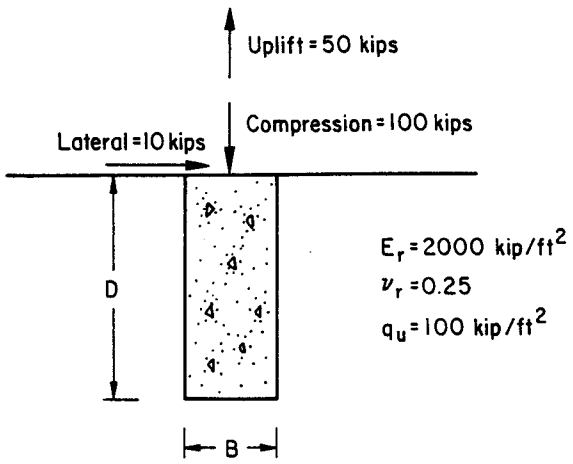

Figure 8-1. Loading and Rock Mass Properties for Lattice Tower Foundation

allows a conservative estimate of the peak unit side shear resistance, $\bar{\tau}_{max}$:

$$\left(\frac{\bar{\tau}_{max}}{p_a}\right) \approx 0.63\left(\frac{q_u}{p_a}\right)^{1/2} \tag{8-1}$$

in which p_a is atmospheric pressure. In English units, $p_a \approx 2$ kip/ft^2 and:

$$\bar{\tau}_{max} \approx 0.63 \times \left(\frac{100}{2}\right)^{1/2} \times 2 = 8.9 \text{ kip/ft}^2$$

A factor of safety of 2.5 implies that the maximum axial load (Q_{max}) is 250 kips. The maximum axial load is related to the unit side shear resistance by:

$$Q_{max} = \pi B D \bar{\tau}_{max} \tag{8-2}$$

which implies that a suitable length of the embedded shaft is:

$$D = \frac{Q_{max}}{\pi B \bar{\tau}_{max}} \tag{8-3}$$

The selection of the shaft diameter often is made on the basis of construction considerations. For the present case, it is assumed that B = 1.5 ft, and therefore from Equation 8-3:

$$D = \frac{250}{\pi \times 1.5 \times 8.9} = 5.96 \text{ ft}$$

Rounding off this result, D is selected to be 6 ft, in which case the factor of safety for axial compression is slightly larger than 2.5.

Before predicting the load-displacement response of a shaft with B = 1.5 ft and D = 6 ft, the relative rigidity of the shaft is considered. The condition for a rigid shaft has been discussed in Section 4 (Equation 4-103). For the present case:

$$\left(\frac{E_c}{E_r}\right)\left(\frac{B}{2D}\right)^2 = \left(\frac{730,000}{2000}\right)\left(\frac{1.5}{2 \times 6}\right)^2 = 5.7 > 1 \qquad (8\text{-}4)$$

in which the modulus of the concrete shaft (E_c) has been taken as 730,000 kip/ft^2. Because the relative rigidity is greater than 1 (Section 4), the shaft behaves rigidly under axial loading.

Consider first the linear elastic response of this rigid shaft. The prediction of its axial stiffness is given below. From Equation 7-2, the parameter ζ is:

$$\zeta = ln[5(1 - \nu_r)D/B] = ln[5 \times 0.75 \times 6/1.5] = 2.708 \qquad (8\text{-}5)$$

From Equation 7-1, the elastic stiffness is:

$$\frac{Q_c}{w_c} = \left[\frac{\pi}{(1 + \nu_r)\zeta}\right]E_r d = \left[\frac{\pi}{1.25 \text{ x } 2.708}\right] \text{ x } 2000 \text{ x } 6 \qquad (8\text{-}6)$$

$$= 11137 \text{ kip/ft} = 928 \text{ kip/in}$$

To determine the response of the shaft once it slips, values of the parameters c and $(\tan\phi \cdot \tan\psi)$ are required. From Equation 7-20, a preliminary design value of c is given by:

$$\left(\frac{c}{p_a}\right) \approx 0.1 \left(\frac{q_u}{p_a}\right)^{2/3} \qquad (8\text{-}7)$$

from which

$$c = 0.1 \times (\frac{100}{2})^{2/3} \times 2 = 2.7 \text{ kip/ft}^2$$

Equation 7-21 gives a value of $(\tan\phi \cdot \tan\psi)$ suitable for use in preliminary design:

$$\tan\phi \tan\psi \approx 0.001(\frac{q_u}{p_a})^{2/3} = 0.001 \times (\frac{100}{2})^{2/3} = 0.0136 \quad (8\text{-}8)$$

The load-displacement curve for full slip is given by Equation 7-3 and, for convenience, it is repeated below:

$$w_c = (\frac{R_1}{\pi E_r D}) Q_c - R_2(\frac{B}{2}) \quad (8\text{-}9)$$

in which

$$R_1 = (1 + \nu_r)(\zeta + \frac{1}{2\tan\phi \tan\psi}) = 1.25 \times (2.708 + \frac{1}{2 \times 0.0136}) = 49.34 \quad (8\text{-}10)$$

and

$$R_2 = (\frac{1 + \nu_r}{\tan\phi \tan\psi})(\frac{c}{E_r}) = (\frac{1.25}{0.0136}) \times (\frac{2.7}{2000}) = 0.124 \quad (8\text{-}11)$$

Therefore

$$w_c = (\frac{49.34}{\pi \times 2000 \times 6}) Q_c - 0.124 \times (\frac{1.5}{2})$$

$$= 1.309 \times 10^{-3} Q_c - 0.093 \qquad \text{(ft. with } Q_c \text{ in kips)}$$

$$= 0.0157 Q_c - 1.116 \qquad \text{(in. with } Q_c \text{ in kips)}$$

The predicted overall axial load-displacement behavior therefore can be represented as in Figure 8-2, which shows an initial linear elastic portion, a linear slip portion, and ultimate failure. Under the design compressive load of 100 kips, the predicted displacement is 0.45 inches (point C in Figure 8-2), which lies within the slip region and also meets the design specification.

In the design calculations presented above, the predicted slip displacements were based on what are likely to be lower bound estimates of c and $(\tan\phi \cdot \tan\psi)$. Because

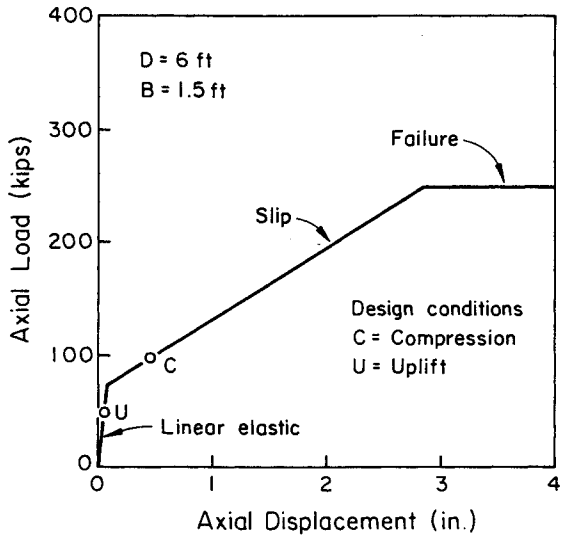

Figure 8-2. Predicted Axial Behavior of Lattice Tower Foundation

this is a conservative approach, it is likely to overpredict the actual displacements at any given load.

The same general axial response can be expected under uplift loading, provided the same values of E_r, $\bar{\tau}_{max}$, c, and $(\tan\phi \cdot \tan\psi)$ can be relied upon. If this is reasonable, then the uplift displacement under an uplift load of 50 kips can be expected to be about 0.05 inches, which lies within the linear elastic region (point U in Figure 8-2). It will not always be reasonable to adopt the same values for the model parameters when examining both compression and uplift behavior. For example, adverse joint orientations may necessitate the reduction of the design values of any or all of E_r, $\bar{\tau}_{max}$, c, and $(\tan\phi \cdot \tan\psi)$ for the uplift case. In the present case, it also would be advisable to examine the possibility of wedge failure during uplift as the aspect ratio D/B = 4 is relatively low, but this is not pursued here.

DESIGN PROCEDURE FOR LATERAL LOADING

The behavior under lateral loading is now considered. Assuming that the shaft is effectively rigid with respect to bending, Equations 5-8 and 5-9 may be used to compute the displacements. The effective shear modulus of the rock is $G^* = G_r(1 + 3\nu_r/4)$ and, since $G_r = E_r/[2(1 + \nu_r)]$, their values are calculated as:

$$G_r = \frac{2000}{2 \times 1.25} = 800 \text{ kip/ft}^2$$

and

$$G^* = 800 \times (1 + 3 \times 0.25/4) = 950 \text{ kip/ft}^2$$

Therefore, the displacement and rotation at the groundline from a horizontal force of 10 kips are:

$$u = 0.4 \frac{H}{G^*B} \left(\frac{2D}{B}\right)^{-1/3} = 0.4 \times \frac{10}{950 \times 1.5} \left(\frac{12}{1.5}\right)^{-1/3} \quad (8\text{-}12)$$

$$= 1.40 \text{ ft} \times 10^{-3} \text{ ft} = 0.02 \text{ in}$$

and

$$\theta = 0.3 \frac{H}{G^*B^2} \left(\frac{2D}{B}\right)^{-7/8} = 0.3 \times \frac{10}{950 \times 1.5^2} \left(\frac{12}{1.5}\right)^{-7/8} \quad (8\text{-}13)$$

$$= 2.28 \times 10^{-4} \text{ radians} = 0.013 \text{ degrees}$$

For the shaft to be effectively rigid in bending, the quantity $(E_c/G^*)(B/2D)^2$ should be larger than 100 (Section 5, Equation 5-7). In the present case, it is only 5.7, and therefore the shaft is of intermediate flexibility. As suggested in Section 5, the displacement and rotation for shafts of this type should be increased by about 25 percent. Even the increased values still meet the design specification.

In the calculations presented above, the same value of rock modulus E_r was used to calculate both the axial and lateral displacements. This may not always be justified, however, and the designer needs to determine that this assumption is reasonable for the site. Axial displacement of the shaft essentially involves shearing of the rock mass on vertical, cylindrical surfaces, while under lateral loading, the deformation pattern in the rock mass is more complex. Therefore, in the application of the linear theories to predict axial and lateral displacements of a shaft, it may be more reasonable on occasion to adopt different values of E_r for the axial and lateral modes.

It is also necessary to check that adequate capacity can be provided by the rock mass to resist the lateral loading, as suggested earlier in Section 3. The shaft considered here has a ratio of D/B = 4, and it is likely that the full plane strain limit pressure will develop at a depth of about 3 diameters. This could be included in the determination of the lateral capacity; however, it will be simpler and even more conservative to assume that the limiting normal stress on the projected area of the face of the shaft is equal to the uniaxial compressive strength of the rock mass, or $q_{ult} = \sqrt{s}\ q_u$, in which s is the parameter used in the Hoek and Brown failure criterion (Section 3). Based on the description of the rock mass given previously, Table 3-1 indicates a representative value of s = 0.1, and therefore:

$$q_{ult} = \sqrt{0.1} \times 100 \text{ kip/ft}^2 = 31.6 \text{ kip/ft}^2$$

The ultimate lateral force can be estimated conservatively (given that values of s and q_u are representative) by:

$$H_{ult} = q_{ult}\ BD = 31.6 \times 1.5 \times 6 = 284.4 \text{ kips} \qquad (8\text{-}14)$$

The factor of safety against failure under lateral loading then is:

$$F = H_{ult}/H = 284.4/10 = 28.4 \qquad (8\text{-}15)$$

which meets the design specification more than adequately.

It should be noted that, for lower quality rock masses, the suggested values of s (Table 3-1) decrease rapidly. For such cases, it may be necessary to increase the shaft dimensions to achieve an adequate margin of safety for the lateral loading.

SUMMARY

The design example presented in this section has illustrated that the equations presented in the previous sections can be used simply and efficiently in the preliminary design process. Both capacities and displacements can be computed for all loading modes, as long as adequate geotechnical data are available.

Section 9

CONCLUSIONS AND RECOMMENDATIONS

This report has addressed the mechanical behavior of cylindrical concrete drilled shafts embedded in rock. Methods of analysis have been described which allow the prediction of the shaft load-displacement behavior and ultimate capacity when subjected to either axial load (compression or uplift), lateral load or moment, or torsion. Coupling between the various modes of loading has not been considered.

Simple models for the mechanical behavior have been suggested, and these allow closed form predictions of the response of a shaft when subjected to any of the individual modes of loading addressed. For axial compression or uplift, initial linear elastic response and shaft slippage in its socket have been considered. Only the initial linear elastic response and the limiting condition have been considered for both the lateral and torsional loading modes.

The application of these models to the interpretation of field loading tests reported in the literature also has been considered. All except two of the field tests involved axial loading and, by fitting the simple model to the observed behavior for these cases, it has been possible to deduce a likely range of values for the model parameters. Furthermore, it has been possible to correlate some of the basic parameters of the model to a single index property, the uniaxial compressive strength of the rock. This is a major simplification, but one of convenience, because it allows preliminary estimates of the model parameters to be made for initial design calculations. Greater confidence in the model and its predictions only can be obtained from further field load testing with proper documentation.

There are very few field data from lateral and torsional load tests on drilled shafts in rock, and therefore research in this area is warranted. Furthermore, very little is known about the behavior of drilled shafts in rock under the combined action of two or more of the loading modes. Problems of this type also warrant further study.

The closed form expressions presented in this report were developed for essentially

homogeneous rock masses. At the present time, comparable expressions do not exist for layered rock masses. However, judicious use of the solutions presented will allow bounds to be established on the shaft behavior for equivalent homogeneous assumptions using the strongest and weakest rock layer properties. An estimate of the actual behavior then can be made by appropriately weighting the actual layer thicknesses and properties. More precise solutions for multi-layered rock masses require a general three-dimensional numerical analysis.

Appendix A

BACK ANALYSIS OF AXIAL LOAD TESTS

The figures in this appendix show details of the field load tests listed in Table 7-1. Each plot shows the actual test data (applied load versus axial displacement) and the fit that was made to obtain the parameters of the simple analytical model for axial loading. In Figures A-1 to A-14, the axial loads are compressive, and the displacements actually are shaft butt settlements. In Figures A-15 to A-25, the loads are uplift, and the displacements are upward movements of the shaft butt. In Figures A-4 and A-5, measured dilations at the shaft walls also have been plotted against axial displacement. The system of units shown on each figure is the same as that given in the corresponding source reference. Note also that the deduced S values always are in the units of load per displacement.

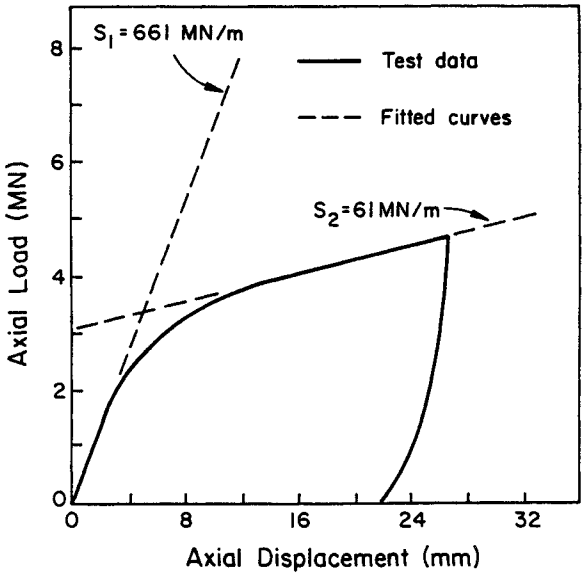

Figure A-1. Load-Displacement Behavior of Shaft P1
(Test Data from Horvath, et al., 1)

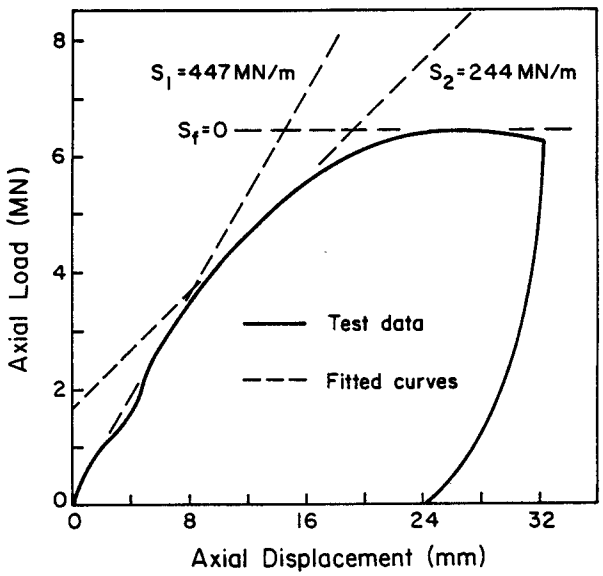

Figure A-2. Load-Displacement Behavior of Shaft P3
(Test Data from Horvath, et al., 1)

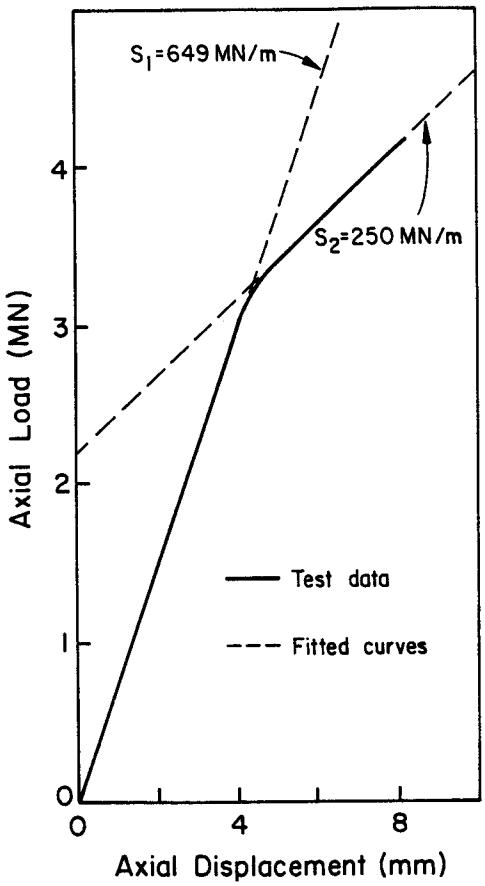

Figure A-3. Load-Displacement Behavior of Bay St. Shaft
(Test Data from Horvath, et al., 2)

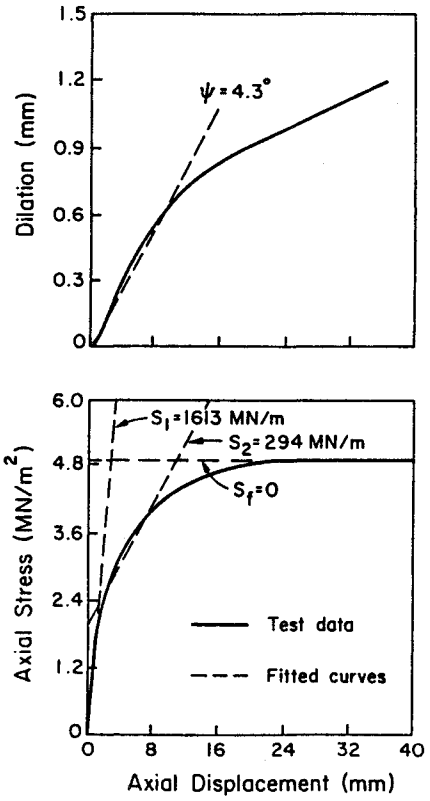

Figure A-4. Load-Displacement and Dilational Behavior of Shaft S3 (Test Data from Williams, 3)

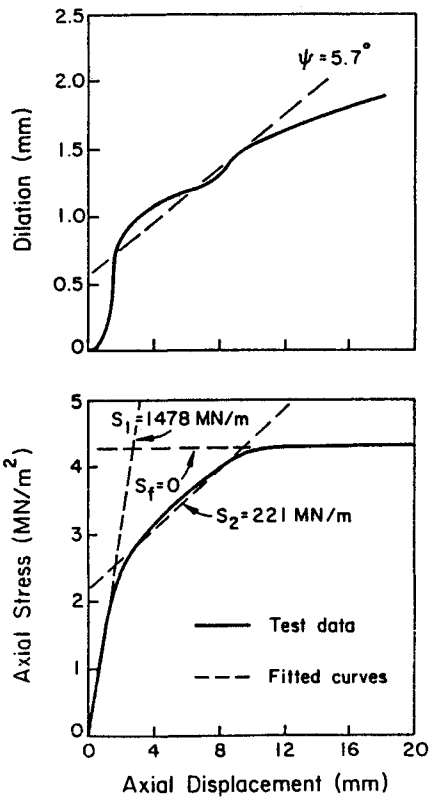

Figure A-5. Load-Displacement and Dilational Behavior of Shaft S5 (Test Data from Williams, 3)

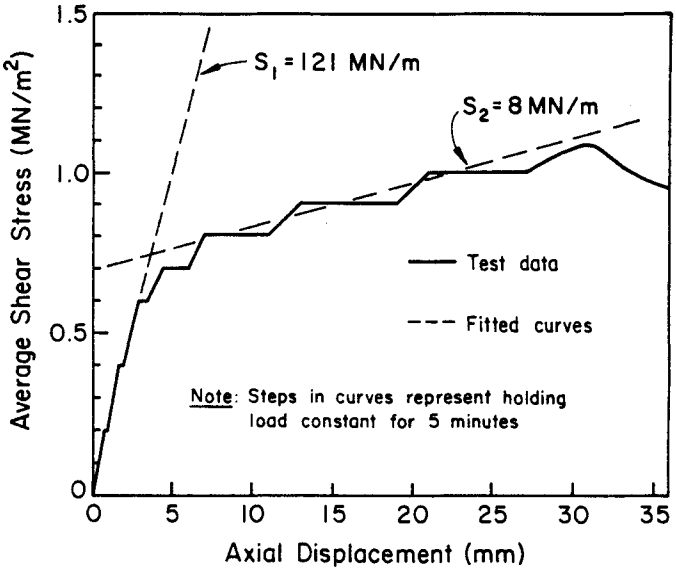

Figure A-6. Load-Displacement Behavior of Shaft A2 (Test Data from Pells, et al., 4)

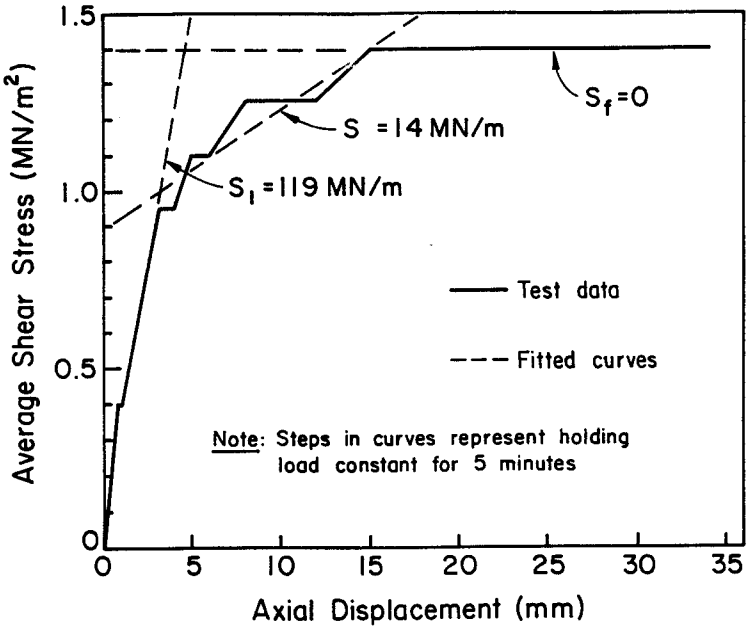

Figure A-7. Load-Displacement Behavior of Shaft A3
(Test Data from Pells, et al., 4)

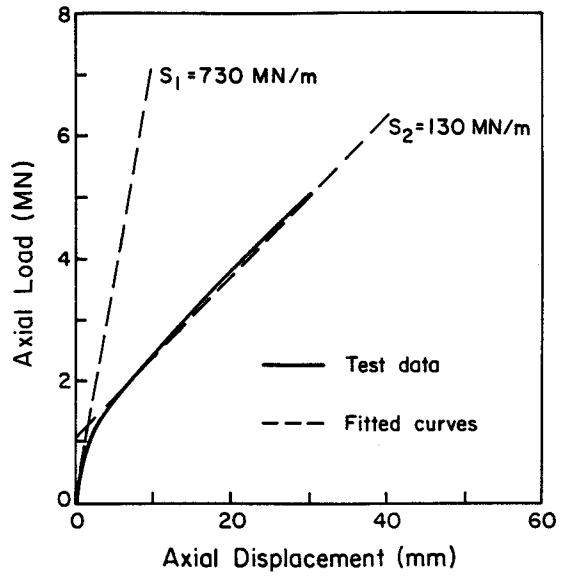

Figure A-8. Load-Displacement Behavior of "Voided Toe" Shaft
(Test Data from Mallard and Ballantyne, 5)

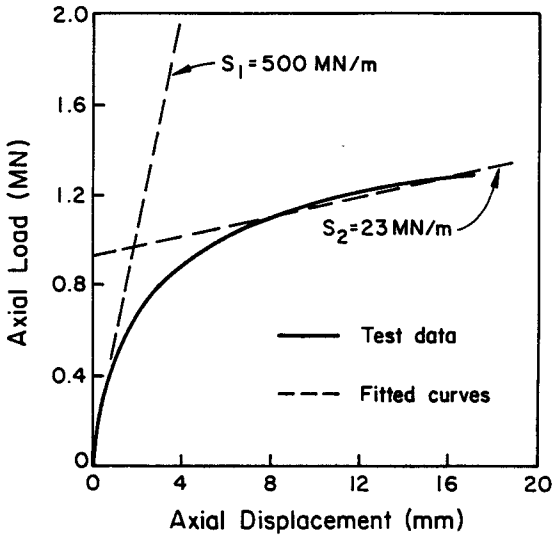

Figure A-9. Load-Displacement Behavior of Shaft A3
(Test Data from Davies, et al., 8)

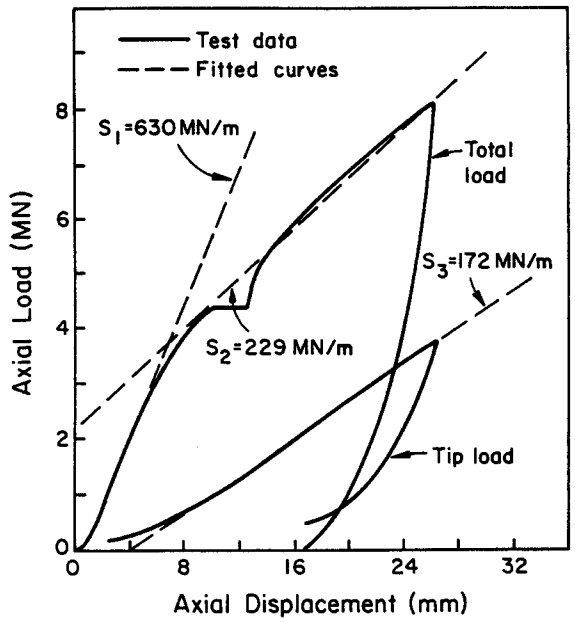

Figure A-10. Load-Displacement Behavior of Shaft P2
(Test Data from Horvath, et al., 1)

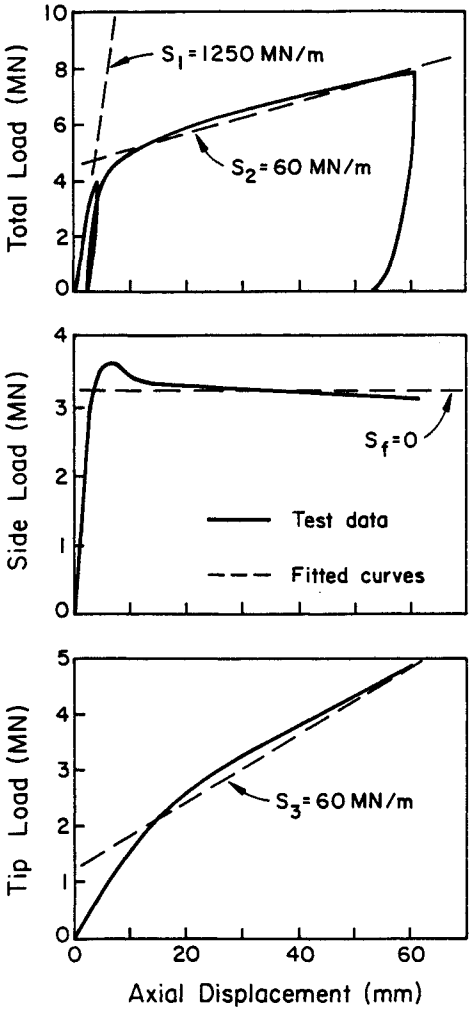

Figure A-12. Load-Displacement Behavior of Shaft M8 (Test Data from Williams, 3)

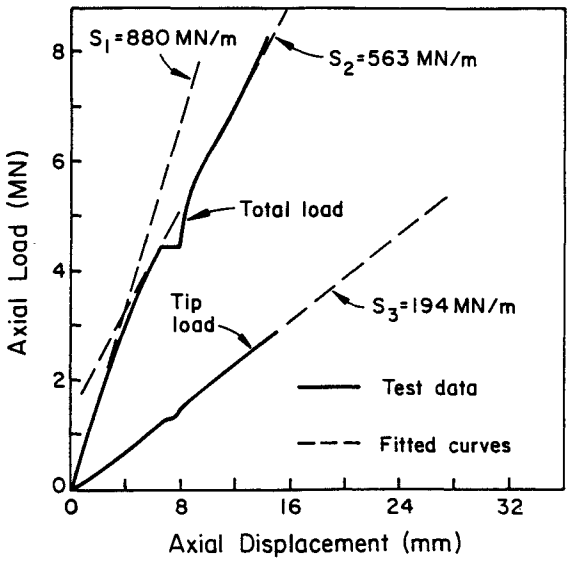

Figure A-11. Load-Displacement Behavior of Shaft P4 (Test Data from Horvath, et al., 1)

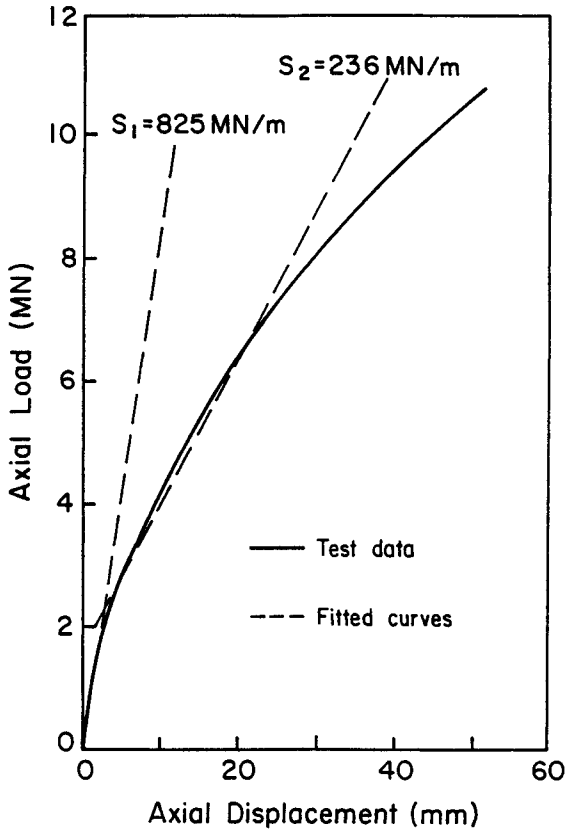

Figure A-13. Load-Displacement Behavior of "Solid Toe" Shaft (Test Data from Mallard and Ballantyne, 5)

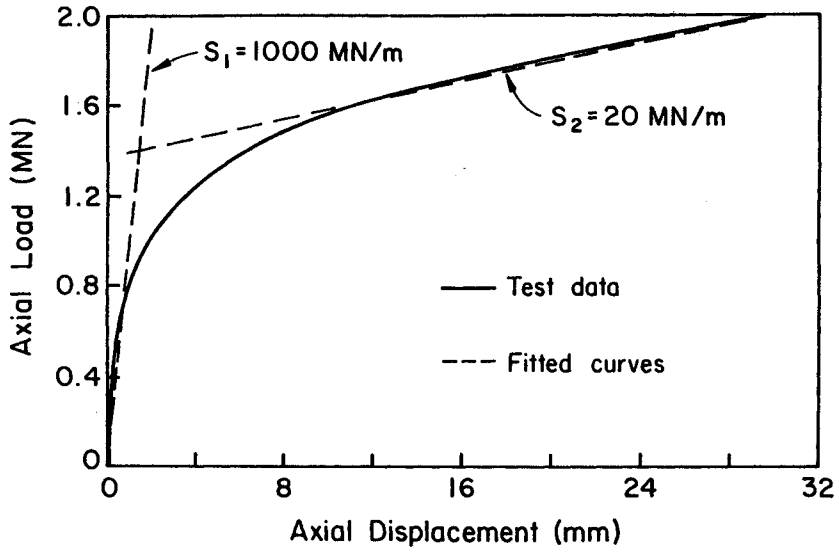

Figure A-14. Load-Displacement Behavior of Shaft A1
(Test Data from Davies, et al., 8)

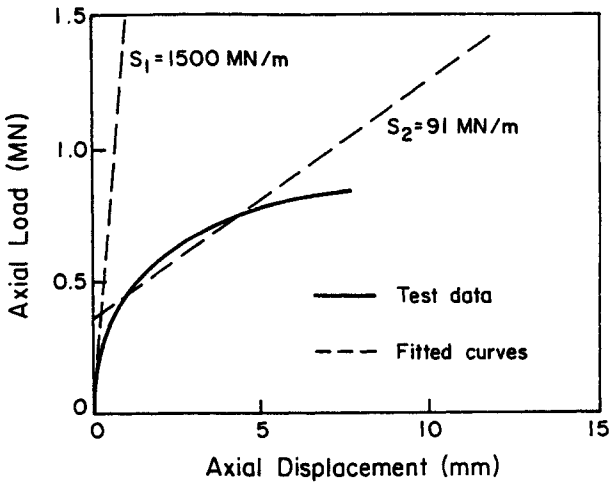

Figure A-15. Load-Displacement Behavior of Shaft 1A
(Test Data from Webb and Davies, 6)

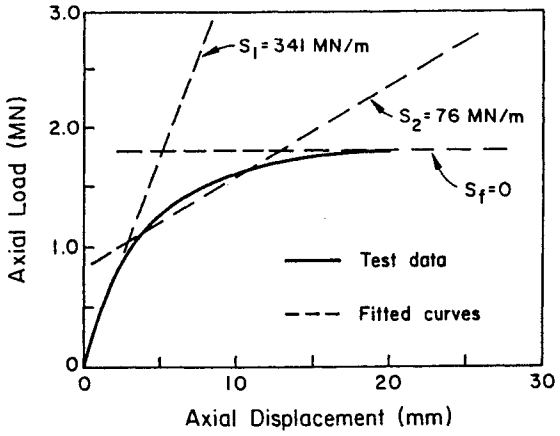

Figure A-16. Load-Displacement Behavior of Shaft 1B (Test Data from Webb and Davies, 6)

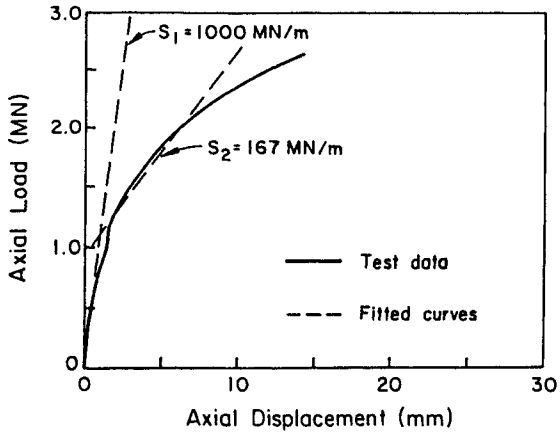

Figure A-17. Load-Displacement Behavior of Shaft 1C (Test Data from Webb and Davies, 6)

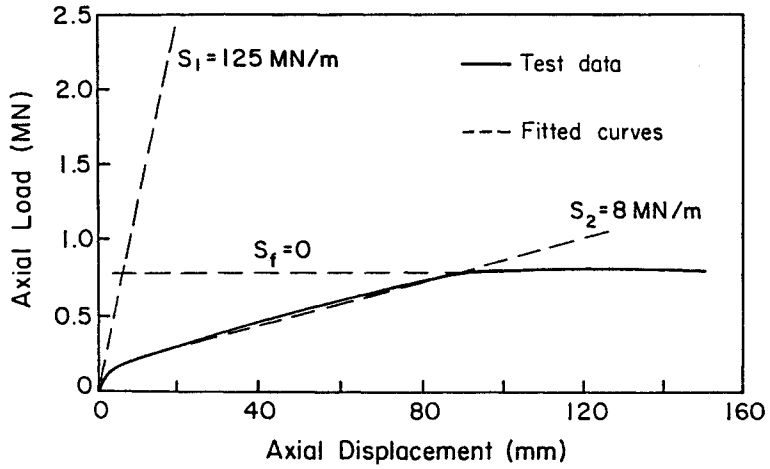

Figure A-18. Load-Displacement Behavior of Shaft 2B (Test Data from Webb and Davies, 6)

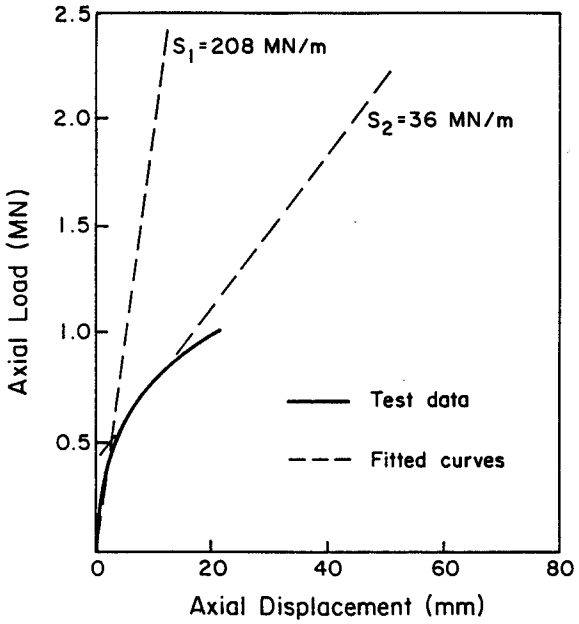

Figure A-19. Load-Displacement Behavior of Shaft 2C (Test Data from Webb and Davies, 6)

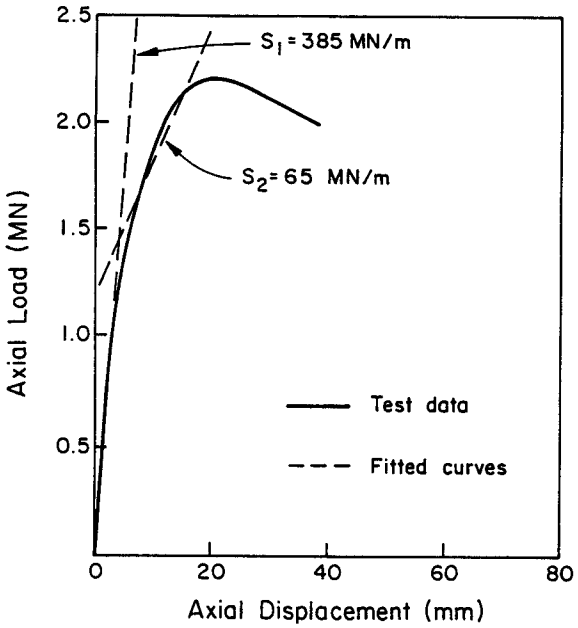

Figure A-20. Load-Displacement Behavior in Shaft 2F (Test Data from Webb and Davies, 6)

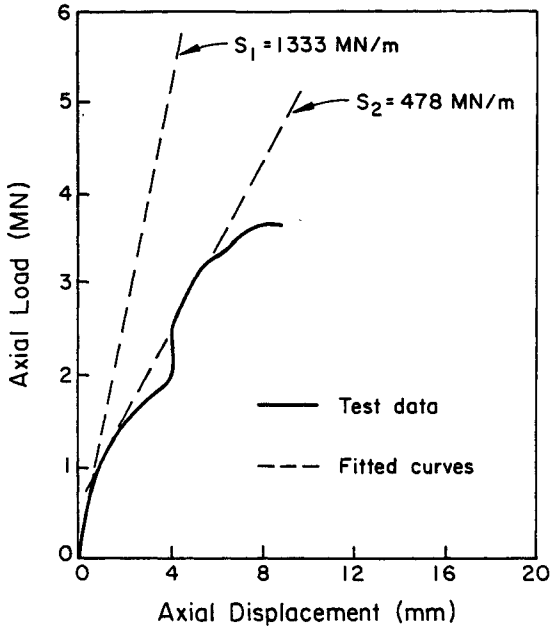

Figure A-21. Load-Displacement Behavior of Shaft 3B (Test Data from Webb and Davies, 6)

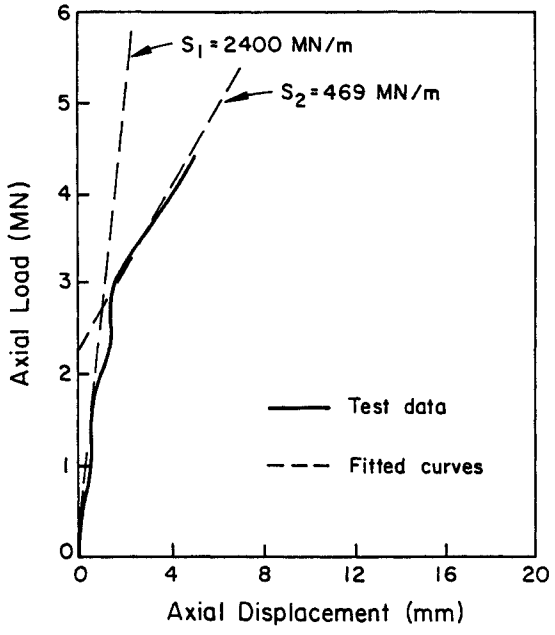

Figure A-22. Load-Displacement Behavior of Shaft 3C (Test Data from Webb and Davies, 6)

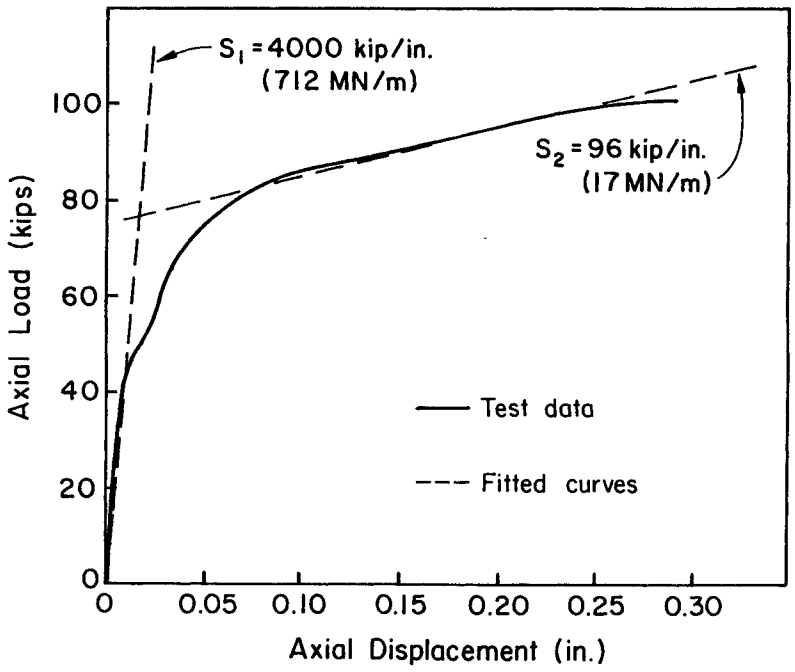

Figure A-23. Load-Displacement Behavior of Shaft 24-2
(Test Data from Kulhawy, et al., 7)

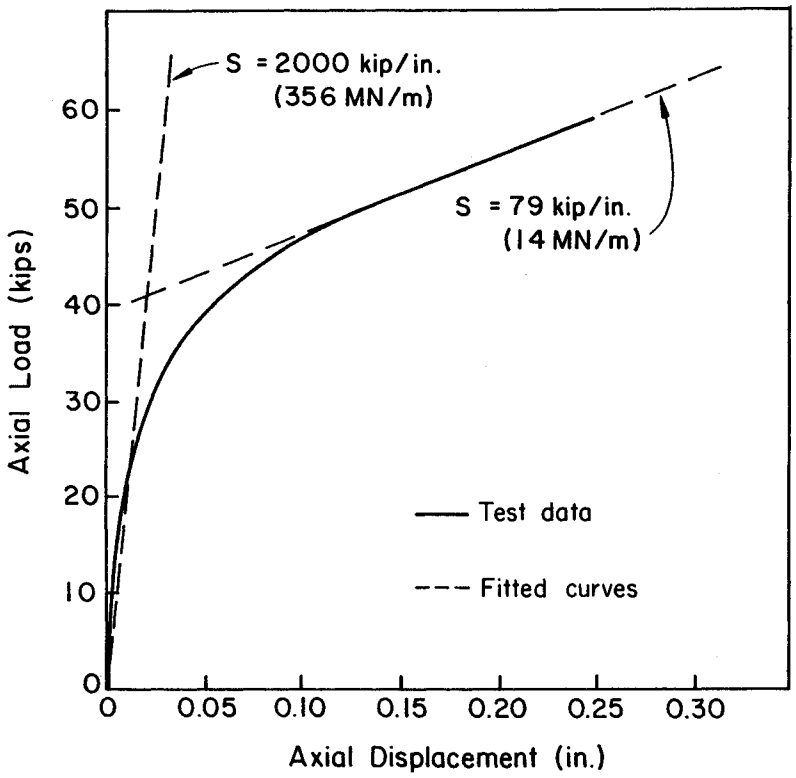

Figure A-24. Load-Displacement Behavior of Shaft 24-3
(Test Data from Kulhawy, et al., 7)

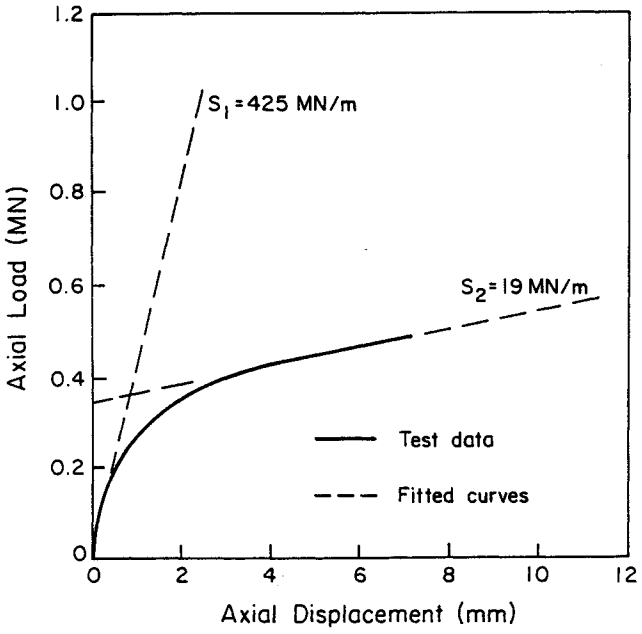

Figure A-25. Load-Displacement Behavior of Shaft A4
(Test Data from Davies, et al., 8)

REFERENCES

1. Horvath, R. G., Kenney, T. C., and Kozicki, P., "Methods of Improving the Performance of Drilled Piers in Weak Rock," Canadian Geotechnical Journal, Vol. 20, No. 4, Nov. 1983, pp. 758-772.

2. Horvath, R. G., Kenney, T. C., and Trow, W. A., "Results of Tests to Determine Shaft Resistance of Rock-Socketed Drilled Piers", Proceedings, International Conference on Structural Foundaitons on Rock, Vol. 1, Sydney, 1980, pp. 349-361.

3. Williams, A. F., "The Design and Performance of Piles Socketed into Weak Rock," Ph.D. Dissertation, Monash University, Melbourne, 1980 (as reported in 9).

4. Pells, P. J. N., Rowe, R. K., and Turner, R. M., "An Experimental Investigation into Side Shear for Socketed Piles in Sandstone," Proceedings, International Conference on Structural Foundations on Rock, Vol. 1, Sydney, 1980, pp. 291-302.

5. Mallard, D. J. and Ballantyne, J. L., "The Behavior of Piles in Upper Chalk at Littlebrook D Power Station," Piles in Weak Rock, Institution of Civil Engineers, London, 1977, pp. 47-72.

6. Webb, D. L. and Davies, P., "Ultimate Tensile Loads of Bored Piles Socketed into Sandstone Rock," Proceedings, International Conference on Structural Foundations on Rock, Vol. 1, Sydney, 1980, pp. 265-270.

7. Kulhawy, F. H., O'Rourke, T. D., Stewart, J. P., and Beech, J. F., "Transmission Line Structure Foundations for Uplift-Compression Loading: Load Test Summaries," Report EL-3160, Electric Power Research Institute, Palo Alto, 1983, 729 p.

8. Davies, P., Webb, D. L., Hooley, P., and Yeats, J. A., "Geotechnical Parameters for Design of Bored Piles Founded in Weathered Siltstone Rock," Proceedings, 7th European Conference on Soil Mechanics and Foundation Engineering, Vol. 3, Brighton, 1979, pp. 43-50.

9. Chiu, H. K. and Dight, P. M., "Prediction of the Performance of Rock-Socketed Side-Resistance-Only Piles Using Profiles," International Journal of Rock Mechanics and Mining Sciences, Vol. 20, No. 1, Feb. 1983, pp. 21-32.

Appendix B

UNITS CONVERSIONS

LENGTH

1 foot (ft) = 0.3048 meters (m)

1 inch (in) = 25.4 millimeters (mm)

MASS

1 pound (lb) = 0.4536 kilograms (kg)

FORCE

1 ton (t) = 2000 pounds (lb)
= 2 kips (k)
= 8.897 kilonewtons (kN)

STRESS

1 ton/square foot (tsf) = 1.024 kilograms/square centimeter (kg/cm^2)
= 95.76 kilonewtons/square meter (kN/m^2)
= 0.0958 meganewtons/square meter (MN/m^2)
= 2 kips/square foot (ksf)
= 13.89 pounds/square inch (psi)
= 0.945 atmosphere (atm)

1 Newton/square meter (N/m^2) = 1 Pascal (Pa)

1 bar = 100 kilonewtons/square meter (kN/m^2)

($\therefore$ 1 tsf $\approx$ 1 kg/cm^2 $\approx$ 100 kN/m^2 $\approx$ 1 atm $\approx$ 1 bar)

UNIT WEIGHT

1 pound/cubic foot (lb/ft^3 or pcf) = 0.016 grams/cubic centimeter (g/cm^3)
= 0.158 kilonewtons/cubic meter (kN/m^3)

About EPRI

EPRI creates science and technology solutions for the global energy and energy services industry. U.S. electric utilities established the Electric Power Research Institute in 1973 as a nonprofit research consortium for the benefit of utility members, their customers, and society. Now known simply as EPRI, the company provides a wide range of innovative products and services to more than 1000 energy-related organizations in 40 countries. EPRI's multidisciplinary team of scientists and engineers draws on a worldwide network of technical and business expertise to help solve today's toughest energy and environmental problems.

EPRI. Electrify the World

Printed on recycled paper in the United States of America

EPRI • 3412 Hillview Avenue, Palo Alto, California 94304 • PO Box 10412, Palo Alto, California 94303 • USA
800.313.3774 • 650.855.2121 • askepri@epri.com • www.epri.com